Examining the adolescent psychosis spectrum: A dimensional approach integrating symptom, cortical morphometric, functional, and transcriptomic data

Alyssa Dai
Integrated Program in Neuroscience
McGill University, Montreal
December 2022

A thesis submitted to McGill University in partial fulfilment of the requirements of the degree of Master of Science

Contents

Abstract

The emergence of the psychosis spectrum (PS; subclinical psychosis-related symptoms) during late childhood and adolescence (i.e., youth) coincides with a period of dynamic cortical remodeling and is linked to greater risk for the later emergence of neuropsychiatric disorders such as psychosis. Prior neuroimaging studies of the PS have reported abnormalities in individual cortical morphometric features, but have largely neglected changes expressed in covariance patterns of multiple interrelated metrics. How these patterns may link to dimensions of latent psychosis-related symptomatology, brain function, and molecular architecture are open areas for investigation.

This thesis contributes a data-driven characterization of multivariate cortical morphometry in the PS by integrating symptom, magnetic resonance imaging (MRI), and transcriptomic data. Using the Philadelphia Neurodevelopmental Cohort, a community-based and non-help-seeking sample, we analyzed data from 266 youth (aged 8–23) who endorsed PS features. Non-negative matrix factorization was used to identify 8 morphometric covariance patterns (MCPs) integrating MRI-based metrics (cortical thickness, surface area, mean curvature, local gyrification index). In a single multivariate model, subject-specific MCP loadings were related to sociodemographic features and three dimensions of PS symptoms derived using factor analysis. We explored the functional and molecular relevance of MCPs associated with symptom dimensions by mapping them to meta-analytic functional activation patterns, maturational cortical functional gradients, and spatial variation in gene expression.

Two latent patterns of brain-behaviour associations were revealed, including a clinically relevant pattern relating metric-specific variation in five MCPs to symptom severity along a PS dimension of ‘disturbed self-experience.’ MCPs contributing to this symptom-morphometry relationship mapped to meta-analytic activation patterns of relevant cognitive functions, as well as to cortical areas reconfiguring along a unimodal-to-transmodal functional hierarchy across maturation. A transcriptomic gradient also differentiated anterior PS-related MCPs from other MCPs by genes enriched for specific cell types, synaptic signalling processes, and affective and psychotic disorder-related genes.

We show that by leveraging shared covariance of multiple MRI metrics along with a dimensional approach to symptoms, we can gain a more nuanced understanding of potential cortical vulnerability during the earliest manifestations of risk for psychosis.

Résumé

L'émergence du spectre de la psychose (SP ; symptômes subcliniques liés à la psychose) à la fin de l'enfance et à l'adolescence (c.-à-d. la jeunesse) coïncide avec une période de remodelage cortical dynamique et est liée à un risque accru d'apparition ultérieure de troubles neuropsychiatriques tels que la psychose. Des études antérieures de neuroimagerie du SP ont signalé des anomalies dans les caractéristiques morphométriques corticales individuelles, mais ont largement négligé les changements exprimés dans les modèles de covariance de plusieurs mesures interdépendantes. La manière dont ces modèles peuvent être liés aux dimensions de la symptomatologie latente liée à la psychose, à la fonction cérébrale et à l'architecture moléculaire sont des domaines ouverts à l'investigation.

Cette thèse contribue à une caractérisation basée sur les données de la morphométrie corticale multivariée dans le SP en intégrant les données sur les symptômes, l'imagerie par résonance magnétique (IRM) et la transcriptomique. À l'aide de la Cohorte neurodéveloppementale de Philadelphie, un échantillon communautaire d'individus qui ne recherchent pas d'aide, nous avons analysé les données de 266 jeunes (âgés de 8 à 23 ans) qui ont présenté les caractéristiques SP. La factorisation matricielle non-négative a été utilisée pour identifier 8 modèles de covariance morphométrique (MCM) intégrant des métriques basées sur l'IRM (épaisseur corticale, surface, courbure moyenne, indice de gyrification local). Dans un modèle multivarié unique, les charges MCM spécifiques au sujet étaient liées à des caractéristiques sociodémographiques et à trois dimensions des symptômes de SP dérivées à l'aide d'une analyse factorielle. Nous avons exploré la pertinence fonctionnelle et moléculaire des MCM associées aux dimensions des symptômes en les cartographiant aux modèles d'activation fonctionnelle méta-analytique, aux gradients fonctionnels corticaux de maturation et à la variation spatiale de l'expression des gènes.

Deux schémas latents d'associations cerveau-comportement ont été révélés, y compris un schéma cliniquement pertinent concernant la variation spécifique à la métrique dans cinq MCM à la gravité des symptômes le long d'une dimension SP de « l'expérience de soi perturbée ». Les MCM contribuant à cette relation symptôme-morphométrie sont cartographiés aux modèles d'activation méta-analytiques des fonctions cognitives pertinentes, ainsi qu'aux zones corticales reconfigurant le long d'une hiérarchie fonctionnelle unimodale à transmodale à travers la maturation. Un gradient transcriptomique a également différencié les MCM antérieurs liés à la SP

des autres MCM par des gènes enrichis pour des types de cellules spécifiques, des processus de signalisation synaptiques et des gènes liés aux troubles affectifs et psychotiques.

Nous montrons qu'en tirant parti de la covariance partagée de plusieurs mesures IRM avec une démarche dimensionnelle aux symptômes, nous pouvons acquérir une compréhension plus nuancée de la vulnérabilité corticale potentielle lors des premières manifestations de risque de psychose.

Acknowledgments

The work presented in this thesis represents the culmination of the support, teaching, and dedication of many individuals I have had the privilege of working alongside over the past two years. Principal among these is my supervisor, Dr. Mallar Chakravarty. Enrolling in your graduate seminar was one of the luckiest decisions I made in my senior year, and I would not be where I am today without the genuine enthusiasm and mentorship you showed me over the course of my first months as a neuroimaging student—and every month since! Thank you for always believing in me, for helping me achieve things I never realized I could, and for always making time for one more read-through of my draft, one more presentation rehearsal, one more commendation. I am so appreciative of all that you have done and continue to do for your students.

To my advisory committee members, Dr. Bratislav Misic, Dr. Martin Lepage, and Dr. Xiaoqian Chai: thank you for your thoughtful and encouraging feedback on my research, and for guiding me towards producing the best work possible. It has been an honour to build upon your contributions and share in your scientific perspectives.

Thank you also to the Healthy Brains for Healthy Lives Initiative, as well as the Canadian Institutes of Health Research, for the funding support that was essential to my master's research.

To my colleagues in the CoBrA Lab: thank you for your companionship, positivity, and willingness to help, and for being my frequent reminders of all that is possible with a curious and open mind. My heartfelt thanks especially to Dr. Raihaan Patel, for your encouragement and guidance since day one, and without whose tools much of the work in this thesis would not be possible. Likewise, a tremendous thank you to Dr. Gabriel Devenyi: you taught me how to be a better problem-solver and more confident programmer, and it was a true privilege to have your expertise and advice always just a message away. To my fellow master's survivors: thank you for sharing in this rollercoaster of conducting research during a pandemic with me, and for being a sounding board all the times I have needed it most. Thank you especially to my friends Justine Ziolkowski and Hannah Owens: it has been wonderful to be a graduate student alongside you.

To my partner, Zach: thank you for your unwavering understanding and support throughout this journey, and for being my cheerleader on all the good days and bad days. Finally, my endless love and gratitude to my parents, Sherry and David, for always keeping me reminded of what's important, and who probably would be just as proud even if this thesis never saw the light of day.

Contributions of Authors

This manuscript contains original unpublished work by the author, Alyssa Dai. All data processing and analyses of the primary dataset of interest, as well as writing and generation of figures were led by the author. Dr. M. Mallar Chakravarty supervised this work, providing guidance on initial project conceptualization, analysis, interpretation, and thesis writing.

The primary data used in this thesis (structural neuroimaging scans and neuropsychiatric/behavioural variables) were obtained from the publicly available Philadelphia Neurodevelopmental Cohort (PNC) (https://www.ncbi.nlm.nih.gov/projects/gap/cgi-bin/study.cgi?study_id=phs000607.v3.p2). Quality control for motion in raw PNC brain scans was performed by Dr. Swapna Premasiri and Aurelie Bussy. Dr. Gabriel A. Devenyi provided technical support (troubleshooting, optimizing) on image processing and analysis pipelines, including developing the iterativeN4_multispectral pipeline used here to preprocess brain images.

Supplementary and secondary data used in this thesis were generously shared by Justine Ziolkowski (cortical morphometric covariance patterns from autism spectrum disorder and matched neurotypical individuals, used in Section 4.3.3) and Drs. Hao-Ming Dong and Avram Holmes (maturational functional connectivity gradients, used in Section 4.7).

Dr. Raihaan Patel developed the code used for one of the data analyses (non-negative matrix factorization, Section 4.3), and additionally provided guidance related to implementation and results interpretation for this method. Several data analyses also employed open-source software toolboxes or code authored by Dr. Ross D. Markello and Justine Y. Hansen, who provided technical support related to their use. Support on methodological choices and/or interpretation of findings was also provided by Dr. Tyler M. Moore (factor analysis, Section 4.4), and Drs. Ross D. Markello and Bratislav Misic (imaging transcriptomic analyses, Section 4.8). Dr. Jakob Seidlitz and Dr. Theodore D. Satterthwaite provided feedback on experimental design.

List of Figures

List of Tables

List of Abbreviations

AHBA	Allen Human Brain Atlas
bPLS	Behavioural partial least squares
BSR	Bootstrap ratio
CCA	Canonical correlation analysis
CT	Cortical thickness
GI	[Local] gyrification index
GO	Gene Ontology
ICA	Independent component analysis
K-SADS	Kiddie Schedule for Affective Disorders and Schizophrenia
MC	Mean curvature
MCP	Morphometric covariance pattern
mcPLS	Mean-centered partial least squares
MPRAGE	Magnetization-prepared rapid acquisition gradient echo
MNI	Montreal Neurological Institute
MRI	Magnetic resonance imaging
NMF	Non-negative matrix factorization
(OP)NMF	(Orthonormal projective) non-negative matrix factorization
PCA	Principal component analysis
PLS	Partial least squares
PNC	Philadelphia Neurodevelopmental Cohort
PRIME	Prevention through Risk Identification, Management, and Education
PS	Psychosis spectrum
PS-R	PRIME Screen-Revised
SA	Surface area
SIPS	Structured Interview for Psychosis-risk Syndromes
WRAT-4	Wide Range Achievement Test, version 4

1. Introduction

1.1. The psychosis spectrum and brain development

1.1.1. The prevalence of psychosis in the population

Schizophrenia and related psychotic disorders (e.g., schizoaffective disorder, psychotic depression) affect roughly 3% of society (W. C. Chang et al., 2017; Perälä et al., 2007), and are increasingly conceptualized as clinical manifestations of phenotypes that are continuously distributed in the general population (McGrath et al., 2015; Nelson et al., 2013; M. J. Taylor et al., 2016; van Os et al., 2000; van Os & Linscott, 2012; van Os et al., 2009; Verdoux & van Os, 2002). Positive (e.g., hallucinations, delusions), negative (e.g., blunted affect, avolition), and disorganized symptoms (e.g., conceptual disorganization, disorganized speech) are hallmark debilitating features of such disorders (Potuzak et al., 2012; van Os & Kapur, 2009), but have also been consistently observed at subclinical levels in otherwise healthy individuals. Approximately 5–8% of the general population report subthreshold positive symptoms such as abnormal auditory perceptions or attenuated paranoid delusional thinking, which are also commonly referred to as "psychotic-like experiences" (Linscott & van Os, 2013; McGrath et al., 2015; van Os et al., 2009; van Os & Reininghaus, 2016). The prevalence of subclinical psychosis symptoms is even higher in children and adolescents, with estimates of around 20% (Calkins et al., 2014; Kelleher, Connor, et al., 2012; Kelleher, Keeley, et al., 2012). These findings provide evidence for the existence of a continuum from mental health to diagnosable psychotic illness, with possible neurodevelopmental underpinnings.

1.1.2. The psychosis spectrum (PS)

Within the psychosis continuum, the range of subclinical positive symptoms, threshold-level positive psychotic symptoms such as hallucinations, and attenuated negative and disorganized symptoms observed in the general population has been collectively described as psychosis spectrum (PS) symptoms (Calkins et al., 2014; J. H. Taylor et al., 2020). Studies of individuals with PS symptoms represent a rising alternative to the clinical high-risk approach for investigating early development of psychosis symptoms. Namely, "clinical high-risk" has been used to describe individuals seeking clinical help for symptoms and who fulfill specific diagnostic criteria for a prodromal stage of psychosis (McGlashan et al., 2010; Schultze-Lutter et al., 2015), or signs and symptoms preceding the acute clinical phase of illness (Fava & Kellner, 1991). Around 30% of clinical high-risk individuals will experience a first episode of psychosis, the onset

of full-blown psychotic symptoms, within 2 years (Fusar-Poli, Bonoldi, et al., 2012; Fusar-Poli et al., 2013). The PS characterization is distinct from clinical high-risk in that individuals are not help-seeking, have a wider range of symptom severity, and show significantly lower rates of both short- and long-term progression to a first episode of psychosis (Dominguez et al., 2011; Kaymaz et al., 2012; J. H. Taylor et al., 2020; van Os & Reininghaus, 2016). PS symptoms thus uniquely provide a window into both normative variation of mental health and potential deviating risk pathways.

Despite their often-transitory nature, substantial evidence suggests that PS symptoms capture a critical phenotype of emerging psychosis vulnerability even before the prodrome, which still poses serious implications for overall health. Like overt psychotic disorders, PS symptoms can cause significant distress (Calkins et al., 2014) and have been associated with a host of negative mental and physical outcomes. These include impairments in neurocognitive (Calkins et al., 2014; Gur et al., 2014; Kelleher et al., 2013; Mollon et al., 2016) and psychosocial functioning (Schimmelmann et al., 2015), alterations in brain structure (see Section 1.5 for a review of neuroimaging findings), increased suicidal ideation (Calkins et al., 2014; Cederlöf et al., 2017), as well as reduced overall quality of life (Alonso et al., 2018). A recent longitudinal study further revealed that school-age youth with distressing PS symptoms show developmental milestone delays (e.g., delayed early motor milestones) and brain structural abnormalities irrespective of the persistence of symptoms (Karcher, Loewy, et al., 2022), corroborating the clinical relevance of even transient expressions of this phenotype. Crucially, PS symptoms early in life not only increase the risk of a later psychotic disorder as much as four-fold (Healy et al., 2019; Kaymaz et al., 2012), but are also linked to higher risk for other psychiatric disorders (Kelleher, Keeley, et al., 2012; McGrath, Saha, Al-Hamzawi, Andrade, et al., 2016; Werbeloff et al., 2012), amplifying their importance as a marker of general psychopathology. Taken together, the increased risk for neuropsychiatric disorders alongside the clear neurodevelopmental and functional impairment associated with PS symptoms suggests that their existence should be considered a public health concern.

1.1.3. Neurodevelopmental and sociodemographic factors of PS symptoms

PS symptoms often first emerge and are most prevalent during late childhood and adolescence (Calkins et al., 2014; Kelleher, Connor, et al., 2012; McGrath, Saha, Al-Hamzawi, Alonso, et al., 2016), an age group we will refer to in this thesis broadly as “youth.” This coincides

with a period during which the brain is in the crux of extensive neurobiological and functional maturation and therefore vulnerable to an array of neuropsychiatric issues (Keshavan et al., 2014; Paus et al., 2008). During this period, processes including increasing myelination as well as active synaptic pruning and refinement contribute to gray matter reorganization, resulting in stereotyped trajectories of both microscale and macroscale cortical features of the brain that collectively support typical neurodevelopment (Keshavan et al., 2014; Paus et al., 2008; Raznahan et al., 2011). The manifestation of PS symptoms during youth may represent a first expression of atypical development processes that in concert with other environmental and biological risk factors may lead to psychotic illness, congruent with the model of schizophrenia itself as a progressive disorder of disrupted neurodevelopment (Keshavan et al., 2014; Murray et al., 2017; Rapoport et al., 2012). Studying the PS in neurodevelopmental samples is thus critical, as it enables the identification of emerging neurobiological abnormalities during a stage when therapeutic intervention may still be able to capitalize on the maturing brain's capacity for plastic change.

As is the case for psychotic disorders, demographic characteristics such as sex, racial identity, and socioeconomic privilege also represent important risk factors for PS symptoms. Findings supporting sex differences in the prevalence of psychotic-like experiences have been mixed (Dolphin et al., 2015; Laurens et al., 2007; Ronald et al., 2014; Stainton et al., 2021), potentially due to the to the predominant focus on only positive subclinical symptoms. Notably, a study of a comprehensive range of PS symptoms in a large ($n > 4000$) US community sample of youth identified male sex as a significant predictor of PS symptoms (Calkins et al., 2014), a result that is potentially concordant with the earlier onset of clinical psychosis in males (Ochoa et al., 2012; van der Werf et al., 2014). Findings related to racial differences, meanwhile, have been more consistent. Youth from racial minority backgrounds, particularly Black individuals, report disproportionately higher levels of PS symptoms when compared with European or White American youths in US-based community samples (Calkins et al., 2014; Karcher, Klaunig, et al., 2022; Paksarian et al., 2016) or with White British youths in UK-based samples (Laurens et al., 2008). Higher prevalence of PS symptoms has also been associated with indicators of socioeconomic disadvantage, including lower education and income levels (Johns et al., 2004; Pignon et al., 2018) as well as fewer years of parental education for youth (Calkins et al., 2014; Zammit et al., 2013). These findings mirror racial-ethnic (C. Morgan et al., 2019; Schwartz &

Blankenship, 2014) and socioeconomic (Kirkbride et al., 2008; Pignon et al., 2018) disparities in clinical psychoses.

Understanding how sociodemographic differences may be reflected in abnormal neurobiology in youth with PS symptoms may therefore be crucial for elucidating the pathophysiology of psychosis development. However, studies of brain correlates of PS symptoms, as well as of clinical psychotic symptoms more broadly, have often treated these characteristics as nuisance variables rather than as potential sources of relevant heterogeneity. Moreover, psychosis studies have overwhelmingly included mainly White participants recruited from narrow geographic catchment areas, thereby limiting sample representativeness of the racial and socioeconomic diversity relevant for symptoms (Burkhard et al., 2021; Harnett, 2020). These factors highlight a need for study designs that explicitly assess the influence of sociodemographic variables on neurobiological phenotypes, particularly in diverse samples of younger individuals experiencing PS symptoms. Recent large-scale, population studies of youth such as the Philadelphia Neurodevelopmental Cohort (PNC) (Calkins et al., 2015) and the Adolescent Brain Cognitive Development study (Garavan et al., 2018) provide this opportunity, and may be instrumental to a more complete understanding of potential neurodevelopmental pathways for psychosis.

1.1.4. Transdiagnostic implications of understanding the PS

In addition to possibly reflecting vulnerability for psychotic disorders, the presence of PS symptoms has been widely shown to index elevated risk for myriad psychiatric disorders in which psychosis is not a core feature, particularly affective disorders and anxiety disorders (Calkins et al., 2017; Giocondo et al., 2021; Kırlı et al., 2019; McGrath, Saha, Al-Hamzawi, Andrade, et al., 2016; van Os & Reininghaus, 2016). An investigation of youth with PS symptoms revealed that both persistent and transient symptoms were associated with increased rates of major depressive disorder after two years (Calkins et al., 2017). Further, a recent meta-analysis of population-based studies of youth found a three-fold increased risk of any mental disorder, psychotic or non-psychotic, for youth with PS symptoms, as well as a 2.8-fold increase in non-psychotic disorders alone compared to peers without PS symptoms (Healy et al., 2019), suggesting that PS symptoms in early life may be a dynamic marker of risk for subsequent psychopathology (Giocondo et al., 2021; van Os & Reininghaus, 2016).

While PS symptoms do show a degree of specificity for psychotic outcomes (Kaymaz et al., 2012; Werbeloff et al., 2012), the transition to differing diagnosable phenotypes is likely modulated by multiscale genetic, environmental, and neurobehavioral susceptibilities (Calkins et al., 2017; Siever & Davis, 2004). Thus, understanding mechanistic underpinnings of the PS may facilitate identification of biologically-grounded markers of risk that have extended relevance beyond the prevention of psychotic illness (van Os & Reininghaus, 2016; Voineskos et al., 2020). As will be explored further in the next sections, an integrated approach that considers the neurodevelopmental, neurobiological, behavioural, and molecular dimensions that shape the PS will move us closer to this goal.

1.2. Magnetic resonance imaging

An important step towards improving our understanding of psychosis pathogenesis or antecedents involves reliably mapping subjective symptom presentations onto underlying neural targets. This can be accomplished using magnetic resonance imaging (MRI), a popular medical imaging technique that allows non-invasive in vivo investigation of the human brain in 3D at high spatial resolution. The MRI modality of most relevance to the current study is structural MRI, which involves sequences that can produce detailed images of neuroanatomical structure (Lerch et al., 2017). The specific type of structural MRI sequence of interest to this work, T1-weighted imaging, will also be discussed in more detail below.

Broadly, structural MRI harnesses the abundance of hydrogen atoms in the body and works by applying a powerful uniform magnetic field (B_0, measured in Tesla (T)) to align hydrogen protons in tissues and cause them to precess (or circle) around the axis of B_0 (Currie et al., 2013). This alignment to B_0 is then perturbed by introducing an external energy, a radiofrequency pulse referred to as B_1. The excited protons will subsequently return to their equilibrium state through two processes of relaxation: the realignment of proton spins with B_0, termed T1 or longitudinal relaxation; and the loss of phase coherence of spinning protons, termed T2 or transverse relaxation (Currie et al., 2013; Elmaoğlu & Çelik, 2011). As relaxation occurs, protons emit a magnetic resonance signal that can be localized in space via the application of additional magnetic gradient fields. Using Fourier transformation, the frequency information contained in the localized signals in the imaged plane can then be converted to intensity levels, which are then displayed as shades of gray in the final MR image or volume. The contrast of individual voxels in a slice depends on

the density of protons, the surrounding tissue environment, and the timing (sequence) of pulses and applied magnetic gradients. By manipulating the latter, different MR image types, in which the signal measures different properties of the brain, can be obtained.

The present study primarily relies on T1-weighted (T1w) structural MRI, which produces images in which differences in voxel signal intensity reflect differences in T1 relaxation time of the underlying imaged tissue. By leveraging short times between the delivery of the radiofrequency pulse and the readout of signal (i.e., echo time) as well as between successive pulses (i.e., repetition time), T1w images provide maximal contrast between different tissue types (Elmaoğlu & Çelik, 2011). In the context of the brain, clear distinction between white matter, gray matter, and cerebrospinal fluid can be achieved, making this imaging technique ideal for examining features of cortical anatomy across health and illness.

Of secondary relevance to this study are functional MRI methods, which enable inference of brain activity through the blood oxygenation level-dependent (BOLD) contrast (Glover, 2011). This form of imaging is designed to detect changes in the relative levels of oxygenated and deoxygenated hemoglobin in blood due to their different magnetic properties. Such changes are known to occur in the brain following neuronal activation (Buxton & Frank, 1997; Buxton et al., 1998) and translate to measurable alterations in BOLD signal, a phenomenon known as the hemodynamic response (Glover, 2011). Functional MRI can be employed to study both spontaneous neural activity in a 'resting-state' setting, as well as patterns of brain activity occurring as a participant engages in a task in the scanner in 'task-based' settings.

1.3. Surface-based analysis of structural brain MRI

In the current thesis we use cortical surface-based measures as a basis for characterizing neuroanatomical profiles of individuals experiencing PS symptoms (Lerch et al., 2017). By applying image processing algorithms to T1w images, it is possible to derive morphometric variables that quantify a variety of surface-based macrostructural features of the cerebral cortex. While volume-based methods of modelling the cortex also exist, they may have limited capacity to capture detailed topological characteristics of the cortical sheet—and, by extension, subtle changes in these characteristics associated with early stages of illness—due to the complex and variable folding pattern of this structure (Van Essen et al., 1998). Surface-based methods help to overcome such limitations by constructing triangular meshes that aim to represent the geometry of

the white matter and pial cortical surfaces, allowing multiple morphological measurements, such as cortical thickness, to be computed at each vertex (i.e., point) along the cortex.

1.3.1. CIVET

One of the most widely used pipelines for performing surface-based analysis is CIVET, which performs automated structural MR image processing including image registration, intensity normalization, and classification of voxels into white matter, gray matter, and cerebrospinal fluid, along with cortical surface extraction (more details on CIVET processing are presented in Section 4.2.1) (Ad-Dab'bagh et al., 2006). A key feature of CIVET is its that it uses the Constrained Laplacian Anatomical Segmentation using Proximities (CLASP) algorithm to construct cortical surface meshes (Ad-Dab'bagh et al., 2006; J. S. Kim et al., 2005). In this approach, the white matter surface is first estimated, and then the pial surface is created via expansion of the white matter surface to the gray matter-cerebrospinal fluid boundary along a Laplacian field (J. S. Kim et al., 2005). In previous comparisons with FreeSurfer, another popular pipeline for cortical surface analysis, CIVET was shown to demonstrate higher reliability and scan-rescan reproducibility of cortical thickness measurements (S. Jeon et al., 2017; Lewis et al., 2017), as well as higher robustness of cortical surface reconstruction (Lewis et al., 2017). There is also evidence that CIVET-derived measurements may be more sensitive to certain early pathological patterns of brain atrophy, such as those associated with the Mild Cognitive Impairment stage of Alzheimer's disease (Redolfi et al., 2015). These findings highlight CIVET as a suitable tool for characterizing cortical surface morphometry in the context of abnormal health.

1.4. MRI-based measures of cortical morphology: cortical thickness, surface area, local gyrification index, mean curvature

Four surface-based metrics that are among the most easily accessible in common structural analysis pipelines including CIVET, and which together can provide a refined description of cortical anatomy at the vertex level, are cortical thickness, surface area, local gyrification index, and mean curvature. Schematic representations of each of these metrics are shown in Figure 1, and methodological details of how each metric was calculated in the current work are presented in Section 4.2.3. We provide brief computational descriptions of each metric below:

- Cortical thickness refers to the distance between the white matter surface and pial surface (J. S. Kim et al., 2005).

- Surface area is a function of the area occupied by the triangular faces surrounding a given vertex (Lyall et al., 2015).
- Local gyrification index describes the amount of surface area packed in a limited spherical volume around a vertex relative to an approximated lissencephalic area of the same region (Toro et al., 2008).
- Mean curvature refers to the average of the two principal curvatures at a vertex, which are the maximum and minimum values of curvature at that point (Ronan et al., 2011).

These morphometric features of the cortex are driven by different properties of the underlying cellular-level morphology, although precise mappings from MRI-derived metrics to biological underpinnings are currently lacking. Rather, they can be interpreted as indirect, putative indices of microscale biological processes that are interrelated but dissociable, which we expand on in the following section for our metrics of interest.

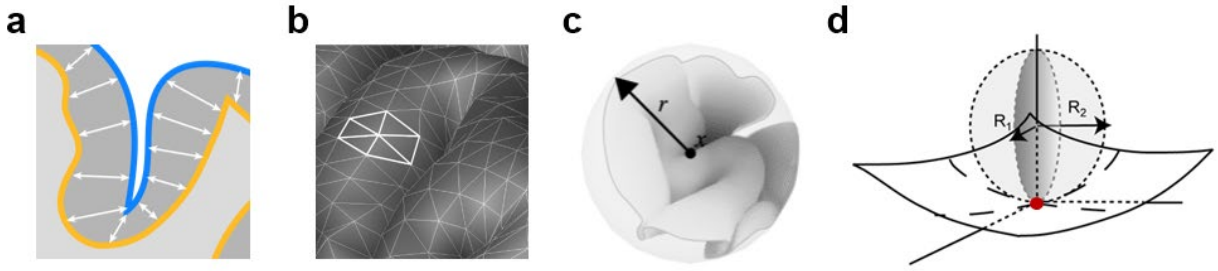

Figure 1. Illustration of four surface-based morphological measurements of the cortical sheet at the vertex level. (a) Cortical thickness refers to the distance (mm) between the white matter surface (denoted by the yellow boundary) and pial surface (blue boundary). **(b)** Surface area is a function of the area (mm^2) occupied by the triangular faces surrounding a given vertex. **(c)** Local gyrification index describes the amount of surface area contained within a limited spherical volume of radius *r* around a vertex *x*. The surface ratio method of computing this index is shown here (Toro et al., 2008). **(d)** Mean curvature denotes the average of the two principal curvatures at a vertex (red dot), each of which are measured as the inverse of the corresponding radius of curvature, i.e., R_1 and R_2. Image adapted from (Ronan et al., 2011).

1.4.1. Interpreting cortical MRI metrics

Cortical thickness has often been related to the number of neurons within radial cortical columns and radial neuronal migration, and is influenced by dendritic arborization, synaptic pruning, and myelination (Huttenlocher, 1990; T. Jeon et al., 2015; Rakic, 1995; Vandekar et al.,

2015). Surface area reflects processes including synaptogenesis and the number of radial columnar units in the cortex (Budday et al., 2015b; Rakic, 1988, 1995, 2009), and is also intrinsically linked to cortical folding (Garcia et al., 2018; Ronan & Fletcher, 2015). Although the biological phenomena underlying folding characteristics of the cortex have been more elusive, local gyrification index has been theorized to estimate folding complexity resulting from differential tangential expansion of cortical layers, which in turn may reflect local patterns in cytoarchitecture (Budday et al., 2015b; Ronan & Fletcher, 2015; Ronan et al., 2013). Finally, the specific biological interpretation of mean cortical curvature remains relatively underexplored, but studies of brain microstructure have highlighted a reliable relationship between this measure and white matter integrity (Deppe et al., 2014; King et al., 2016). The above metrics are not independent, but can contribute complementary information to a neurostructural signature of symptoms. For example, since local gyrification index and mean curvature are both measures related to cortical folding, they likely share a dependency on forces of folding hypothesized to arise from axonal fibres and neuronal dispersion at the biomechanical level (Im et al., 2008; Kroenke & Bayly, 2018; Llinares-Benadero & Borrell, 2019; Nie et al., 2012), and on the spatial patterning of neurogenesis at the cellular level (Borrell, 2018; Llinares-Benadero & Borrell, 2019). However, these two metrics offer distinct resolutions of insights into the local surface topology. Whereas local gyrification index has a more direct association with surface area and measures the complexity of surface convolution on the centimeter scale (Schaer et al., 2008; Toro et al., 2008), mean curvature is a mathematically well-defined measure that quantifies the sharpness and concavity or convexity of the folding of a surface, thus providing sensitivity to millimeter-scale changes in gyral and sulcal shape (Pienaar et al., 2008; Ronan et al., 2011).

We note here that another MRI-based metric which has been extensively studied in healthy and psychosis populations is gray matter volume (Fusar-Poli et al., 2011; Fusar-Poli, Radua, et al., 2012; Nenadic, Dietzek, et al., 2015; Witthaus et al., 2009), which can be estimated through various combined analyses of cortical thickness and surface area variation (Winkler et al., 2018). However, given evidence that cortical thickness and surface area have distinct cellular and genetic substrates (Chenn & Walsh, 2002; Panizzon et al., 2009; Winkler et al., 2010) as well as dissociable developmental trajectories (Raznahan et al., 2011; Wierenga et al., 2014), considering these two metrics separately may help parse differential psychopathological contributions of their

underlying processes (Rimol et al., 2012). The current manuscript thus evaluates cortical thickness and surface area as individual variables.

1.4.2. Cortical MRI metrics in normative development

Consistent with the notion that different macrostructural cortical features reflect different underlying biological processes, different metrics are also associated with divergent spatiotemporal patterns of maturation. Globally, cortical thickness peaks in early childhood and then undergoes a protracted decline throughout late childhood and adolescence (Amlien et al., 2016; Lyall et al., 2015; Raznahan et al., 2011; Wierenga et al., 2014). By contrast, surface area begins to increase rapidly as early as the third trimester of pregnancy, and pronounced expansion continues after birth until late childhood (Clouchoux et al., 2012; Raznahan et al., 2011; Wierenga et al., 2014). For both cortical thickness and surface area, transmodal association areas of the brain display more sustained refinement throughout later developmental epochs compared to earlier-maturing primary and unimodal cortical areas (Sydnor et al., 2021). By comparison, cortical gyrification is established primarily in utero, occurring from the late second trimester to about 2 years of age, by which point folding has largely attained an adult-like morphology (Budday et al., 2014, 2015b; G. Li et al., 2014). Folding complexity may continue to increase subtly throughout childhood and early adolescence (Budday et al., 2015a; Remer et al., 2017) and potentially undergoes modest decline starting in late adolescence (D. Klein et al., 2014; Raznahan et al., 2011), but is generally thought to be relatively stable during postnatal development compared to metrics such as cortical thickness, particularly in sensory regions of the cortex (Damme et al., 2019; Hill, Dierker, et al., 2010; Hill, Inder, et al., 2010; Mutlu et al., 2013). Therefore, in the context of investigating neural markers of vulnerability to psychosis, incorporating metrics such as local gyrification index and mean curvature may provide unique insights into the contribution of pathological early development that compliment structural metrics more sensitive to aberrant neuromaturational processes during adolescence (e.g., cortical thickness).

1.5. Cortical morphometric features in the PS and early psychosis

Compared to studies on psychotic disorder or clinical high-risk patients, neuroimaging investigations of the PS are still in their infancy. Nonetheless, select existing MRI studies have found diverse cortical structural abnormalities in individuals with PS symptoms, which importantly appear to mirror abnormalities in patient cohorts. Such studies have predominantly

evaluated changes in gray matter volume and have reported both distributed reductions and increases in regional volume associated with PS symptoms, which commonly converge on prefrontal cortical regions, the precuneus and lateral posterior parietal cortex, and the temporal lobe (Drakesmith et al., 2016; Jacobson et al., 2010; Karcher, Paul, et al., 2022; Meller et al., 2020; Nenadic, Lorenz, et al., 2015; Roalf et al., 2017; Satterthwaite et al., 2016; Schoorl et al., 2021). More recently, studies examining cortical thickness have indicated an association between psychotic-like experiences and reduced cortical thickness, including in frontal and paracentral regions, the inferior parietal lobule, the insula, and temporal regions (Karcher, Paul, et al., 2022; van Lutterveld et al., 2014; Vargas & Mittal, 2022), although increased cortical thickness has also been observed in the medial orbitofrontal/ventromedial prefrontal cortex (Kirschner et al., 2021). van Lutterveld et al. additionally found that adults with non-clinical auditory visual hallucinations demonstrated a similar, but milder pattern of cortical thinning compared to psychotic disorder patients (van Lutterveld et al., 2014), providing support for a continuum of neural risk for psychosis within which PS may represent an intermediate phenotype. In youth, PS symptoms have further been associated with reduced surface area in prefrontal, primary sensorimotor, and cingulate cortical regions (Jalbrzikowski et al., 2019; Vargas & Mittal, 2022).

While measures of cortical folding remain under-studied in subclinical subjects, recent work has linked lower local gyrification index in the midcingulate cortex and superior parietal lobule (Hua et al., 2021) as well as in vertex clusters in the middle frontal, occipital, and temporal gyri (Fonville et al., 2019) to positive psychotic-like experiences. Notably, these circumscribed reductions overlap spatially with patterns of gyrification abnormalities observed in individuals at clinical and familial high risk for psychosis (Damme et al., 2019; I. Park et al., 2021; Sasabayashi et al., 2017). This further suggests possible continuity in neural vulnerability to psychosis that may manifest through changes in multiple cortical macrostructural features. To our knowledge, the metric of cortical mean curvature has only been examined in PS individuals in one study to date, in which positive psychotic-like experiences were associated with greater mean curvature within a left precuneus cluster (Evermann et al., 2020). Nonetheless, findings of both mean curvature increases (Damme et al., 2019; Jessen et al., 2019; Schultz et al., 2010) and decreases (Damme et al., 2019; Liu et al., 2020) across multiple lobes in clinical high-risk or first-episode psychosis patients relative to healthy controls underscore its potential as an imaging marker of early pathophysiology. Furthermore, Damme et al. showed that local gyrification index and mean

curvature demonstrate distinct aberrations in clinical high-risk youth, corroborating the idea that considering both metrics offers a more comprehensive view of altered properties of cortical folding (Damme et al., 2019).

While the relationship of age with morphometric alterations in the PS remains poorly understood, select studies along with evidence from high-risk cohorts have highlighted the existence of abnormal trajectories of cortical metrics predating psychotic illness onset. For example, greater cortical thinning with age has been observed in both clinical and familial high-risk youth compared to healthy controls (Cannon et al., 2015; Sugranyes et al., 2021), while less age-related reduction in surface area has been found in familial high-risk youth (Sugranyes et al., 2021). Taking this a step further, a prior study revealed that the developmental course of cortical thickness among schizotypal youth is linked to scores on different symptom-like dimensions (Derome et al., 2020). Meanwhile, local gyrification index has been recently shown to undergo greater age-related decline in frontal and temporal areas in schizotypal individuals compared to controls (Pham et al., 2021). These findings offer evidence that aberrant cortical morphometry in the PS may be part of atypical patterns of neuromaturation, and that considering the effect of age can yield more nuanced insights into brain-behaviour relationships in the PS.

1.5.1. Limitations of existing PS neuroimaging research

Existing PS neuroimaging efforts have several limitations which may have contributed, in part, to the heterogeneity in neuroanatomical findings. Pronounced among these is the reliance on univariate statistical methods that treat the cortex as a collection of independent regions or vertices. In these methods, a single feature is modelled separately at individual locations across the cortex, which are typically defined by an *a priori* anatomical parcellation or, more commonly, at the level of single cortical vertices in "mass univariate" analyses. This approach has drawbacks for both statistical and biological interpretations. First, the potentially large number of statistical tests performed requires stringent corrections for multiple comparisons, which in turn lowers power to detect more subtle effects that may be characteristic of emerging psychopathology (Genon et al., 2022; Marek et al., 2022; McIntosh & Mišić, 2013). Second, univariate analyses fail to consider the highly networked nature of the brain, in which the morphological properties of different regions are interdependent and covary with each other (Alexander-Bloch et al., 2013). As a result, prior PS studies employing such analyses have lacked sensitivity to detect shared patterns of

abnormalities across vertices that may be eclipsing pronounced effects at any single location in the brain.

Previous attempts to characterize PS neuroanatomy have been further limited by a focus on adult samples (e.g., (Drakesmith et al., 2016; Evermann et al., 2020; Fonville et al., 2019; Kirschner et al., 2021; Meller et al., 2020; Nenadic, Lorenz, et al., 2015; Schoorl et al., 2021; van Lutterveld et al., 2014)) rather than on age ranges when PS symptoms first emerge, as well as by examining individual MRI-derived cortical metrics in isolation from one another. The historical lack of large, comprehensive symptom and imaging datasets of PS youth has further contributed to this issue. While some recent PS studies have applied univariate linear regression to query multiple structural metrics at each cortical vertex or region of interest (Fonville et al., 2019; Hua et al., 2021; Jalbrzikowski et al., 2019), such designs still model each metric separately and thus undermine the complementary biological information carried by different morphometric indices. As a result, univariate approaches to neuroanatomy may have precluded the discovery of more complex patterns of covariance that could reconcile heterogeneous changes across different cortical features. How different morphometric abnormalities currently associated with PS symptoms might relate to one another therefore remains an open question.

1.6. Covariance-based methods for deriving imaging signatures of abnormal cortical morphology

Converging evidence suggests that modelling the coordinated variation of multiple morphometric features enables more nuanced estimation of cortical organization (Glasser et al., 2016; R. Patel et al., 2020; Seidlitz et al., 2018; Vandekar et al., 2016). For example, Seidlitz et al. showed that morphometric similarity mapping, which quantifies interregional similarity based on the correlation of multiple MRI-based structural metrics (i.e., "morphometric similarity"), generates individualized networks of cortical regions that have greater cytoarchitectonic similarity than in single metric covariance networks, in addition to having high transcriptional similarity (Seidlitz et al., 2018). This approach has uncovered morphometric similarity differences between psychotic disorder patients and healthy controls that also align with spatial patterning of transcriptional vulnerability to schizophrenia (S. E. Morgan et al., 2019), exemplifying the clinical utility of considering covariation of multiple features. However, a key limitation of morphometric similarity mapping is that it cannot parse the influences of individual features on interregional

morphometric similarity, thereby restricting insights into putative neurobiological substrates of abnormal cortical macrostructural patterning.

More classical multivariate analysis techniques, which assess relationships between multiple input variables simultaneously, can also be used to integrate information from multiple morphometric features in a single statistical framework (R. Patel et al., 2020; Smith & Nichols, 2018). In a neuroimaging context, these analyses can harness the mutual dependencies between vertices to identify informative patterns, termed components, within brain data. In particular, recent work has highlighted non-negative matrix factorization (NMF) as a promising alternative for investigating neurobiologically meaningful covariance structure of multiple MRI-derived metrics (R. Patel et al., 2020; Robert et al., 2021). Conceptually similar to popular multivariate methods such as principal component analysis (PCA) and independent component analysis (ICA), NMF is an unsupervised technique that decomposes a dataset into its dominant patterns of covariance, thus providing a data-driven way to significantly reduce the dimensionality of typically vertex-wise subject brain data. In addition to bolstering interpretation beyond segregated local cortical properties, this dimensionality reduction helps to guard against concerns regarding the low stability of downstream multivariate brain-behaviour associations where the number of features vastly outnumbers the number of observations (Helmer et al., 2020).

1.6.1. Non-negative matrix factorization: advantages and applications

NMF offers several interpretational advantages over the more commonly applied PCA and ICA. First, NMF uniquely enforces a non-negativity constraint on its outputs (Sotiras et al., 2015). Covariance components extracted using this method are associated with purely positive weights of input features and loadings of individual observations (i.e., subjects), enabling more straightforward interpretation of neuroanatomical variation than when effects of opposing direction are present.

Furthermore, the orthonormal projective variant of NMF (OPNMF) has the ability to aggregate variance in imaging data in a parcellation-like fashion, contrasting with challenges of PCA and ICA in defining clear boundaries between variance components (Sotiras et al., 2015). This property of OPNMF leads to parsimonious representations of coordinated cortical structural variation that serve as alternatives to *a priori* defined anatomical atlases. For example, applications of OPNMF to single-metric cortical data have delineated reproducible and biologically plausible whole-brain covariance ‘networks’ of gray matter volume (Shan et al., 2022; Sotiras et al., 2015;

Varikuti et al., 2018; Wen et al., 2022), cortical thickness (Kaczkurkin et al., 2019; Neufeld et al., 2020; Sotiras et al., 2017), and local gyrification (Sanfelici et al., 2021). The resulting networks have in turn demonstrated sensitivity to a range of clinical phenotypes, including capturing psychiatric disorder-related morphometric abnormalities (Neufeld et al., 2020; Sanfelici et al., 2021), revealing neuroanatomically homogeneous subtypes of autism spectrum disorder (Shan et al., 2022), as well as predicting broad dimensions of psychopathology (Kaczkurkin et al., 2019). Notably, Wen et al. found that gray matter volume signatures consistently achieved better patient/control classification across multiple diseases (including schizophrenia) when formed from OPNMF-derived networks as opposed to a conventional brain atlas or voxel-wise maps (Wen et al., 2022). A study by (Neufeld et al., 2020) also observed a specific pattern of hypogyrification in OPNMF-derived gyrification networks that was shared across three different early psychiatric illness groups as well as related to poorer cognition and functioning. These findings illustrate that data-driven covariance patterns identified by NMF can provide novel imaging signatures of neuropathological processes, and may have the potential to capture transdiagnostic effects linked to developmental vulnerability.

In recent years, our group has adapted NMF to investigate shared patterns of covariance across multiple MRI-based metrics simultaneously, thus harnessing their complementary information (R. Patel et al., 2020). This work demonstrated the greater stability of spatial components derived using multiple metrics compared to single-metric NMF decompositions, corroborating conclusions from morphometric similarity network studies. In healthy individuals, this novel 'multi-metric' analysis has revealed multimodal microstructural components of the human hippocampus (R. Patel et al., 2020) and striatum (Robert et al., 2021) subcortically, as well as whole-brain components of covariance across several vertex-wise measures of both cortical macrostructure and microstructure (R. Patel et al., 2022). Importantly, these studies showcased the ability of NMF to recover subject 'loadings' onto covariance components that are metric-specific, such that downstream brain-cognition associations identified using these components could still be resolved at the level of the contributing structural features (R. Patel et al., 2022, 2020). This approach has recently also been shown to be sensitive in a psychosis context: using covariance components derived from anterior cingulate cortex structural indices in schizophrenia patients, Ochi et al. discovered component-level patterns of abnormality in specific metrics that were differentially related to antipsychotic treatment response or resistance (Ochi et al., 2022). Thus,

the multi-metric implementation of NMF holds promise for establishing more refined profiles of neurostructural vulnerability while circumventing limitations of morphometric similarity approaches.

1.7. A dimensional approach to symptom heterogeneity within the PS

Progress towards precise neuroanatomical mappings of PS symptoms has likely been limited by overly simplistic behavioural perspectives. PS neuroimaging studies have often sought brain morphometric correlates of an aggregate score of symptoms based on *a priori* clinical scales, with a majority considering only the positive subclinical symptom domain or subtypes (e.g., auditory verbal hallucinations) (Fonville et al., 2019; Kirschner et al., 2021; van Lutterveld et al., 2014; Vargas & Mittal, 2022). Another common strategy has been to investigate group-average differences in cortical features between individuals with and without PS symptoms (Drakesmith et al., 2016; Jacobson et al., 2010; van Lutterveld et al., 2014). However, *a priori* composite symptom scores may not optimally capture neural variation due to eschewing the possibility that neural alterations reflect a more complex weighted combination of symptoms. Similarly, single-domain and case-control approaches assume a monolith of PS expression and do not account for the heterogeneity in symptom presentation and neural alterations observed before the onset of frank illness (Kaczkurkin et al., 2020; Unterrassner, 2018; Voineskos et al., 2020; Yung et al., 2009). For example, population-based studies have indicated that subclinical negative symptoms can be as prevalent as subclinical positive symptoms in adolescents and young adults, and that the co-occurrence of these experiences amplifies the risk of poor functioning, help-seeking behaviour, and later onset of clinical psychosis (Calkins et al., 2017; Dominguez et al., 2010; Werbeloff et al., 2015).

In line with these findings, accumulating evidence suggests that PS phenotypes may be better understood in terms of the simultaneous variation of multiple salient symptom *dimensions* gleaned through data-driven modelling (Armando et al., 2010; Calkins et al., 2015; Fonseca-Pedrero et al., 2018; Shevlin et al., 2017; Stefanis et al., 2002; Wigman et al., 2011; Yung et al., 2006). In such a model, each dimension describes a phenotypic axis underlying a weighted combination of measurable symptoms that co-occur, along which individuals can vary continuously (Kaczkurkin et al., 2020). These dimensional models are thus compatible with the view of PS features as lying on a continuum from possibly benign to maladaptive processes, while

also enabling insights into the potentially varied clinical significance of dissociable groupings of behavioural phenomena. This approach is aligned with two increasingly pursued, large-scale frameworks for a dimensional re-envisioning of psychopathology more broadly: the Research Domain Criteria, which seeks to characterize psychopathology dimensions using multiple biobehavioural levels or "units" of analysis (Cuthbert & Insel, 2013; Insel et al., 2010); and the Hierarchical Taxonomy Of Psychopathology, which seeks to organize diverse psychopathological phenomena according to their shared and unique covariance to yield more informative research targets (Kotov et al., 2018, 2017).

Factor analytic approaches have long been applied to investigate the latent dimensional structure of clinical psychotic symptoms (Potuzak et al., 2012), and can derive interpretable dimensions with improved robustness and prognostic value over categorical classifications of illness (data-driven or diagnostic) (Martin et al., 2021; Ravichandran et al., 2021). However, there has been a paucity of factor analytic studies of symptoms in non-help-seeking individuals (i.e., PS), especially youth, and existing investigations have found inconsistent factors due to generally limited types of items being included in analyses. Select population-based studies of a broader range of PS symptoms have suggested the existence of three symptom dimensions, including 'unusual thoughts/perceptions', 'ideas about special abilities/persecution', and 'negative/disorganized symptoms' (Calkins et al., 2015); or, alternatively, 'cognitive-perceptual', 'interpersonal/negative', and 'disorganized' features (Fonseca-Pedrero et al., 2018). Critically, these dimensions show overlap with the dimensional structure seen in clinical psychosis (Kotov et al., 2016; Liddle, 1987; Maj et al., 2021; Potuzak et al., 2012), and may be differentially related to functional and health outcomes (Martin et al., 2021; Reininghaus et al., 2013).

As data-driven symptom dimensions are likely to have more coherent etiology than measures of total symptom burden or than is captured by a general PS group, a dimensional characterization of PS features may also provide improved linkage with neurobiology. Limited but promising findings in this direction have indicated that certain dimensional PS factors in youth, namely ideas about special abilities/persecution and negative/disorganized symptoms, are related to volume reductions of distinct regions in the medial temporal lobe (Roalf et al., 2017). However, contrary to the one-to-one relationships targeted by existing brain-behaviour studies of the PS, it is conceivable that broad dimensions of PS symptoms are multi-determined with regards to brain circuits as opposed to mapping to isolated regions. Multivariate analytical approaches which can

resolve complex associations between symptom and neurobiological domains thus could offer unprecedented insight into the biobehavioural underpinnings of the PS.

1.8. Multivariate brain-behaviour associations

To achieve refined mappings between dimensional PS symptoms and neurobiological variation, it is necessary to consider the mutual dependencies existing not only between brain variables as previously discussed, but also among different clinical-behavioural measurements (Voineskos et al., 2020). For example, PS symptom domains often co-occur and are highly correlated (Dominguez et al., 2010; Stefanis et al., 2002), and their expression is also linked to sociodemographic characteristics (Dominguez et al., 2010; Werbeloff et al., 2015). Rather than individual clinical features mapping to cortical alterations, then, it is conceivable that their shared variation within a complex behavioural profile of risk may have a neuroanatomical signature in distributed or overlapping brain circuits, as has been observed for clinical psychosis samples (Kirschner, Shafiei, Markello, Makowski, et al., 2020).

"Doubly multivariate" analyses refer to approaches that can leverage this multiplicity to map a set of behavioural variables jointly to patterns among a set of brain structural variables (Genon et al., 2022). These analyses thus avoid *a priori* assumptions regarding one-on-one symptom-neuroanatomy relationships as well as the limited view gained by focusing on only a single behavioural aspect (Genon et al., 2022; C. Song et al., 2022). More broadly, these approaches can summarize a complex constellation of associations among two sets of variables by a smaller number of parsimonious latent patterns or "variables." When the two datasets correspond to clinical and brain structural data, the latent variables define dissociable aspects of brain-behaviour covariance or correlation, and importantly, capture inter-individual differences via subject-specific scores which quantify expression of the identified patterns (McIntosh & Mišić, 2013). Doubly multivariate approaches may offer a means of parsing heterogeneous biobehavioural mechanisms of the PS in line with a dimensional understanding of psychopathology (Cuthbert & Morris, 2021; Xia et al., 2018).

One popular data-driven doubly multivariate approach, which is also the most relevant to the current work, is partial least squares correlation (PLS). Compared to its sister techniques including canonical correlation analysis (CCA) (Wang et al., 2020), PLS has commonly-used reliability or bootstrapping assessments that provide insight into the stability of the derived brain-

behaviour relationships (McIntosh & Lobaugh, 2004). Both PLS and CCA have demonstrated utility for uncovering multimodal phenotypic axes of psychotic disorders, including a clinical-anatomical pattern linking cognitive impairments and negative symptom factors to distributed gray matter volume loss in schizophrenia (Kirschner, Shafiei, Markello, Makowski, et al., 2020); as well as cognitive-anatomical patterns (Jessen et al., 2019; Rodrigue et al., 2018) that show promise for differentiating patients of different psychotic diagnoses along an affective-nonaffective psychosis dimension (Rodrigue et al., 2018). Together, these studies illustrate that relating low-dimensional symptom axes to whole-brain neural alterations can uncover novel pleiotropic-like links between brain and behaviour that nonetheless remain highly interpretable.

1.9. Morphometric abnormalities in the context of a macroscale functional hierarchy

Contextualizing patterns of anatomical abnormalities in terms of the functional specialization of the cortex offers a bridge between brain structure, function, and symptomatology. There has been extensive evidence for a macroscale hierarchy of cortical organization that can be quantified as a "gradient" extending from primary sensory and motor (i.e., unimodal) areas to distributed association (i.e., transmodal) areas (Huntenburg et al., 2018; Margulies et al., 2016; Sydnor et al., 2021). This gradient corresponds to the primary axis of variation in a low-dimensional representation of cortical vertices' similarity in functional connectivity patterns, and is thus known as the principal functional gradient in the context of functional MRI data (Margulies et al., 2016). Notably, this gradient captures the spatial ordering of and gradual transitions between cortical resting-state functional networks (Yeo et al., 2011), but how large-scale patterns in morphological features might map to this functional gradient is less well known.

Across structural neuroimaging studies of psychotic disorder and clinical high-risk patients, the topography of morphological disturbances has consistently converged on the extreme ends of the unimodal-to-transmodal functional gradient. In particular, changes in individual cortical morphometric features have frequently been localized to association regions anchoring the transmodal end of this hierarchy, such as regions involved in the frontoparietal or default mode resting-state networks (Andreou & Borgwardt, 2020; Fusar-Poli et al., 2011; Fusar-Poli, Radua, et al., 2012; Matsuda & Ohi, 2018; Palaniyappan et al., 2011; van Erp et al., 2018). The same networks have also demonstrated significantly reduced morphometric similarity, as assessed by morphometric similarity networks, in psychosis patients relative to healthy controls (S. E. Morgan

et al., 2019). These results are consistent with transmodal cortical areas showing increased and protracted vulnerability of structural properties to the aberrant neurodevelopment that may underlie variation related to the PS (Mueller et al., 2013; Reardon et al., 2018). Further still, these regions also support higher-order psychological functions commonly affected in psychopathology (Sydnor et al., 2021), such as the belief evaluation and reality monitoring processes typically impaired in psychosis (Corlett et al., 2010; Lee et al., 2015). Therefore, the unimodal-transmodal hierarchy naturally offers a potential organizing principle for morphometric abnormalities linked to PS symptoms. Importantly, it was also recently shown that the organization of macroscale functional gradients reconfigures during development, such that a unimodal-transmodal structure takes a backseat to a somatomotor- and visual-anchored gradient in childhood, but is gradually converged upon as sensorimotor and association areas are increasingly differentiated in adolescence, reaching a mature cortical architecture (H.-M. Dong et al., 2021). Situating patterns of morphology within maturational functional gradients thus could in turn situate PS symptom-brain structure relationships within the context of dynamic functional neurodevelopment.

1.10. Meta-analytic functional contextualization of morphometric abnormalities

Beyond large-scale cortical gradients, the availability of comprehensive meta-analytical databases derived from functional neuroimaging also offers a window into structure-function coupling in the PS. One such resource that has attained widespread use is Neurosynth, a framework for the automated generation of meta-analytical brain activation maps related to common psychological terms in functional MRI studies (Yarkoni et al., 2011). The Neurosynth database can be used to query direct spatial correspondences between psychological function-based brain patterns and novel brain maps derived from structural MRI features, a process known as functional "decoding" (L. J. Chang et al., 2013). Notably, this technique has recently been leveraged to explore the potential functional relevance of components of structural covariance defined using NMF (Robert et al., 2021; Shan et al., 2022). These studies illustrated the capacity of NMF-derived neuroanatomical patterns to capture distinct yet coherent cognitive functional profiles within the context of both healthy (Robert et al., 2021) and psychopathological brain structural landscapes (Shan et al., 2022). Since past analyses of this nature have focused on subcortical data or a single cortical metric, meta-analytic functional associations of more complex cortical covariance patterns remain to be elaborated. In particular, decoding functions of patterns that integrate multiple cortical

structural features may offer new perspectives into how brain structure and function interact to shape symptom expression.

1.11. Transcriptomic fingerprints of brain structural vulnerability to psychosis

The MRI-derived phenotypes discussed thus far allow for incisive dimensional characterization of neuroanatomical variations underlying PS symptoms, but can only provide indirect measures of putative pathophysiological mechanisms. Meanwhile, recent advancements in imaging transcriptomics, particularly the development of brain-wide gene expression atlases, have opened new opportunities to investigate the molecular basis of macroscopic changes related to psychopathology (Arnatkeviciute et al., 2021). The Allen Human Brain Atlas (AHBA), which was constructed via microarray profiling of post-mortem brain tissue, represents the most neuroanatomically comprehensive transcriptomic atlas to date (Hawrylycz et al., 2012). Significantly, this resource has enabled unparalleled inference regarding transcriptional enrichment of molecular and biological functions that is consistent with the patterning of neuroimaging markers (Arnatkeviciute et al., 2021; Martins et al., 2021).

Neuroimaging studies incorporating the AHBA have increasingly highlighted how macrostructural alterations can provide a mechanistic link between variation in gene expression and psychotic experience. Using multivariate analysis, a prior study co-located psychosis case-control differences in morphometric similarity with expression of genes found to be dysregulated in post-mortem studies of schizophrenia, as well as genes involved in neurotransmission-related processes (S. E. Morgan et al., 2019). Specific gene expression patterns have further been linked directly to individual imaging-based cortical morphometric indices, in the context of both mental health and illness. For example, normative spatiotemporal variation in cortical thickness, including during adolescence, has been correlated with expression of transcriptional markers of astrocytes, microglia, and excitatory neurons (Ball et al., 2020; Y. Patel et al., 2020; Shin et al., 2018; Vidal-Pineiro et al., 2020). Interestingly, regional deviations from normative thickness in schizophrenia patients were found to demonstrate alignment with markers of overlapping cell types, including astrocytes, endothelial cells, oligodendrocyte precursors, and neurons (Di Biase et al., 2022). This link has also been extended to nonclinical psychosis populations: schizotypy-related variations in magnetization transfer, an index of intracortical myelin content, was related through multivariate analysis to genes with neuronal, astrocyte, and microglial affiliations, and which are dysregulated

in schizophrenia (Romero-Garcia et al., 2020). These findings suggest a reasonably tight coupling between changes in brain macrostructure and expression levels of both specific cell types and relevant disorder-related genes.

Strikingly, in recent work which integrated NMF on brain volumetric data with a genome-wide association study, associations were found between the resulting whole-brain patterns of structural covariance and sets of genes enriched in both common and dissociable biological pathways (Wen et al., 2022). The NMF-derived covariance patterns were also correlated with a number of novel genomic loci, implying that this data-driven representation of neuroanatomical data may be able to capture more subtle molecular organization than other T1w MRI-based phenotypes (Wen et al., 2022). The above findings suggest that in the context of the PS, establishing transcriptomic signatures of symptom-related morphometric covariance patterns may clarify critical feature- or pathway-specific molecular mechanisms driving the observed neurostructural vulnerability.

2. Rationale

Despite significant conceptual and empirical progress, an integrated understanding of neuroanatomical signatures of dimensional PS symptoms and their potential biological underpinnings is lacking. Attempts thus far to characterize cortical abnormalities in the PS have been hampered by a focus on adult age ranges, examining individual morphometric features in isolation using univariate analyses, and case-control comparisons or one-dimensional measures of symptoms. By contrast, growing research supports data-driven multivariate analyses as a means of resolving more nuanced patterns of cortical morphometric variation expressed during critical maturational epochs, which may in turn better capture dimensional symptom variation as well as multimodal cortical properties.

Building on these perspectives, the current study leveraged an analytic framework linking morphometric, behavioural, functional, and transcriptomic information to characterize neural PS phenotypes in the context of neurodevelopment. Using a community-based sample of PS youth, we derived multivariate mappings between symptom dimensions and morphometric covariance patterns integrating multiple cortical features, and then contextualized these relationships by drawing on insights from functional (Neurosynth, functional connectivity gradients) and molecular (AHBA gene expression) architectures of the brain.

3. Objectives

The objectives of this work were threefold. **(1)** We aimed to use NMF to identify covariance patterns among interrelated cortical morphometric features in PS youth, and to investigate how they mapped to latent factors of PS symptoms. **(2)** We aimed to contextualize PS-related morphometric covariance patterns functionally by evaluating their spatial similarity to meta-analytical activation patterns of psychological processes, and their spatial organization with respect to the unimodal-to-transmodal cortical functional hierarchy. **(3)** We aimed to explore molecular underpinnings of PS vulnerability in morphometric covariance patterns by aligning them with spatial expression of specific biological functions, canonical brain cell types, and genes associated with psychiatric disorders.

4. Methods

An overview of the analytic workflow can be found in Figure 2. Briefly, morphometric covariance patterns (MCPs) based derived from four structural metrics across the cortex were used to derive a multivariate representation of cortical morphology (cortical thickness, surface area, mean curvature, local gyrification index) from 266 youth who met psychosis spectrum (PS) criteria. We mapped PS-related MCPs to known large-scale cognitive and cortical functional architectures via functional MRI results, as well as to cortical gene expression patterns to better understand their putative functional and neurobiological relevance.

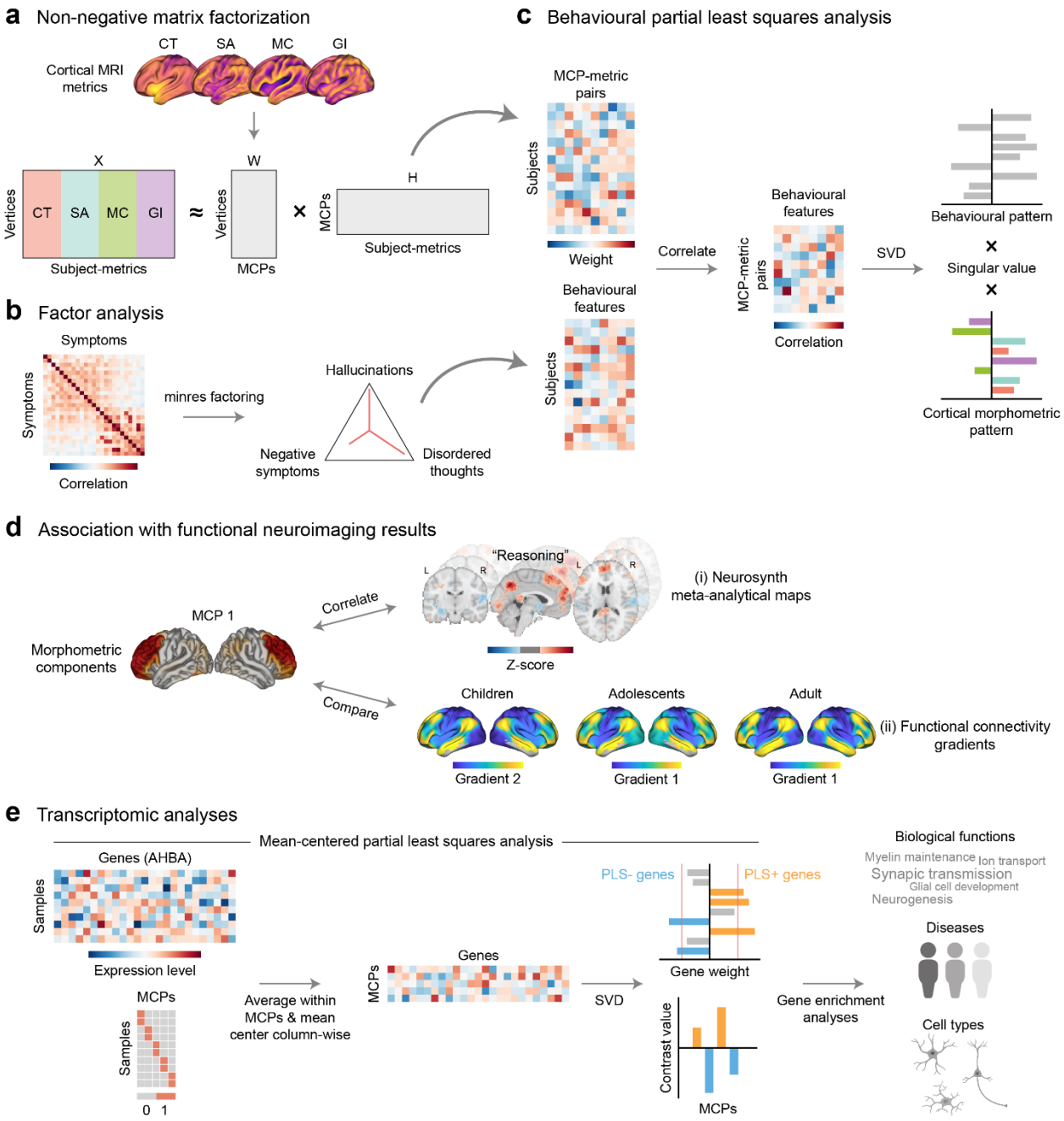

Figure 2. Workflow. *(Continued on next page)* **(a)** Four cortical metrics derived from T1-weighted MRI data of 266 psychosis spectrum youth were subjected to orthonormal projective non-negative matrix factorization (OPNMF) to identify components representing morphometric covariance patterns (MCPs). OPNMF decomposed the matrix of concatenated subject metrics into a component matrix (W), describing spatial properties of MCPs in the data, and a loading matrix (H), describing subject-specific loadings of metrics for each MCP. **(b)** Minimum residual factor analysis was applied on the correlation matrix of PS symptom measures to identify major latent symptom dimensions. **(c)** Behavioural PLS analysis was used to relate subject-specific MCP-metric loadings to scores on each symptom dimension as well as sociodemographic features. This resulted in latent variables representing maximally covarying patterns of the brain and behavioural

data. **(d)** Two methods were used to contextualize MCPs functionally. Each MCP was correlated with (i) meta-analytic activation maps of psychological functions (Neurosynth), as well as aligned with (ii) previously reported functional gradients across maturation, to compare within-MCP gradient value distributions. **(e)** Using the Allen Human Brain Atlas (AHBA), we obtained tissue sample-level gene expression data corresponding spatially to each MCP. Mean-centered PLS analysis was used to extract patterns of gene expression that maximally differentiated the MCPs. The resulting latent variables comprised a weighted combination of genes, describing an expression profile, and a set of contrast values describing the MCPs covarying with the expression profile in a separable way. The strongest weighted genes, segregated by sign, provided gene sets characterizing specific MCPs and were further analyzed for enrichment for certain biological functions, disease-related genes, and cell types. SVD = singular value decomposition; PLS = partial least squares

4.1. Data

4.1.1. Overview of PNC dataset

We used cross-sectional T1w structural MRI and psychiatric data from the publicly available PNC (study version 3) (Satterthwaite et al., 2014). The PNC is a large, racially and socioeconomically diverse community-based sample of youth reflecting the demographics of the greater Philadelphia area (Calkins et al., 2015; Moore et al., 2016). Importantly, PNC subjects were not recruited from psychiatric services (i.e., not seeking help for psychiatric symptoms), but screened into specific psychiatric diagnoses at rates aligning with epidemiologically ascertained samples (Calkins et al., 2015). Thus, this sample offers a glimpse into the continuum of 'normal' to 'abnormal' mental health in the developing population, as championed by recent symptom dimension mapping doctrines such as the Research Domain Criteria (Cuthbert & Insel, 2013; Insel et al., 2010), and brain abnormalities associated with subthreshold psychosis symptoms at a young age.

4.1.2. MRI acquisition and psychiatric assessment

Within the PNC, T1w images were collected for a subsample of 1598 physically healthy participants (8-23 years old) on a single 3T Siemens TIM Trio scanner (Satterthwaite et al., 2014). A magnetization-prepared rapid acquisition gradient echo (MPRAGE) sequence was used with the following imaging parameters: repetition time, 1810 ms; echo time, 3.5 ms; inversion time, 1000 ms; flip angle, 9°; voxel size, 0.9375 mm×0.9375 mm×1.0 mm; and right-to-left/anterior-to-posterior field of view, 180/240. All participants additionally underwent psychopathology assessment with the GOASSESS interview, the purpose of which was to capture subject

experiences of symptoms across multiple disorder domains including mood, anxiety, behavioural, eating, and psychosis spectrum disorders (Calkins et al., 2015). Specifically, GOASSESS comprises a mixture of dichotomous (yes/no) and Likert scale (e.g., 0–"Definitely disagree" to 6–"Definitely agree") questions that are adapted from three widely-used diagnostic instruments: the Kiddie Schedule for Affective Disorders and Schizophrenia (K-SADS) (Kaufman et al., 1997); the Prevention through Risk Identification, Management, and Education (PRIME) Screen-Revised (PS-R) (Kobayashi et al., 2008); and the Structured Interview for Psychosis-risk Syndromes (SIPS) (Miller et al., 2003). All study procedures were approved by the institutional review boards of the University of Pennsylvania and The Children's Hospital of Philadelphia. Informed written consent was obtained from participants over 18 and parents/guardians of participating children, and informed written assent was obtained from children.

4.1.3. Definition of psychosis spectrum (PS) sample

We identified PNC youth as PS if they met any of the following criteria: (1) endorsed any hallucination or delusion on the K-SADS with a duration of at least one day, outside the context of substance use or physical illness, and accompanied by significant impairment or distress; (2) had a total PS-R score at least two standard deviations (SDs) higher than age-matched peers, at least 1 PS-R item rated 6 ("Definitely agree"), or at least 3 PS-R items rated 5 ("Somewhat agree"); (3) scored a total of at least 2 SDs above age-matched peers on SIPS negative and disorganized symptom items (Calkins et al., 2015, 2014). Excluding individuals with significant non-psychiatric medical conditions that could affect central nervous system function (determined by an impact severity rating of 3 ["Significant"] or higher), PS symptoms were identified in 427 participants. After additional exclusion of participants whose MRI scans did not pass rigorous quality assurance procedures (see Section 4.2.1 for details), we arrived at a final study sample of 266 youth with PS features (Table 1).

Table 1. Sociodemographic characteristics of physically healthy psychosis spectrum youth from the PNC.

Variable	Psychosis spectrum (n = 266)
Age in years, mean ± SD (range)	15.8 ± 3.1 (8.8–23.2)
Sex, n (%)	
Female	149 (56.0)
Male	117 (44.0)
Race, n (%)	
African American or Black	154 (57.9)
European American	78 (29.3)
Mixed[a] or other race	34 (12.8)
WRAT-4 Reading standard score, mean ± SD	98.5 ± 16.7
Parent education in years, mean ± SD	13.5 ± 2.0

[a] Includes combinations of African American or Black, European American, Hispanic/Latino, and other race, as well as unknown race

SD = standard deviation; WRAT-4 = Wide Range Achievement Test, version 4

4.2. Data processing

4.2.1. MRI processing and quality control

A summary flowchart of PS subject exclusion due to the below MRI quality control steps can be found in Appendix Figure 1. All raw T1w scans were previously inspected for motion and scan quality by two independent raters, following our laboratory's quality control protocol (Bedford et al., 2020) (https://github.com/CoBrALab/documentation/wiki/Motion-Quality-Control-(QC)-Manual). Consensus of these quality ratings was determined for exclusion of scans with movement artefacts, such as image blur or ringing. Since certain neuroimaging pipelines perform better if provided with T1w images with brain masks, we preprocessed scans using the automated iterativeN4_multispectral pipeline (https://github.com/CoBrALab/iterativeN4_multispectral) to obtain brain masks in native space, generated using Brain Extraction based on nonlocal Segmentation Technique (BEaST) (Eskildsen et al., 2012). Outputs were quality controlled for accurate coverage of brain tissue by each subject's derived brain mask.

The raw T1w images and their corresponding brain masks were then submitted to the CIVET processing pipeline (http://www.bic.mni.mcgill.ca/ServicesSoftware/CIVET, version (v)2.1.1) to estimate four gray matter morphometric features: cortical thickness (CT), surface area (SA), mean curvature (MC), and local gyrification index (GI). Briefly, CIVET first performs image

registration to Montreal Neurological Institute (MNI) space using the MNI ICBM152 average (Collins et al., 1994; Fonov et al., 2009), followed by intensity inhomogeneity correction using the N3 algorithm (Sled et al., 1998). Voxels are then classified into white matter, gray matter, and cerebrospinal fluid (Tohka et al., 2004; Zijdenbos et al., 2002), and cortical surfaces (81924 vertices per surface mesh) are extracted using the Constrained Laplacian Anatomic Segmentation using Proximities method (J. S. Kim et al., 2005). We employed the N3 correction in CIVET rather than supplying bias field-corrected images from iterativeN4_multispectral as inputs as we observed that the former approach produced fewer image processing failures for CIVET. All CIVET outputs were quality controlled according to an in-house manual (Bedford et al., 2020) (https://github.com/CoBrALab/documentation/wiki/CIVET-Quality-Control-Guidelines); only scans in which the extracted cortical surfaces generally followed the apparent anatomy were included in our analyses.

4.2.2. Behavioural measures and missing data imputation

In addition to subject responses on the 30 PS-related symptom items from GOASSESS, we included age, sex, and race for analysis to capitalize on the diverse demographic composition of the PNC and of the PS subgroup. As well, following previous studies on the PNC, we estimated full-scale intelligence quotient (IQ) for subjects using their age-adjusted standard scores on the Reading subtest of the Wide Range Achievement Test, version 4 (WRAT-4) (Calkins et al., 2014; Wilkinson & Robertson, 2006). WRAT-4 Reading standard scores range from a minimum score of 55 to a maximum score of 145, with a mean of 100 and a SD of 15. Finally, parent education (mean years of mother and father, unless only one was available) provided a proxy for socioeconomic status (Moore et al., 2016).

Since 28 subjects (11%) had missing values for one or more of the 35 behavioural variables of interest, we performed data imputation using random forests, implemented in R v3.5.1 (package missForest, v1.4) (Stekhoven & Bühlmann, 2012). This algorithm fits a random forest on the observed part of a data matrix to predict the missing observations for a specific variable, and can robustly handle relationships in mixed-type data involving both continuous and categorical variables (Cui & Wang, 2020; Stekhoven & Bühlmann, 2012), such as those present in the PS behavioural dataset. To impute missing values more accurately, we sought to leverage all available observed values of the variables of interest as well as auxiliary information about subjects' comorbid psychopathology. Random forests were trained using behavioural data from all PS youth

regardless of MRI data quality (n = 427), and attributes in the input data matrix included a total of 122 symptom items from GOASSESS covering 16 psychological clinical domains (including PS), in addition to our sociodemographic variables of interest. The number of decision trees per random forest was set to 1000.

4.2.3. Morphometric feature estimation

Vertex-wise CT, SA, and MC values for each subject were estimated automatically as part of the CIVET pipeline, while vertex-wise GI was computed separately from cortical mid-surface reconstructions from CIVET using code adapted from (Toro et al., 2008) (https://github.com/r03ert0/surfaceratio, v5). Specifically, CT at each vertex was estimated as the curved distance along streamlines computed between the white matter surface and the gray matter (pial) surface at that point, following the Laplace method (J. S. Kim et al., 2005). CT was smoothed across the surface using the default 30-mm full-width half-maximum (FWHM) blurring kernel for this measure to diminish the impact of noise (Boucher et al., 2009; Lerch & Evans, 2005); default smoothing kernel sizes were used for the other measures estimated by CIVET as well. SA was estimated as the area of the polygon formed by one-third of the triangles surrounding each vertex on the mid-surface (FWHM = 40 mm) (Lyttelton et al., 2009). MC was calculated as the average of the principal curvatures at each vertex, which were derived from the inverse of the radii of orthogonal osculating circles at each vertex on the mid-surface (FWHM = 30 mm) (Ronan et al., 2011). Thus, larger values of MC indicate 'sharper' curvature. Finally, GI was estimated through the "surface ratio": the ratio between the mid-surface area contained in a small sphere centered at each vertex and the area of a circle of equivalent radius (Toro et al., 2008). We used the recommended sphere radius of 20 mm for surface ratio calculation. Morphometric data of medial wall vertices were excluded in all analyses.

4.3. Multivariate analysis of morphometric covariance: Non-negative matrix factorization

To identify spatial patterns of neuroanatomical covariance, we applied the orthonormal projective extension of non-negative matrix factorization (OPNMF) to our cortical metrics (Figure 2a). OPNMF is an unsupervised multivariate statistical technique that decomposes an input matrix (in our case, cortical morphometric features, $\mathbf{X}_{m\times n}$) into a component matrix ($\mathbf{W}_{m\times k}$) and a loading coefficient matrix ($\mathbf{H}_{k\times n}$) such that the reconstruction error between the original ($\mathbf{X}$) and

reconstructed (**W**×**H**) inputs is minimized (R. Patel et al., 2020; Sotiras et al., 2015; Yang & Oja, 2010). OPNMF thus solves the following minimization problem:

$$\|X - WH\| \text{ subject to } W \geq 0;\ W^T W = I;\ H = W^T X$$

where $\| \|$ represents the squared Frobenius norm and **I** represents the identity matrix (Boutsidis & Gallopoulos, 2008; Yang & Oja, 2010). Importantly, **W** is initialized using non-negative double singular value decomposition, which promotes sparsity of the output component matrix (Boutsidis & Gallopoulos, 2008). The OPNMF decomposition results in k output components (where k is defined *a priori* by the user) each describing an underlying pattern of covariance in the input data (Sotiras et al., 2015). Given that the input in this case comprised multiple morphometric indices, we refer to the resulting components as morphometric covariance patterns (MCPs) in the current manuscript. Specifically, in the OPNMF output, **W** contains weights representing the contribution of each of m imaging variables (vertices) to each identified covariance pattern or component, while **H** contains the weights of the contributions of each covariance pattern to the reconstruction of each of n data points (subject-level metrics) in the original input. In other words, **W** conveys information regarding the spatial properties of each MCP, while the entries of **H** are loadings that specify the strength of expression of the MCP in each subject-metric.

When applied to neuroimaging data, OPNMF offers several advantages over other common dimensionality reduction techniques such as PCA or ICA, which tend to produce components that can be challenging to interpret by virtue of being either too widespread or too spatially dispersed and comprising overlapping brain areas with opposite-sign weights (Sotiras et al., 2015). By contrast, the non-negativity and orthogonality constraints of OPNMF lead to sparse and parsimonious output components that have minimal spatial overlap. This is ideal for obtaining a purely additive, parts-based representation of the cortex that is readily interpretable, in which each vertex can be associated with a distinct MCP.

4.3.1. Implementation

We implemented OPNMF and the accompanying stability analysis in Python (v3.6.8) using a set of in-house scripts (https://github.com/CoBrALab/cobra-nmf) (R. Patel et al., 2020) that builds on publicly available code from (Sotiras et al., 2015). In the current study, the rows of the OPNMF input matrix **X** corresponded to the 77122 (m) non-medial wall cortical vertices considered for analysis across the whole brain, while the columns comprised the CT, SA, MC, and GI values for all 266 subjects, stacked horizontally by metric to form 1064 subject-metric

combinations (*n*) (Figure 2a). Importantly, the vertex-wise values for each metric were residualized for subjects' mean CT and total SA prior to input matrix construction. We implemented this residualization step based on the observation that MCPs derived using the raw metrics, as well as brain-behaviour relationships subsequently identified based on those MCPs (see Section 4.5), tended to be dominated by global differences in CT and SA, features which undergo drastic global reorganization during maturation (Raznahan et al., 2011). Through correcting OPNMF input for mean CT and total SA, we sought to encourage output MCPs which capture more nuanced patterns of covariance, and thereby refine mappings from anatomy onto variation in symptoms. Additionally, to adjust the data for each of the four cortical metrics to all be on the same scale, we first performed within-metric z-scoring for each row (vertex) in the input data matrix, and then shifted all the z-scored data by the minimum z-score (R. Patel et al., 2020).

4.3.2. Stability analysis

To select the number of MCPs (*k*) to retain, we assessed both the gradient of the reconstruction error, which quantifies the gain in accuracy achieved by increasing the number of MCPs from one granularity to the next (Durran, 2013; Fornberg, 1988; Quarteroni et al., 2007), and the similarity of output MCPs across varying half-splits of the input data, which provides a measure of the stability of the decomposition for a given *k* (R. Patel et al., 2020). Specifically, the sample was randomly split into two halves (n_a = 133, n_b = 133), and OPNMF was performed on each half separately to produce two different component matrices ($\mathbf{W}_a$, $\mathbf{W}_b$). The spatial similarity of the two sets of MCPs was then assessed by first computing the cosine similarity matrix $\mathbf{C_W}$ of rows of **W** for each decomposition, where the *i*th row of $\mathbf{C_W}$ represents the similarity of component weights between vertex *i* and all other vertices. The mean Pearson correlation between corresponding rows (vertices) of $\mathbf{C_W}$ for each split-half was taken to represent the stability of the employed granularity.

We repeated the above procedure for each of *k* = 2 to *k* = 30 for 10 random half-splits, evaluating *k* in steps of two for computational efficiency. To estimate accuracy for a given *k*, we computed the change in reconstruction error between *k*-2 and *k* and averaged the differences from all 20 random halves of the data to report the gradient of the reconstruction error at that granularity.

4.3.3. Exploring the generalizability of morphometric covariance patterns

Previous studies have suggested that structural covariance networks derived by applying OPNMF on a single morphometric feature have the capacity to capture abnormalities across

different dimensions (Kaczkurkin et al., 2019) as well as severity (Neufeld et al., 2020) of psychopathology. To explore whether our multivariate implementation of OPNMF identified morphometric patterns that may generalize to the neuroanatomy of non-PS groups, we qualitatively compared our identified MCPs to MCPs defined using the same four T1w cortical features in two other non-overlapping samples. OPNMF was first independently repeated, using the resolution selected for the primary PS sample after the stability analysis above, in 681 youth from the PNC who did not meet PS criteria and were free of nervous system-affecting medical conditions ("non-PS PNC" sample; see Appendix Table 1 for demographic summary). Additionally, to probe the transdiagnostic relevance of the MCPs identified in our PS sample, we compared them to a 6-MCP cortical decomposition recently observed by our group to be stable in a harmonized multi-site dataset of 486 autism spectrum disorder patients and matched neurotypical individuals ("autism spectrum" sample; see Appendix Table 1 for demographic summary per site) (Ziolkowski et al, in prep). Both 'replication' samples were processed using the same pipelines and had passed all stages of MRI quality control.

4.4. Exploratory factor analysis of PS symptoms

Exploratory factor analysis was used to identify major latent dimensions from the 30 PS measures from GOASSESS using the R package psych (v2.0.12; William Revelle) (Figure 2b). This technique seeks to identify a smaller set of meaningful, unmeasured constructs (factors) underlying a set of measured variables, which exert a causal influence on the relationships observed between those variables (Russell, 2002). We first used the 'mixedCor' function to find appropriate pairwise correlation metrics between the various combinations of dichotomous and polytomous (Likert) PS symptom items (Holgado–Tello et al., 2008). The resulting mixed correlation matrix was then factored (using the 'fa' function) using the default minimum residuals method, which aims to minimize the off-diagonal residuals between the empirical correlations and those reproduced by the extracted factors using a least squares procedure (Harman & Jones, 1966). Oblique factor rotation (oblimin) was applied to increase factor interpretability (Russell, 2002). The output of a given factor model included factor loadings of each original symptom item, which described the unique contribution of each factor to that item's variance, and regression-based factor scores for each subject reflecting the extent to which an individual expresses each extracted

underlying symptom dimension (DiStefano et al., 2009). Factor scores were used to represent the latent dimensions of PS at the subject level in downstream analyses.

To determine the number of factors to extract, we first inspected the scree plot to obtain initial estimates of the factor structure (Cattell, 1966). Factor models with the numbers of factors around the inflection point were then individually estimated, and the optimal solution was identified using the criteria of (1) minimal cross-loadings, or items that load strongly (≥ 0.35) onto more than one of the extracted factors (Costello & Osborne, 2005; Rosenblad, 2009), and (2) factor interpretability (Henson & Roberts, 2006).

4.5. Identifying MCP-behaviour correlations: Behavioural partial least squares analysis

Behavioural partial least squares correlation (bPLS) analysis was used to relate subject-specific MCP loadings to scores on the identified PS symptom dimensions (Figure 2c). bPLS is an unsupervised multivariate statistical technique that decomposes relationships between two datasets (**X** and **Y**) into orthogonal latent variables, which are linear combinations of the original data with maximum covariance (Krishnan et al., 2011; McIntosh & Lobaugh, 2004; McIntosh & Mišić, 2013).

In our case, **X** contained MCP loadings for each cortical metric (k×4 loadings in total) per subject (brain data); and **Y** contained age, sex, race (binarized for African American, European American, and Mixed/other race), parent education, WRAT-4 Reading standard score, and PS symptom factor scores for each subject (behavioural data) (Figure 2c). To perform bPLS, the data matrices were z-scored column-wise and correlated, and singular value decomposition was applied on the resulting correlation matrix $\mathbf{R} = \mathbf{X}'\mathbf{Y}$ such that $\mathbf{X}'\mathbf{Y} = \mathbf{USV}'$ (Eckart & Young, 1936).

Each output latent variable (LV) comprises a pair of left and right singular vectors (from matrices **U** and **V**) which weight the original brain and behaviour variables, respectively, in the extracted multivariate pattern, as well as a singular value (from matrix **S**) proportional to the covariance between morphometry and behaviour captured by the LV (McIntosh & Lobaugh, 2004). Thus, each output LV describes an association between a spatial pattern of cortical morphometry and behavioural characteristics. Following previous studies (R. Patel et al., 2020; Zeighami et al., 2019), we also computed behavioural variable loadings for each LV as the correlation between each feature in the **Y** matrix and brain scores representing how well each

subject exhibits the bPLS-derived morphometry pattern. These loadings can be interpreted as directly indexing the degree of contribution of each behavioural variable to an LV.

4.5.1. Assessing model significance, stability, and feature importance

Statistical significance of each LV was assessed using permutation tests. The rows (observations) of the brain data matrix were randomly shuffled 10000 times, and bPLS was performed using the permuted brain matrices and non-permuted behaviour matrix (Krishnan et al., 2011). This generated a distribution of singular values under the null hypothesis that no relationship exists between morphometric covariance patterns and PS behavioural measures. We used this null distribution to estimate a non-parametric p-value for each LV observed in the original data, setting the alpha at 0.05.

We also assessed the reliability of each LV via split-half resampling. The original data were randomly split into two halves, and correlation matrices were computed for each half separately (i.e., $\mathbf{R_1}$ and $\mathbf{R_2}$). The left and right singular vectors derived from the full-sample PLS were then separately projected onto each half-correlation matrix to obtain the corresponding pairings of half-sample singular vectors (i.e., $\mathbf{U_1}$ and $\mathbf{V_1}$; $\mathbf{U_2}$ and $\mathbf{V_2}$) (Kovacevic et al., 2013). We repeated this procedure for 200 half-splits of the data and computed the mean correlations between $\mathbf{U_1}$ and $\mathbf{U_2}$ (Ucorr) and $\mathbf{V_1}$ and $\mathbf{V_2}$ (Vcorr) across splits. To generate a null distribution for these split-half correlations, the split-half resampling process above was repeated for each permutation of the original data (n = 10000) in the permutation testing procedure. We used this distribution to estimate the probability of surpassing the correlations from the non-permuted data (p_{Ucorr}, p_{Vcorr}), interpreting LVs with both $p_{Ucorr,\ Vcorr} < 0.05$ as representing stable pairings between morphometry and behavioural patterns across subjects (Kovacevic et al., 2013).

Finally, the contribution of individual variables (MCP-metrics or behavioural measures) to an LV was estimated by bootstrap resampling. Subjects (rows of data matrices $\mathbf{X}$ and $\mathbf{Y}$) were randomly sampled with replacement 10000 times and subjected to bPLS to generate a sampling distribution of singular vector weights per variable for each LV. A bootstrap ratio (BSR) was calculated for each MCP-metric pairing as the ratio of its true singular vector weight over its bootstrap-estimated standard error, with large BSRs isolating variables that contribute strongly to the morphometric pattern of an LV and are stable across subjects (McIntosh & Lobaugh, 2004). BSR values were thresholded at ±2.58, corresponding to a p-value of 0.01 (Kirschner, Shafiei,

Markello, Markowski, et al., 2020). All PLS-related analyses were implemented using the pyls package (https://github.com/rmarkello/pyls).

4.6. Meta-analytic functional decoding of morphometric covariance patterns using Neurosynth

To contextualize OPNMF-derived MCPs in terms of functional MRI findings, we used Neurosynth, a meta-analytic database of high-frequency keywords and study-level activation coordinates from 14371 functional MRI studies (Figure 2d, top) (Yarkoni et al., 2011). Cortical surface maps of weights for each MCP were first projected to volumetric MNI 152 standard space and dilated once using a median dilation approach (as implemented in mincmorph: https://github.com/andrewjanke/mincmorph) to increase the cortical anatomical coverage of the maps, similar to the approaches taken in previous studies (Margulies et al., 2016; M. T. M. Park et al., 2018). The resulting volumetric maps served as inputs to the open-ended image "decoding" function of Neurosynth, which aims to quantitatively infer psychological states associated with a provided brain pattern (Yarkoni et al., 2011). Specifically, each input image was correlated with the association test meta-analysis maps of all psychological terms in the Neurosynth database, which contain z-scores of posterior probabilities describing voxels whose activation are preferentially related to the use of a given term (L. J. Chang et al., 2013).

A total of 1342 terms (encompassing all terms available through the Neurosynth web interface, https://neurosynth.org/) were used to decode the broad functional role of each MCP. The 50 most positively correlated terms per MCP were retained, and any redundant, anatomical, or non-specific terms were removed to capture only unique psychological or cognitive processes associated with the spatial pattern of an MCP. All Neurosynth analyses were performed using the Neuroimaging Meta-Analysis Research Environment (NiMARE) package (v0.0.1rc2) (Salo et al., 2022).

4.7. Situating morphometric covariance patterns along cortical functional gradients

To situate OPNMF-derived MCPs along the primary sensorimotor-transmodal hierarchy within the context of development, we leveraged previously reported functional connectivity gradients in healthy children (aged 6-12), adolescents (aged 12-18), and adults (aged 22-35) (H.-M. Dong et al., 2021; Margulies et al., 2016) (Figure 2d, bottom). These gradients represent

ordered components of variance derived from diffusion map embedding of resting-state functional connectivity data, and each describes the positions of vertices along a lower-dimensional embedding axis that encodes dominant differences in vertex-level connectivity patterns (Coifman et al., 2005; Margulies et al., 2016). Vertices with similar values in a gradient thus have similar connectivity patterns. We first assigned each cortical vertex to a single MCP based on the highest component weight of the vertex in the **W** matrix of the OPNMF output (Figure 2a) (R. Patel et al., 2020). Using the resulting morphometric 'parcellation,' we then extracted the distribution of gradient values in each MCP from the map of the first gradient of functional connectivity in adults, which has been characterized by its clear unimodal and transmodal poles (Margulies et al., 2016). We repeated this for the first gradient in adolescents and the second gradient in children, as these maturational gradients have been observed to capture a similar axis of organization as the canonical principal gradient in adults (H.-M. Dong et al., 2021). To enable comparisons with the OPNMF parcellation and with each other, all gradient maps were transformed into MNI 152 space using the neuromaps toolbox (Markello et al., 2022) and z-scored prior to gradient value extraction. For all three gradients, more positive values indicate proximity to transmodal regions, while more negative values denote vertices closer to primary sensory and motor regions.

Due to the vast number of gradient observations (i.e., 1000s of vertices) per MCP, traditional hypothesis testing using summary statistics (e.g., analyses of variance) was not appropriate for interrogating differences in patterns of gradient values. Instead, to explore the maturational 'trajectories' of MCP gradient profiles along the unimodal-transmodal axis, we first qualitatively compared both the shape of the gradient value distribution of MCPs between the three age group maps, as well as the within-map relative positions of MCPs with respect to either end of this hierarchy.

As a secondary analysis, we formally tested for within-MCP maturational shifts in gradient position using the shift function, a graphical method that quantifies how pairs of distributions differ based on their deciles (rogme R package, v0.2.0) (Rousselet et al., 2017). Three pairwise comparisons (adolescent-child, adult-adolescent, adult-child) were made between the age group-specific distributions of gradient values associated with each MCP. A percentile bootstrap technique (2000 samples) was used to estimate 95% confidence intervals for the differences between corresponding deciles of the distributions (Wilcox et al., 2014). A significant decile difference suggests a change in the relative position of a MCP along the unimodal-transmodal axis

between age groups, at specific vertices that are either more 'unimodal' (the lower deciles) or 'transmodal' (the higher deciles) within the MCP. By examining the overall trends in the directions of significant decile differences for a MCP, we can obtain a refined description of how its gradient profile shifts between age groups. This, in turn, allowed us to determine MCPs that may exhibit dynamic functional architectures during maturation.

4.8. Characterizing morphometric covariance patterns and their associated PS significance in terms of transcriptomic architectures

4.8.1. Obtaining gene expression information

Microarray expression data were obtained from six post-mortem adult brains provided by the AHBA (http://human.brain-map.org/) (Hawrylycz et al., 2012). The data were preprocessed using the abagen toolbox (v0.1.3) (Markello et al., 2021) following previously developed best practice recommendations for microarray probe-to-gene annotation, probe filtering and selection, and normalization of both tissue sample and gene expression values (Arnatkeviciute et al., 2019; Markello et al., 2021). In addition, since only two brains had tissue samples from the right hemisphere, we mirrored all available samples across the left-right hemisphere axis to increase the spatial coverage of the expression data (Romero-Garcia et al., 2019). This was important as two of the identified OPNMF-derived MCPs did not appear bilaterally symmetric (see OPNMF results in Section 5.1). The above preprocessing steps yielded a 6932 (samples)×15633 (genes) expression matrix. Finally, using binary masks of each identified MCP and the MNI coordinates of tissue samples generated via nonlinear registration (https://github.com/chrisgorgo/alleninf), we obtained MCP-specific expression matrices (of size samples×genes) containing the gene expression values of all samples located within the boundaries of each MCP. Fetching and subsequent analysis of AHBA data were implemented in Python v3.8.5.

4.8.2. Identifying major axes of gene expression differences between MCPs: Mean-centered partial least squares analysis

We used mean-centered PLS (mcPLS) to identify patterns of gene expression that maximally differentiate the MCPs (Figure 2e). Like behavioural PLS, mcPLS is a PLS correlation technique that searches for orthogonal latent variables expressing maximally covarying patterns of two data matrices **X** and **Y**. However, in mcPLS, the observations (rows) of **X** belong to and are arranged by experimental 'groups,' while **Y** is a dummy coded matrix representing the actual

groups themselves (Krishnan et al., 2011). This variant can thus be interpreted as suitable for finding relationships between predefined *groupings* in a single set of variables.

In this study, **X** (the whole-brain expression matrix) contained the sample-level gene expression matrices obtained for each MCP concatenated vertically, such that each MCP was treated as a group, and each tissue sample an observation (Figure 2e). **Y** was a binary matrix coding the MCP membership of each sample. To perform mcPLS, we computed a matrix **M** containing the MCP-wise averages within each column (gene) in **X**, which was then mean-centered column-wise (Krishnan et al., 2011; McIntosh et al., 2004). Singular value decomposition was performed on the resulting $\mathbf{M}_{\text{mean-centered}}$, producing LVs that identify gene expression patterns optimally separating the MCPs. Each LV comprises a singular value, which describes the proportion of covariance accounted for between MCPs (i.e., tissue sample groupings) and the expression data; gene weights, which identify the expression profile most related to the effect captured by the LV; and contrast values, which illustrate the extent to which each MCP is associated with that expression profile. Each LV has dissociable positive and negative dimensions, expressed through the sign of the contrast values; these dimensions reflect two distributions of gene expression levels that covary with the spatial MCPs in a separable way.

The significance of LVs was assessed against a null model constructed by repeatedly permuting MCP assignments of tissue samples (i.e., the **X** matrix) while preserving spatial autocorrelation. This was done using a spin test, in which a spherical projection of the CIVET surface was randomly rotated and original vertices were reassigned the MCP value of the closest rotated vertex (Alexander-Bloch et al., 2018), effectively rotating the spatial map of all the MCPs. We then reextracted and concatenated the sample-level expression data for each MCP of the 'spun' MCP parcellation following Section 4.8.1, to compare against the observed expression profiles of the original, data-driven MCPs. This procedure was repeated 1000 times, and each resulting null expression matrix was subjected to mcPLS analysis, generating a distribution of null singular values. The p-value of each LV in the original mcPLS result thus indicates the proportion of null singular values greater in magnitude than the empirical singular value.

To assess the stability of the gene weights onto each LV, we performed bootstrap resampling as described in Section 4.5.1 for the behavioural PLS analysis. Due to the high computational cost of additionally implementing bootstrapping per spatial permutation performed for the mcPLS analysis, 1000 bootstrap resamples were used here instead of 10000.

Per significant LV, we derived a positive gene set (PLS+) and a negative gene set (PLS-) which comprised the reliably contributing positively weighted (BSR ≥ 2.58) and negatively weighted (BSR ≤ -2.58) genes, respectively. PLS+ genes show higher expression in the MCPs with positive contrast values and lower expression in MCPs with negative contrast values, while PLS- genes show the inverse pattern for the same LV. The PLS+ and PLS- gene sets for each LV were thus interpreted as characterizing distinct MCPs and were further analyzed using gene enrichment analyses.

4.8.3. Biological process gene enrichment

To determine the biological processes in which the gene sets identified by mcPLS are most involved, we followed the analysis approach used in (Hansen et al., 2021), adapting code from the Gene Category Enrichment Analysis toolbox (https://github.com/benfulcher/GeneCategoryEnrichmentAnalysis) (Fulcher et al., 2021). Using Gene Ontology (GO) data (2022-01-13 release) (Ashburner et al., 2000; Gene Ontology Consortium, 2021), we first generated GO term hierarchy-propagated annotations of individual genes to biological process categories. An enrichment analysis was then performed separately on the PLS+ genes and PLS- genes for each significant LV, since each gene set covaries with different MCPs. For each biological process category, we calculated a 'category score' representing the mean BSR, or normalized weight, of genes annotated to that category within each gene set. Category scores were compared against a null distribution of scores constructed by applying mcPLS to spatial permutations of the MCP-grouped sample expression matrix (see Section 4.8.2 for a detailed description of the spin test implementation). Specifically, null BSRs for the empirical PLS+ and PLS- gene sets were obtained from each permutation, and null category scores were then computed for each GO biological process following the procedure above. The p-value per category in each gene set thus indicates the proportion of null category scores that are greater in magnitude than the empirical category scores (alpha = 0.05). P-values were false discovery rate (FDR)-corrected ($q < 0.05$) across categories for each gene set.

Since we were interested in the unique biological involvement of the PLS+ and PLS- gene sets, we limited interpretation to significantly enriched categories surviving FDR correction that did not overlap between the two gene sets. Given the vast number of biological process categories available (> 10000), we also focus in the results on significant categories with a clear relation to brain development or neurobiological function, to avoid over-interpreting generic cell maintenance

processes (e.g., “protein-DNA complex assembly”, “phosphorylation”) that may lack meaningful spatial specificity at the resolution of our MCPs. A list of terms used to systematically exclude certain non-brain-specific categories prior to our data visualization step can be found in Appendix Table 2.

4.8.4. Cell type-specific gene enrichment

To determine whether the mcPLS-identified gene sets were preferentially expressed in specific cell types, we leveraged cell-specific aggregate gene sets across five different single-cell studies using post-mortem cortical samples in human postnatal subjects (Darmanis et al., 2015; Habib et al., 2017; Lake et al., 2018; M. Li et al., 2018; Y. Zhang et al., 2016), as presented previously (Seidlitz et al., 2020). Briefly, hierarchical clustering of regional topographies across the 58 study-specific cell types in the AHBA resulted in seven canonical cortical cell classes: astrocytes, endothelial cells, microglia, excitatory neurons, inhibitory neurons, oligodendrocytes, and oligodendrocyte precursors (Seidlitz et al., 2020). Using the omnibus gene list for each cell class, we calculated the ratio of genes in each PLS+ and PLS- gene set that are preferentially expressed in one of the seven cell types, following (Hansen et al., 2021). Significance of each enrichment ratio was assessed against a null distribution of ratios constructed by repeating the process 10000 times on random gene sets drawn from the AHBA. Resulting two-tailed p-values were FDR-corrected ($q < 0.05$).

4.8.5. Disease gene enrichment

To explore whether genes associated with psychotic or other psychiatric disorders may be enriched among the mcPLS-identified gene sets, we performed over-representation analysis of diseases from the DisGeNET database (v5.0), a comprehensive catalogue of human-disease associated genes (Piñero et al., 2017). Briefly, fold enrichment ratios were calculated for each disease in the database as the proportion of disease-associated genes in the PLS+ or PLS- gene set of interest, compared to the proportion in a reference gene set. The hypergeometric distribution was used to calculate the p-value for over-representation of a disease or disorder (B. Zhang et al., 2005):

$$p = 1 - \sum_{i=0}^{x} \frac{\binom{K}{i}\binom{M-K}{N-i}}{\binom{M}{N}}$$

where p is the probability of finding x or more genes from the K-length list of associated genes for the disease in a set of N randomly selected genes, drawn from a reference set of M genes. Specifically, N corresponded to the size of each PLS+ or PLS- gene set, and the reference set was selected as the full preprocessed list of 15633 brain-expressed genes from the AHBA. The over-representation analysis results thus allow us to obtain a data-driven disease association profile for each PLS+ or PLS- gene set, and by extension the MCPs covarying with expression of that gene set. Given our focus on the psychosis spectrum, we also compared the calculated fold enrichment ratios for schizophrenia and bipolar disorder among the different evaluated gene sets, to characterize MCPs capturing relatively higher expression of psychotic disorder genes. Over-representation analysis was performed using WebGestalt (http://www.webgestalt.org/) (Liao et al., 2019), and statistics were FDR-corrected across diseases ($q < 0.05$).

5. Results

5.1. Multivariate patterns of cortical morphometric covariance in PS youth

Results of the OPNMF stability analysis are shown in Figure 3a. Since stability coefficients remained roughly consistent at around 0.6 with $k \geq 4$, we focused on the gradient of the reconstruction error to select the optimal number of MCPs. We observed that when moving to increasingly higher resolutions, the last sizeable drop in the magnitude of the reconstruction error gradient occurs between $k = 8$ to $k = 10$, after which the gradient gradually levels off. Recalling that in this curve, the value plotted per k represents the *decrease* in reconstruction error when moving from the previous resolution to the specified resolution, this result indicates that increasing the number of MCPs yields only relatively small gains in accuracy for $k > 8$ (Sotiras et al., 2015). These observations suggest that with $k = 8$, the most prominent patterns in the input data have been captured and any added complexity has diminishing returns on reconstruction accuracy. The 8-MCP solution was thus interpreted as a suitable representation of the intrinsic data dimension and was retained for further analysis.

The 8 MCPs estimated by OPNMF represent groups of vertices that share a pattern of covariation of four morphometric features (CT, SA, MC, GI) across the sample. Spatially, the MCPs were non-overlapping and highly localized, and exhibited bilateral symmetry in all but two MCPs (3 and 8) (Figure 3b), lending to their interpretability.

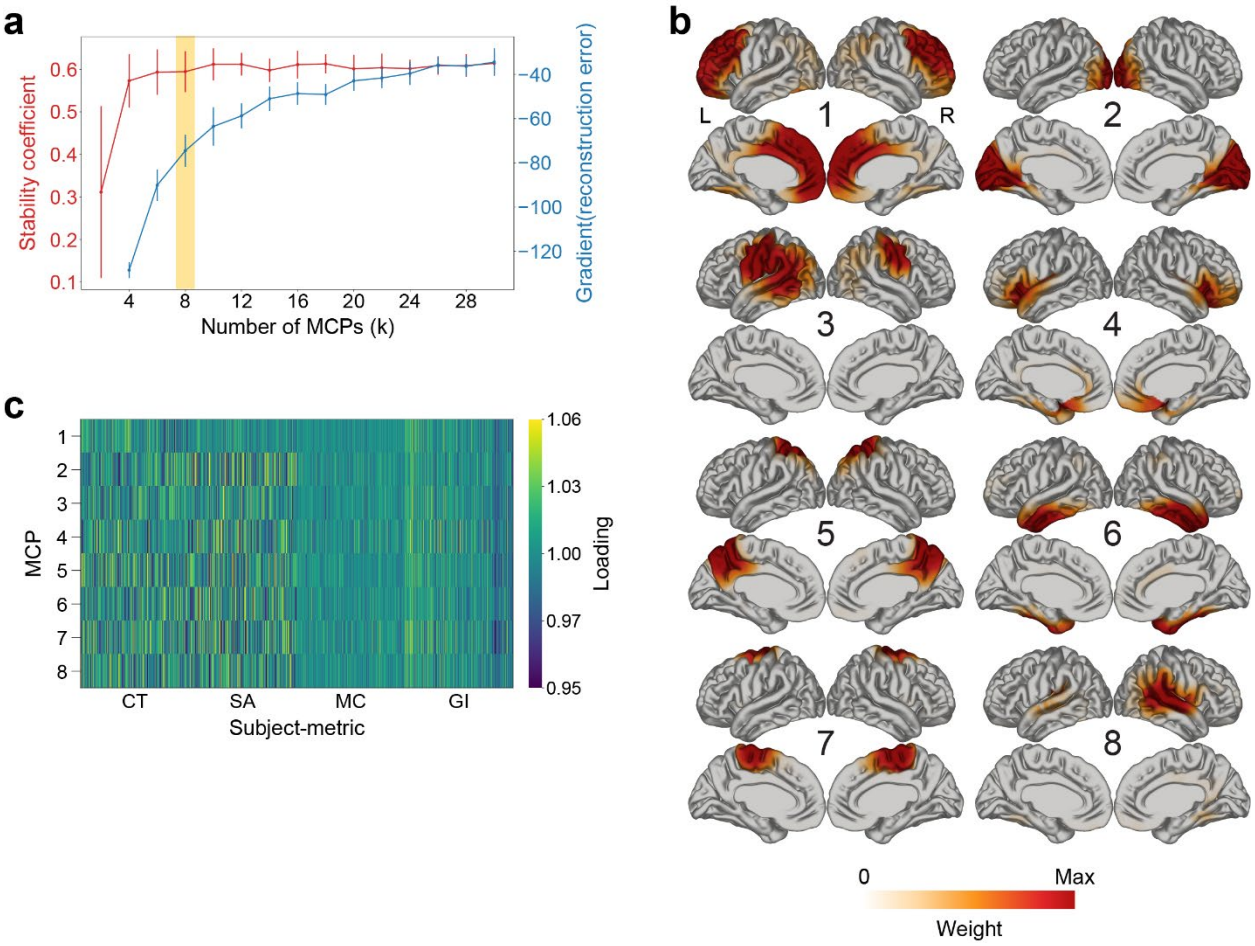

Figure 3. Morphometric covariance patterns delineated by OPNMF. (a) Stability coefficient (red curve) and gradient of the reconstruction error (blue curve) for solutions of 2 to 30 components or MCPs, in steps of two. The yellow box indicates the 8-MCP granularity selected for further analysis. **(b)** Spatial patterns of the 8 MCPs identified by OPNMF, visualized on the group-average brain. Darker colours indicate greater contribution of a vertex to the MCP. **(c)** The loading matrix for the 8-MCP solution, showing the subject-level relative contribution of each metric to each MCP (subject-metric loadings). The loadings for each MCP have been divided by the mean for visualization purposes. Subjects are arranged in ascending age order per metric along the x-axis.

We provide the anatomical description of each MCP below, along with shortened naming conventions:

i. MCP 1 (anterior frontal) encompasses mainly dorsolateral and medial prefrontal cortex.

ii. MCP 2 (visual) approximates the visual cortex.

iii. MCP 3 (left-lateralized sensorimotor/language) captures primary sensorimotor cortex, the left inferior parietal lobule, and posterior portions of the left superior and middle temporal gyri, including Wernicke's area.

iv. MCP 4 (ventral prefrontal/insular) comprises ventrolateral and ventromedial prefrontal cortex, and parts of the insular cortex and temporal operculum.
v. MCP 5 (precuneus) primarily comprises the precuneus.
vi. MCP 6 (anterior/ventral temporal) captures the anterior middle and inferior temporal gyri, including the temporal pole as well as ventromedial temporal areas.
vii. MCP 7 (paracentral) comprises the paracentral lobule, including parts of the supplementary motor area.
viii. MCP 8 (right-lateralized temporoparietal) mainly captures the inferior parietal lobule and posterior portions of the superior and middle temporal gyri in the right hemisphere.

We observed that despite the pronounced anatomical localization of each MCP, the overall decomposition defined cortical boundaries that diverged (e.g., the anterior-posterior division of temporal cortex in MCPs 3 and 6) from those in traditional structural parcellations based on a single morphometric feature, such as the Automated Anatomical Labeling atlas (Tzourio-Mazoyer et al., 2002) or the Desikan-Killiany-Tourville atlas (A. Klein & Tourville, 2012). Further, visual examination of the subject-specific metric loadings for each MCP indicated that individual MCPs were not characterized by a single anatomical metric (Figure 3c); however, MC appeared to have the lowest relative contribution across MCPs, while the highest metric loadings for MCPs 2 to 8 were generally seen in SA. By comparison, MCP 1 appeared to have comparable neuroanatomical representation from all four metrics.

The 8 stable patterns of cortical morphometric covariance we identified in PS youth showed marked overlap with an 8-MCP cortical morphometric decomposition derived using the same methodology from medically healthy youth without PS features (n = 681), as well as with a 6-MCP decomposition observed to be stable among a combined neurotypical and autism spectrum disorder sample enriched for adolescents and young adults (n = 486) (Appendix Figure 2). Similar representation of the visual cortex (e.g., PS MCP 2), anterior temporal cortex (e.g., PS MCP 6), and frontoparietal and temporal opercula (e.g., PS MCP 8) within distinct MCPs was especially pronounced across the three samples, although the symmetry of MCPs varied slightly. This suggests that while macroscale patterns of neurostructural covariance across the cortex are not completely invariant to different neurodevelopmental conditions, the covariance of certain areas may represent a stable phenotype of neurodevelopment that potentially has transdiagnostic relevance.

5.2. Latent dimensions of PS symptoms

Visual examination of the scree plot suggested the existence of 2 to 4 factors in the PS symptom data (Figure 4a). Further evaluation of these solutions revealed that 2 factors broadly distinguished positive symptoms from negative or disorganized symptoms. In the 3-factor solution, the positive symptoms split into two separate factors that remained well-defined, with one factor capturing hallucinations and abnormal perceptions (e.g., verbal hallucination, tactile hallucination, auditory perception) and the other capturing symptoms related to disturbances of self-experience (e.g., external control over thoughts, loss of sense of self, paranoia). Finally, the 4-factor solution produced a factor whose loadings were dominated by a single item (disorganized communication), indicating factor overextraction. Correlations among factors themselves were relatively low in all tested resolutions (e.g., average $r = 0.22$ for 3-factor model) (Appendix Table 3), indicating that the addition of an overarching general factor, such as in a bifactor model, was not warranted in our data (Bornovalova et al., 2020; Reise et al., 2010). Therefore, we determined that 3 factors were optimal for explaining the data, as this solution captured conceptually distinct symptom dimensions while also having few cross-loadings of symptoms (Figure 4b; see Appendix Table 4 for full descriptions of items loading onto each factor). Based on the item loadings per factor, we summarize the identified symptom dimensions as negative/disorganized symptoms, hallucinations/abnormal perceptions, and disturbed self-experience.

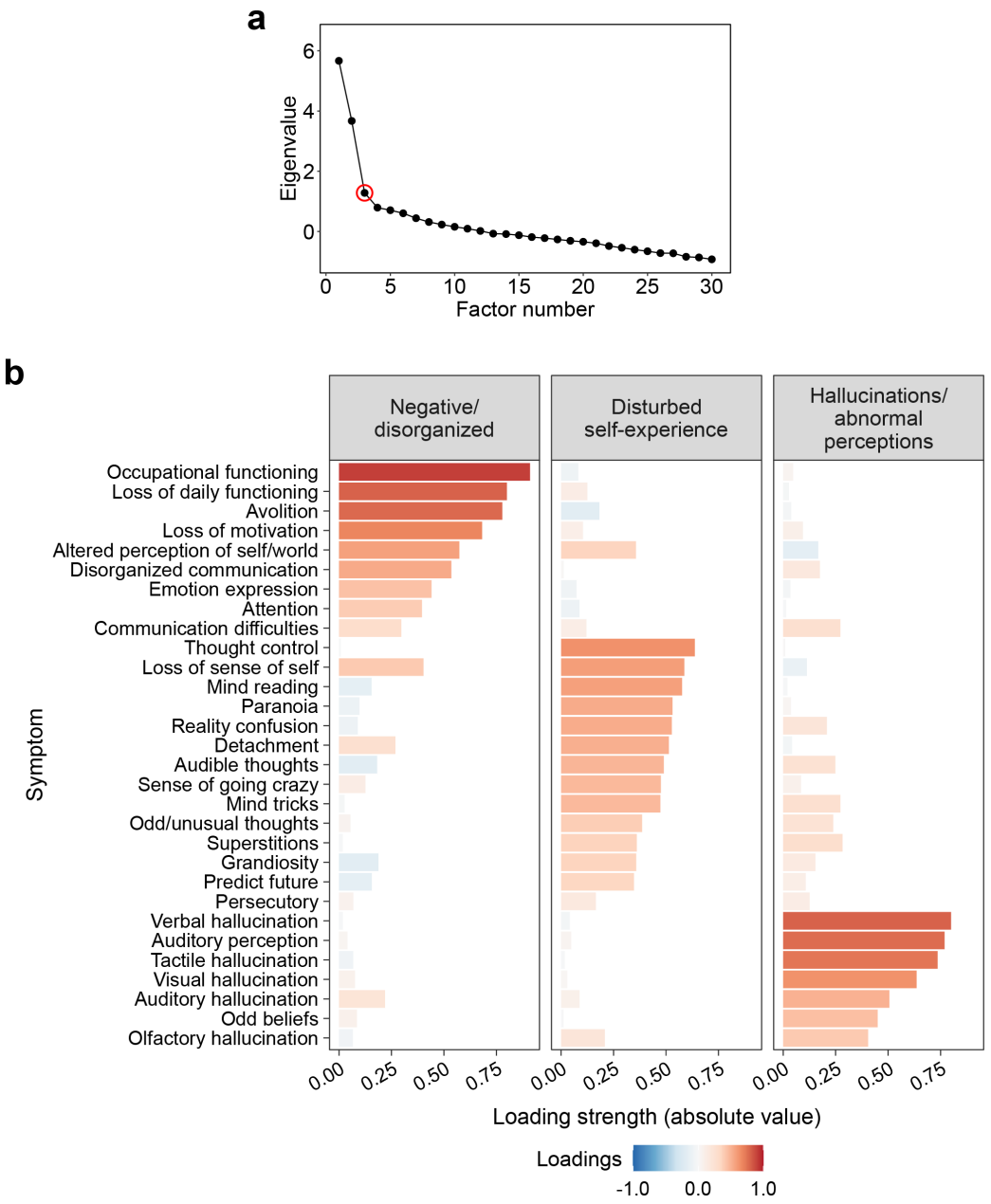

Figure 4. Latent factors of psychosis spectrum symptoms. (a) Scree plot showing the first 30 eigenvalues of the mixed correlation matrix of the 30 PS symptom items. Circled is the 3-factor solution selected for further analysis. **(b)** Loadings of each PS symptom item onto the 3 extracted factors. Positive loadings are shown in red and negative loadings in blue, with larger loadings indicating higher relevance of a variable to the specified factor. Variables with loadings > 0.35 were considered 'important' to a factor and were used in factor interpretation. A descriptive name for the factor is shown at the top of each panel.

5.3. Morphometry-behaviour relationships

The bPLS analysis revealed two statistically significant latent variables relating sociodemographic features and factor analysis-derived symptom dimensions to corresponding cortical morphometric covariance patterns in PS youth. These LVs survived split-half resampling (Appendix Figure 3) and respectively accounted for 52.8% and 24.1% (total of 76.9%) of the covariance between the behavioural and cortical data (Figure 5a).

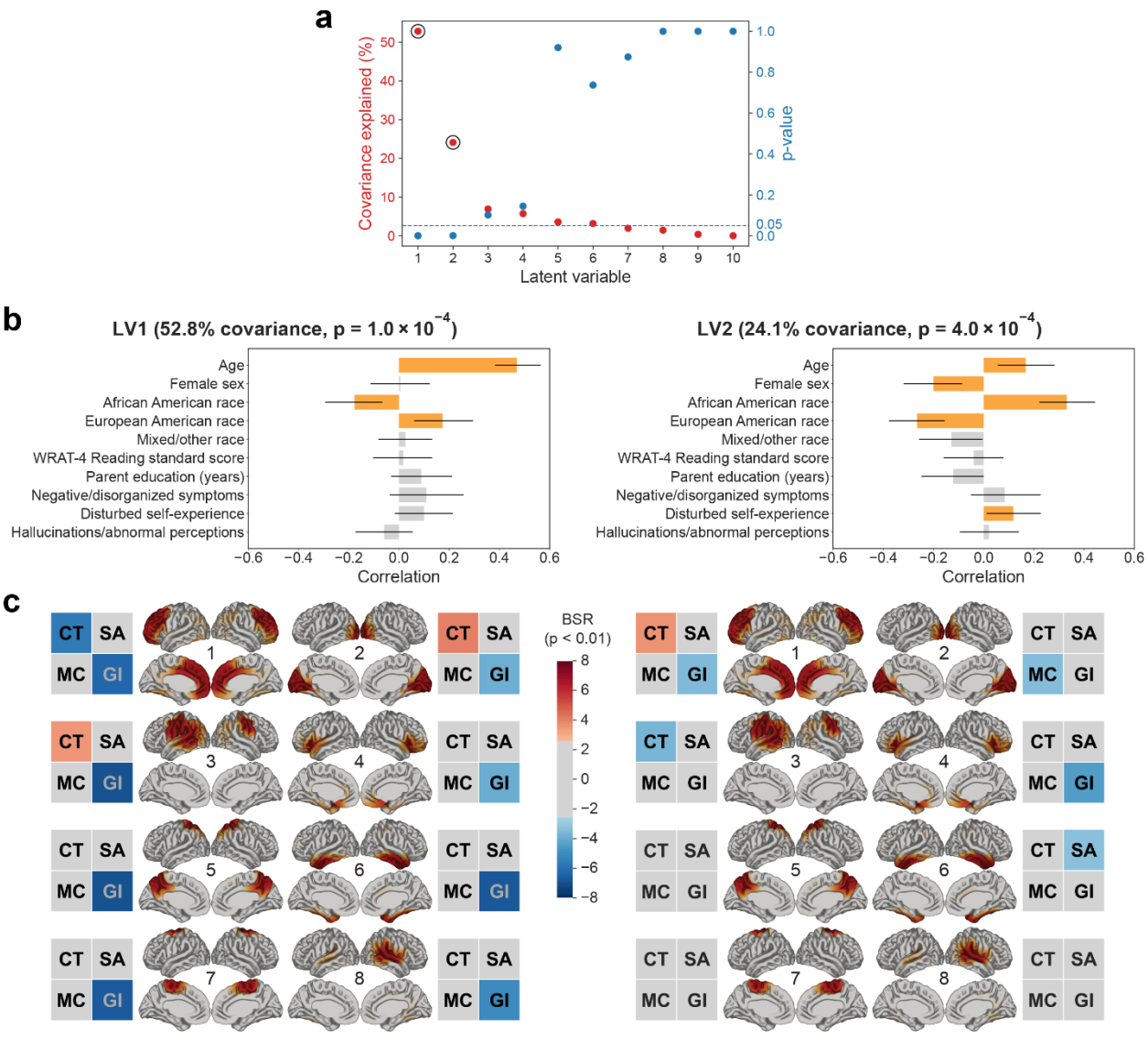

Figure 5. Latent morphometry-behaviour relationships detected by bPLS analysis. *(Continued on next page)* **(a)** Covariance explained (red) and permutation p-values (blue) for all latent variables (LVs) in the bPLS analysis. Black circles indicate significant LVs, which were retained for further analysis. **(b)** Behavioural patterns of LV1 (left) and LV2 (right). Contributions of individual sociodemographic and clinical features are shown as correlations between subject-

specific feature scores and scores on the multivariate pattern (loadings). Yellow bars indicate significantly contributing features; error bars denote 95% bootstrap confidence intervals. **(c)** Morphometric patterns of LV1 (left) and LV2 (right). The 2x2 grids summarize the profile of cortical metrics contributing to the LV within each MCP, as indexed by bootstrap ratios (BSRs). Cortical maps show the MCPs corresponding to each effect. Warmer and cooler colours indicate that higher and lower values of a metric, respectively, contribute to the LV.

The demographic features contributing to LV1 (permuted $p = 1.0\times10^{-4}$; split-half $p_{Ucorr} < 0.0001$, $p_{Vcorr} = 0.034$) included older age ($r = 0.47$, 95% confidence interval (CI) [0.37 0.56]), non-African American race ($r = -0.18$, CI [-0.29 -0.060]), and European American race ($r = 0.17$, CI [0.053 0.29]) (Figure 5b, left). The covarying morphometry pattern involved globally decreased GI, decreased CT in MCP 1 (anterior frontal), and increased CT in MCPs 2 (visual) and 3 (left-lateralized sensorimotor/language) (Figure 5c, left).

The demographic features contributing to LV2 (permuted $p = 4.0\times10^{-4}$; split-half $p_{Ucorr} = 3.6\times10^{-3}$, $p_{Vcorr} = 4.0\times10^{-4}$) included older age ($r = 0.17$, CI [0.053 0.28]), male sex ($r_{female} = -0.20$, CI [-0.31 -0.080]), African American race ($r = 0.33$, CI [0.22 0.44]), and non-European American race ($r = -0.27$, CI [-0.38 -0.15]) (Figure 5b, right). Notably, higher scores on the disturbed self-experience symptom factor ($r = 0.12$, CI [0.0092 0.22]) also contributed to the behavioural pattern. Although race was the strongest contributor to LV2, the lack of significant race differences in symptom factor scores (as assessed by linear regression; Appendix Table 5) suggested that this brain-behaviour pattern was not purely driven by race but captured, in part, a clinical dimension of the PS. The covarying morphometry pattern was more heterogeneous than in LV1, involving increased CT in MCP 1 (anterior frontal), decreased GI in MCPs 1 (anterior frontal) and 4 (ventral prefrontal/insular), decreased MC in MCP 2 (visual), decreased CT in MCP 3 (left-lateralized sensorimotor/language), and decreased SA in MCP 6 (anterior/ventral temporal) (Figure 5c, right).

Given that LV1 captured a mainly demographics-driven pattern, we focus on LV2 to contextualize subsequently explored functional and transcriptomic signatures of MCPs in terms of cortical vulnerability in the PS. For brevity, the five MCPs contributing to LV2 are referred to hereafter as PS-related MCPs.

5.4. Functional associations of morphometric covariance patterns

The Neurosynth psychological term maps most correlated with each MCP map are shown in Figure 6. We observe distinct domains of functional associations for each morphometric

covariance pattern, which can be summarized as cognitive control processes (MCP 1); visuo-spatial functions (MCP 2); verbal and non-verbal communication (MCP 3); affect (MCP 4); attentional processes and numerical reasoning (MCP 5); semantic memory faculties and impairments (MCP 6); higher-level motor functions (MCP 7); and auditory processing (MCP 8). Notably, the associated functional terms align with the anatomical descriptions of each MCP. For example, the high relative correlation of the terms "taste," "pleasant," and "disgust" with the MCP surrounding the anterior insula (MCP 4) is congruous with the role of this cortical region in both the evaluative and expressive aspects of taste valence and other emotions (Jabbi et al., 2007; Phan et al., 2002). Similarly, the dominant correlation of terms such as "speech production" and "verbs" with MCP 3 supports the observed asymmetry of this MCP, given the expected lateralization of language-related functions to the left hemisphere and the associated involvement of cortical areas in and around the temporoparietal junction (Binder et al., 1997).

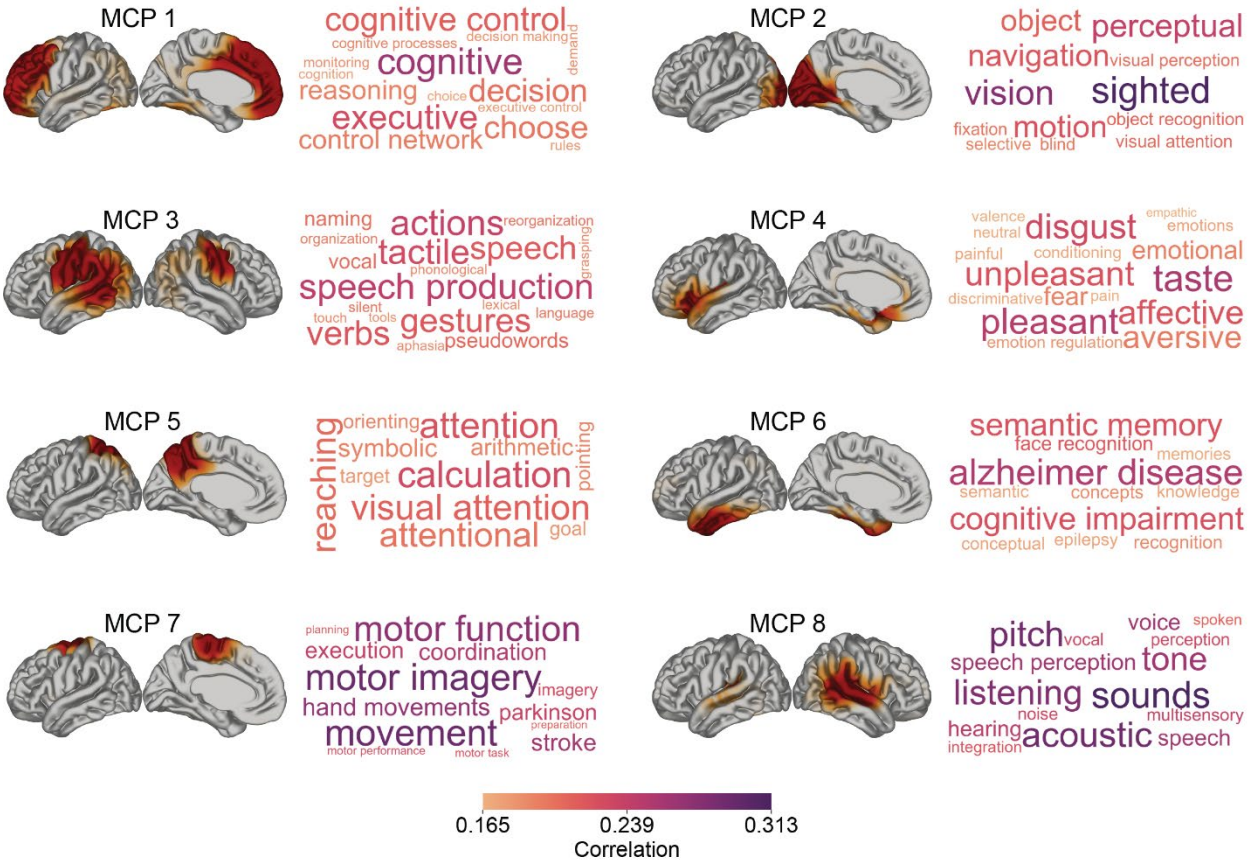

Figure 6. Results of Neurosynth image decoding of morphometric covariance patterns. *(Continued on next page)* Word clouds depict psychological concept terms whose meta-analytic functional maps were most positively correlated with voxel projections of each MCP shown. Font

size denotes the Pearson correlation between a Neurosynth term map and an MCP map relative to other terms in the same word cloud, while term colour denotes the true correlation value. For symmetrical MCPs, only the left hemisphere is shown; for MCPs with contributing vertices in lateral cortex only, only the relevant views are shown.

MCPs that were related to the disturbed self-experience symptom dimension (MCPs 1-4, 6) comprised those functionally associated with cognitive control processes, visuo-spatial functions, verbal communication, affect, or semantic memory.

5.5. Maturational shifting of PS-related morphometric covariance patterns along functional gradients

To characterize the maturational positions of MCPs implicated in PS within the unimodal-transmodal cortical hierarchy, we focus below on the results of mapping PS-related MCPs (MCPs 1-4, 6) onto macroscale functional gradients. Examining MCP-specific distributions of values in the principal gradient in adolescents, we observed that this gradient only loosely captures the spatial layout of PS-related MCPs identified in our comparable age cohort (Figure 7a, middle violin plot). Specifically, PS-related MCPs included both clusters of vertices preferentially located near one extreme of the unimodal-transmodal axis (MCPs 1, 3, 4) and vertex clusters that are distributed more broadly (MCP 6) or at more intermediate positions (MCP 2) along this functional dimension. Given limited MCP localization within the adolescent principal gradient, we additionally asked whether PS-related MCPs undergo dynamic functional reorganization across developmental epochs, indexed by the age-related shifting of MCP positions along the unimodal-transmodal gradient.

Visually, we observe that the PS-related MCPs occupying positions relatively closer to the unimodal end of this gradient in children (MCPs 2-4) shift in position most noticeably along the unimodal-transmodal axis across maturation (Figure 7a and c). The more heteromodal PS-related MCPs, MCPs 1 and 6, are situated more stably at the transmodal apex of the gradient across the three age group gradient maps, but nonetheless show noticeable changes in their gradient value distributions (Figure 7a), which possibly indicates a lesser extent of maturational functional reconfiguration occurring within these cortical areas as well.

To further characterize the possible maturational shifting of PS-related MCPs across the unimodal-transmodal axis, we quantified changes in their gradient value distributions between age

group maps. For each of the five MCPs of interest, shift function analysis indicated significantly different gradient values at nearly all deciles between each pair of age groups (Figure 8). These results support the idea that MCPs associated with disturbances of self-experience in the PS overlap with cortical areas functionally redistributing along the unimodal-transmodal hierarchy across child, adolescent, and adult age windows.

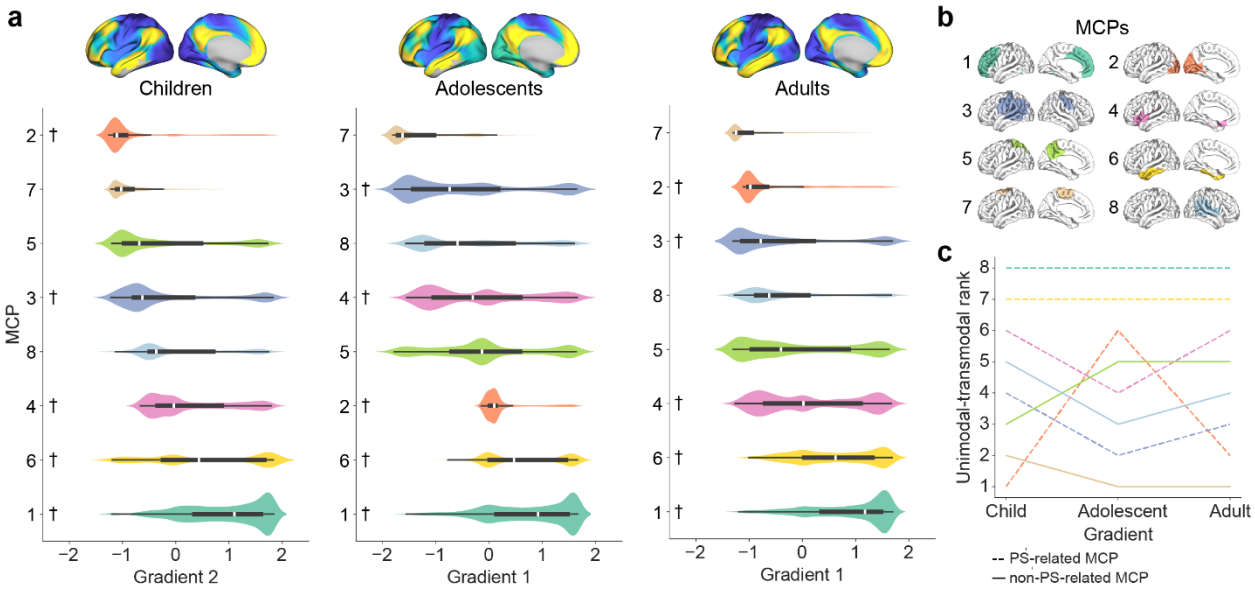

Figure 7. Distributions of the maturational unimodal-transmodal gradients across MCPs. (a) Violin plots depict MCP gradient values per age group map (top), ordered by median. More negative values indicate proximity to the unimodal end of the gradient, and more positive values indicate proximity to the transmodal end of the gradient. The overlaid box plots represent the first, second (median, white) and third quartiles, and the whiskers represent non-outlier end points of the distribution. **(b)** Brain map of each MCP, binarized by labeling each vertex according to its highest weighting. **(c)** The line plot shows the rank of each MCP in each of the ordered violin plots on the left, from 1 (closest to the unimodal end of the gradient) to 8 (closest to the transmodal end of the gradient). In the violin plots (a) and line plot (c), the PS-related MCPs identified by the behavioural PLS analysis are indicated by daggers (†) and dashed lines, respectively.

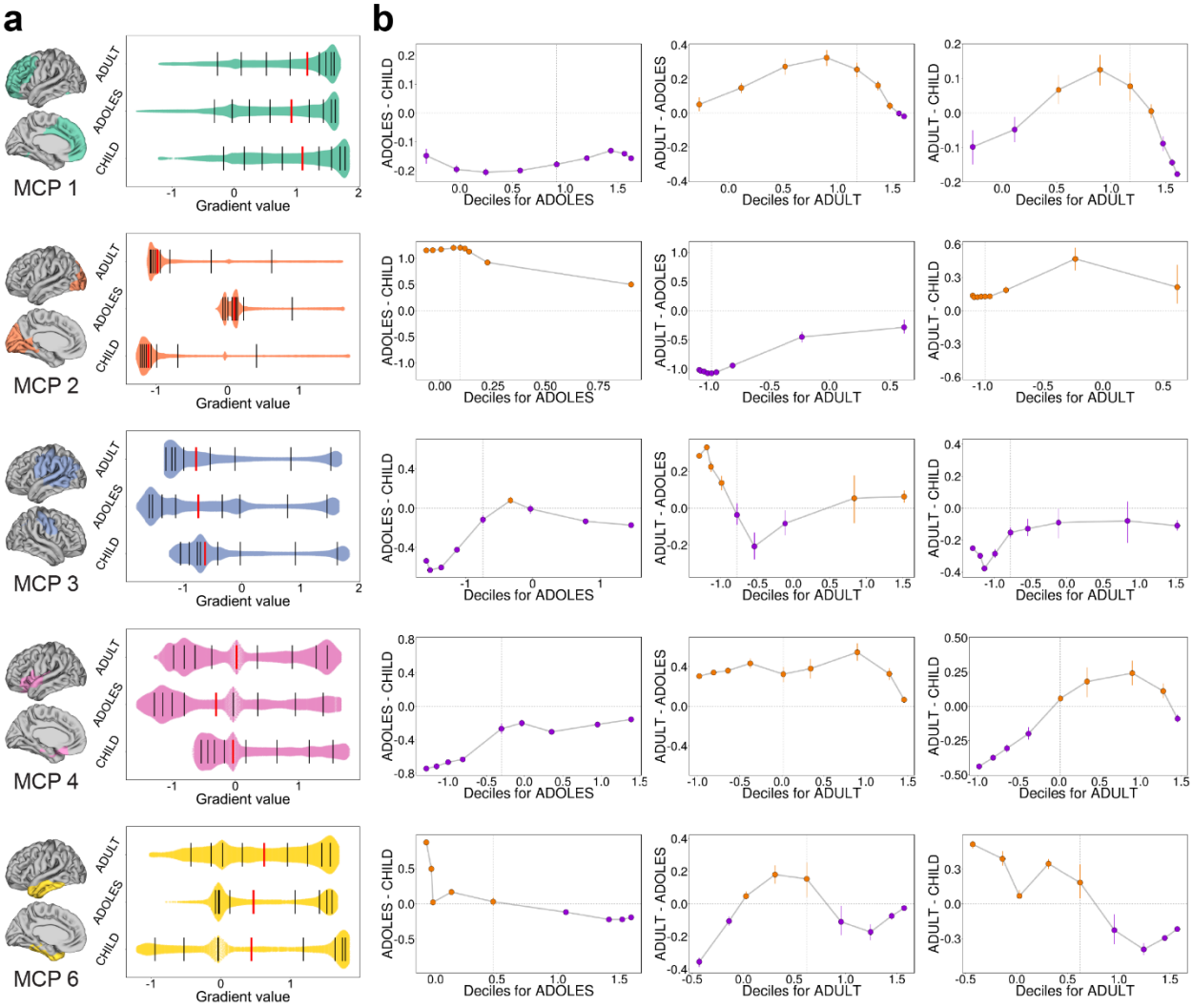

Figure 8. Functional gradient value distributions of PS-related morphometric covariance patterns across maturational gradients. Each row corresponds to a PS-related MCP. **(a)** Column 1: 'Parcel' versions of the PS-related MCPs derived from winner-takes-all assignment of vertices to MCPs. Column 2: Z-scored gradient value distributions from the child (CHILD), adolescent (ADOLES), and adult (ADULT) gradient maps for each MCP, where more positive values indicate proximity to the transmodal end of the gradient. Black lines denote deciles, red lines denote medians. **(b)** Decile differences computed by the shift function for each pair of gradient value distributions per MCP, as a function of the deciles of the older age group map in the pair. The sign of a decile difference is indicated by its colour; error bars denote 95% confidence intervals. E.g., All ADOLES-CHILD decile differences < 0 in row 1 shows that MCP 1 vertices are located significantly closer to the unimodal end of the gradient in the adolescent map than in the child map. The relatively flat curve for this contrast also suggests a consistent magnitude of difference across deciles.

5.6. Dominant transcriptional signatures of morphometric covariance patterns

The first latent variable identified by the mcPLS analysis was significant ($p_{spin} = 0.0020$), and explained 64.8% of the covariance between tissue sample expression levels and MCP membership (Figure 9a). In other words, LV1 revealed a data-driven difference between gene expression patterns of samples located in certain MCPs. The genes contributing most strongly to this difference (i.e., $|BSR| \geq 2.58$) included 6,093 positively weighted genes and 6,888 negatively weighted genes. The contrast values for LV1, which describe the extent to which individual MCPs were associated with the expression of the PLS+ or PLS- gene sets for this LV, are presented in Figure 9b. They indicate that the LV differentiated MCPs 1, 4, and 6 from MCPs 2, 3, 5, 7, and 8, but predominantly separated MCPs 4 (ventral prefrontal/insular) and 6 (anterior/ventral temporal), which most strongly expressed the PLS+ gene pattern, from MCP 2 (visual), which most strongly expressed the PLS- gene pattern. Thus, neuroanatomically, LV1 represents a pattern of gene expression which has a putative frontotemporal–visual cortical gradient (Figure 9b, inset).

Interestingly, we observe that all MCPs corresponding to PLS+ genes (MCPs 1, 4, 6) had been identified as PS-related in our bPLS analysis linking the same MCPs to sociodemographic features and PS symptom dimensions (see Section 5.3).

5.6.1. Genes differentiating MCPs converge with specific cell classes

To better understand the biological significance of the gene sets contributing most strongly to LV1 of MCP expression pattern differences, we examined their enrichment for specific cell classes relative to an ensemble of random gene sets (Figure 9c). PLS+ genes (associated most strongly with ventral frontal/insular and anterior/ventral temporal MCPs) are significantly more expressed in astrocytes (enrichment ratio (ER) = 0.078, $p_{FDR} = 1.4\times10^{-4}$), microglia (ER = 0.049, $p_{FDR} = 1.4\times10^{-4}$), oligodendrocyte precursors (ER = 0.013, $p_{FDR} = 1.4\times10^{-4}$), excitatory neurons (ER = 0.084, $p_{FDR} = 1.4\times10^{-4}$), and inhibitory neurons (ER = 0.060, $p_{FDR} = 0.0030$), and significantly less expressed in oligodendrocytes (ER = 0.034, $p_{FDR} = 1.4\times10^{-4}$) and endothelial cells (ER = 0.049, $p_{FDR} = 0.041$). PLS- genes (associated most strongly with the visual cortical MCP) are significantly more expressed in oligodendrocytes (ER = 0.061, $p_{FDR} = 2.3\times10^{-4}$) and endothelial cells (ER = 0.059, $p_{FDR} = 0.021$), and significantly less expressed in astrocytes (ER = 0.030, $p_{FDR} = 2.3\times10^{-4}$), microglia (ER = 0.034, $p_{FDR} = 0.0049$), and oligodendrocyte precursors (ER = 0.0049, $p_{FDR} = 2.3\times10^{-4}$).

5.6.2. Differential biological process involvement of genes associated with different MCPs

We also explored whether the gene sets differentiating the MCPs in PS youth were preferentially involved in specific biological processes, using annotations from Gene Ontology. Genes from the PLS+ gene set were annotated to a total of 11436 GO biological process categories and showed significant enrichment for 7456 categories. Meanwhile, PLS- genes were annotated to a total of 11497 categories and showed significant enrichment for 8151 categories. A selection of the biological processes that were uniquely enriched in each gene set (PLS+ = 1983 categories; PLS- = 2678 categories) and were most related to brain structure and function are visualized as word clouds in Figure 9d. In general, genes associated with anterior frontal and anterior and ventromedial temporal-localized MCPs (PLS+) appear to be enriched for processes related to signalling between and differentiation of specific neural cell types, while genes associated with posterior frontal, posterior lateral temporal, parietal, and occipital-localized MCPs (PLS-) appear enriched for processes related to the production of supporting cells as well as initial stages of neural development. Notably, each of the positive and negative gene sets shows enrichment for processes directly relevant to the cell classes observed to be over-represented in that gene set based on the cell type enrichment analysis (Figure 9c).

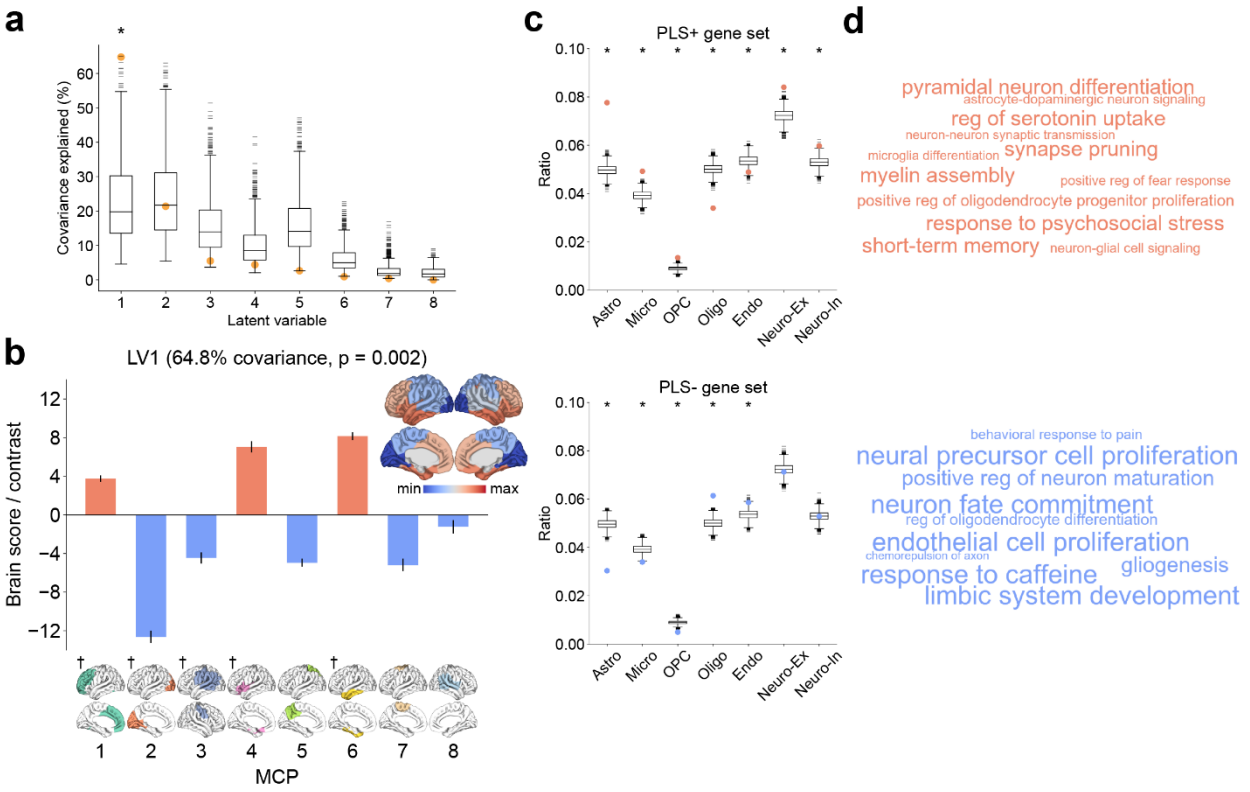

Figure 9. Gene expression patterns maximally differentiating MCPs. (a) The covariance explained by latent variables derived using mean-centered PLS analysis (yellow dots) against distributions of null singular values from a spatial autocorrelation-preserving null model (box plots; 1000 repetitions). * $p < 0.05$. Only the first latent variable was statistically significant and was retained for further analysis. **(b)** MCP contrast values for LV1, as a bar graph and visualized on the group-average brain (inset). MCPs separable by the latent variable have opposite sign contrast values. MCPs with positive values are positively associated with (i.e., show higher expression of) the PLS+ genes, while MCPs with negative values are positively associated with the PLS- genes. Red and blue bars indicate significantly contributing MCPs by their sign; error bars denote 95% bootstrap confidence intervals. The PS-related MCPs identified by the behavioural PLS analysis are indicated by daggers (†). **(c)** Cell class-specific enrichment in the PLS+ (top) and PLS- (bottom) gene sets for LV1. Per gene set, coloured dots represent the true ratio of genes that are preferentially expressed in a cell class. Box plots depict distributions of null ratios obtained using 10000 random gene lists of the same size. * $p_{FDR} < 0.05$. Astro = astrocytes; Micro = microglia; OPC = oligodendrocyte precursors; Oligo = oligodendrocytes; Endo = endothelial cells; Neuro-Ex = excitatory neurons; Neuro-In = inhibitory neurons **(d)** A selection of the neurobiologically-relevant GO biological processes that were significantly enriched in the PLS+ (top) and PLS- (bottom) gene sets for LV1. Note that font size is not informative and was varied only to maximize use of the word cloud space. The box plots in **(a)** and **(c)** represent the first, second (median) and third quartiles, the whiskers represent the non-outlier end points of the distribution, and the horizontal lines represent outliers.

5.6.3. Strongly contributing positive genes are enriched for psychiatric disorders

To explore differences in putative neuropathological relevance of the positive and negative gene sets, we tested the hypothesis that the gene set over-expressed exclusively in PS-related MCPs (i.e., PLS+) is enriched for genes related to psychotic disorders. Using the DisGeNET database, we performed over-representation analysis of Disease Ontology terms in each PLS gene set. Overall, 2421 of the 6093 PLS+ genes (39.7%), and 1394 of the 6888 PLS- genes (20.2%) were annotated to diseases or disorders in DisGeNET. All significantly enriched disease terms are shown in Figure 10, and their corresponding enrichment ratios and FDR-corrected p-values can be found in Appendix Table 6 and Appendix Table 7.

Our results indicate clear differences in the major domains of diseases over-represented in each gene set of interest. Specifically, the PLS+ gene set shows significant overlap with genes associated with several psychiatric disorders, including Unipolar Depression ($p_{FDR} = 6.1\times10^{-3}$), Major Depressive Disorder ($p_{FDR} = 0.016$), and Bipolar Disorder ($p_{FDR} = 0.019$) (Figure 10a). Interestingly, schizophrenia was also among the top 15 most over-represented diseases in the PLS+ gene set, although did not survive FDR correction ($p = 6.8\times10^{-4}$, $p_{FDR} = 0.18$). In contrast, the PLS- gene set showed significant overlap primarily with genes associated with intellectual and developmental disabilities (e.g., Intellectual Disability, Mental Retardation, Cognitive Delay; all $p_{FDR} = 0.021$), but lacked similar enrichment for psychiatric disorder terms (Figure 10b). These differences imply that genes over-expressed in MCPs linked to neuropsychological features of the PS do not necessarily show specific enrichment for psychotic disorder genes, but may instead be uniquely related to the emergence of a variety of psychopathology.

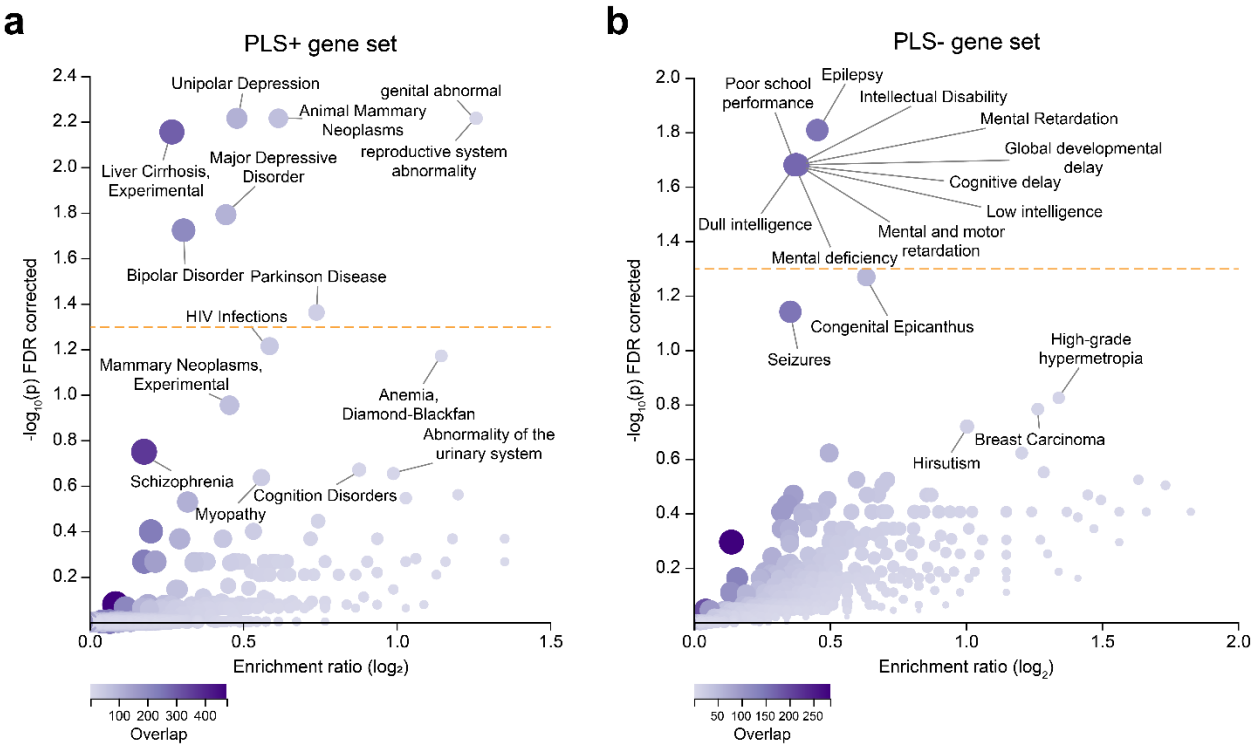

Figure 10. Positive and negative genes contributing to between-MCP differences are differentially enriched for psychiatric disorders. Volcano plots show diseases with gene sets over-represented in the **(a)** PLS+ gene set and **(b)** PLS- gene set for the first latent variable from the mcPLS analysis. The top 15 terms (by FDR-corrected p-value) are annotated. The shade and size of each dot are proportional to the overlap between the disease gene set and the genes in the PLS+ or PLS- gene set that are annotated to a disease in the DisGeNET database. The dashed yellow line corresponds to $p_{FDR} = 0.05$.

6. Discussion

Here, we capitalize on data-driven multivariate methods to decompose cortical morphometry of PS youth into 8 stable, modular patterns of covariance, and find evidence that these morphometric covariance patterns capture individual variation in specific dimensions of PS symptoms. Integrating information from functional connectivity gradients, meta-analytical cognitive states, and gene expression, we further show that MCP vulnerability to PS-related changes are related to large-scale cortical functional and transcriptomic architectures.

6.1. A cortical phenotype of PS integrating multiple morphometric features

There has been ample evidence that the networked nature of brain structure in atypical neurodevelopment may be better characterized via the coordinated variation of different imaging-derived metrics across the cortical sheet (Alexander-Bloch et al., 2013; Kaczkurkin et al., 2019; S. E. Morgan et al., 2019; Seidlitz et al., 2018). In line with this notion, the 8 MCPs identified in the present study, which summarized the spatial covariance of CT, SA, MC, and GI across PS youth, delineated structural units that eschewed classic lobar and gyral boundaries while still remaining highly localized and interpretable. For example, the data-driven PS MCPs subdivided temporal cortex into anterior-ventral, posterior-dorsal, and anterior-dorsal portions that were grouped with other areas in functionally meaningful ways (e.g., left auditory cortical areas belonged to the same MCP as primary sensorimotor areas). This extends previous findings that single-metric covariance patterns derived using OPNMF diverge from traditional atlases based on coarse anatomical characteristics (e.g., Desikan-Killiany-Tourville), and highlight the importance of data-driven parcellations of cortex for better capturing inherent neurobiological coordination (Sanfelici et al., 2021; Sotiras et al., 2017). Notably, although our input to OPNMF contained cortex-wise measurements of 4 different features, the resulting components did not individually resemble the average spatial variation of any single metric. Qualitative comparisons also indicated differences to both thickness-based (Sotiras et al., 2017) and gyrification-based cortical components (Sanfelici et al., 2021). These findings support the efficient integration of information from different morphometric features in all PS MCPs.

Interestingly, despite the present sample being enriched for PS symptoms, the 8 extracted MCPs bear resemblance to similar resolutions of modular cortical communities previously identified using a morphometric similarity network approach (10 morphometric variables) in typically developing adolescents and young adults (Seidlitz et al., 2018). Combined with our exploratory finding that PS MCPs resemble those derived from PNC youth without PS symptoms, these results suggest that the shared patterns of covariance of different macrostructural features may represent variation attributable to a consistent neurodevelopmental phenotype of cortical organization. Additionally, the boundaries of the PS MCPs showed modest qualitative overlap with those of a coarser MCP decomposition in a sample containing autism spectrum individuals. This observation, while also exploratory, is potentially congruent with evidence that OPNMF-derived patterns can capture morphometric signatures across a range of psychopathology (Kaczkurkin et al., 2019; Sanfelici et al., 2021). As PS symptoms themselves are thought to

represent a transdiagnostic psychiatric phenotype (Giocondo et al., 2021; van Os & Reininghaus, 2016), future work investigating cortical areas of high variability or 'instability' between the MCPs found here and those present in different neurodevelopmental psychiatric populations may refine our understanding of cortical vulnerability during maturation.

6.2. Dissociable dimensions of PS symptom variation in youth

The rich assessment of PS features in the PNC presented a unique opportunity to pinpoint major axes of phenotypic variation among youth with distressing levels of symptoms in a data-driven way (Calkins et al., 2015). Specifically, exploratory factor analysis revealed three symptom factors reflecting negative/disorganized symptoms, disturbances of self-experience, and hallucinations/abnormal perceptions. The parsimonious loadings of PS screening items onto these factors suggested that they were well-defined within the sample. Within these factors, the differentiation of negative and disorganized symptoms from positive symptoms is consistent with previous factor analyses of both subthreshold psychotic features (Calkins et al., 2015; Fonseca-Pedrero et al., 2018) and clinical psychotic symptoms (Kotov et al., 2016; Stefanis et al., 2002). Symptoms of disturbed self-experience, such as detachment and feelings of thought control, and perceptual abnormalities, such as verbal hallucinations and auditory perceptions, additionally emerged as dissociable dimensions of positive PS symptoms. These factors captured a separation of sub-delusional (loading onto 'disturbed self-experience') and hallucinatory perceptual symptoms, as has been observed in previous studies examining similarly wide ranges of psychotic symptoms (Calkins et al., 2015; Cardno et al., 1999, 2001). Notably, the three factors identified here also represent a near-replication of a larger-scale factor analysis of the same PS screening tools in the broader PNC cohort (Calkins et al., 2015), further supporting the validity of our findings. This prior study described three specific PS factors (termed '(ideas about) special abilities/persecution', 'unusual thoughts/perceptions', and 'negative/disorganized' symptoms) that largely map onto the symptom dimensions in the current study, along with a general psychosis spectrum factor indicated by all variables (Calkins et al., 2015). While our analysis did not show support for a strong overarching PS factor, this discrepancy could be due to the current sample comprising only PNC participants meeting PS criteria, or the more detailed list of symptom items provided as input for factoring in this study. Nonetheless, our results reinforce that distinct, yet related dimensions of psychosis-related symptoms are present in youth even before the onset of

frank illness. In turn, these findings corroborate the potential of refined symptom clusters over summed scores for resolving heterogeneous neurobiological correlates of the PS (Kirschner, Shafiei, Markello, Makowski, et al., 2020; Peralta & Cuesta, 1999).

6.3. Cortical morphometric signatures of behavioural features in the PS

Our bPLS analysis identified two significant patterns of associations linking MCPs and behavioural features in PS youth. The first brain-behaviour LV captured both previously reported and novel associations between demographic characteristics and cortical morphometry. This LV indicated that among PS youth, older age and European American race are correlated with widespread reduced GI as well as regionally specific cortical thinning or thickening across anterior frontal (MCP 1) or visual and sensorimotor regions (MCPs 2 and 3). These associations align with past findings of age-related decreases in GI (Chung et al., 2017; D. Klein et al., 2014; Raznahan et al., 2011), as well as with the well-established heterogeneity in timeframe of CT maturation between sensorimotor and association cortex, particularly anterior frontal areas (Ball et al., 2020; Sotiras et al., 2017; Whitaker et al., 2016). Intriguingly, the positive direction of CT change in MCPs 2 and 3 contributing to this LV is inverse to the modest cortical thinning typically observed in these primary cortical areas across adolescence (Ball et al., 2020; Raznahan et al., 2011), and also contrasts with the relatively spared or steeper rates of thinning seen in overlapping areas in early stages of clinical psychosis (Lin et al., 2019; Pina-Camacho et al., 2022; Ziermans et al., 2012). However, consistent with a link between thicker cortex in motor and occipital regions and psychological resilience (de Wit et al., 2016; Kahl et al., 2020), it is possible that our results point to early compensatory mechanisms that serve to protect against emerging PS-related neural changes. In addition, our inclusion of race variables in the bPLS analysis provided insights into how social environment may influence cortical morphology that increases risk for neuropsychiatric disorders. To our knowledge, we present the first evidence that a global pattern of primarily decreased GI with age may be related to European American race in PS youth. This result complements increasing reports that both cross-sectional measurements (Isamah et al., 2010) and age-related slopes (Assari & Mincy, 2021; Choi et al., 2020) of cortical morphological features are associated with race and ethnicity.

Significantly, the second brain-behaviour LV highlighted associations involving the disturbed self-experience PS dimension, suggesting the relevance of this pattern to distinct

phenomenological aspects of the PS. In this LV, greater disturbances of self-experience, alongside characteristics of older age, male sex, and African American race mapped onto diverse morphometric alterations across five MCPs. Contributing cortical features were specifically distributed across anterior frontal (CT increase, GI decrease), ventral prefrontal/insular (GI decrease), anterior/ventral temporal (SA decrease), and visual (MC decrease) as well as primary sensory and motor regions (CT decrease). Notably, while the morphometric pattern of this LV recapitulated certain abnormalities previously found in high-risk or PS individuals (e.g., reduced cortical folding in prefrontal (Damme et al., 2019; Drobinin et al., 2020) and occipital regions (Drobinin et al., 2020; I. Park et al., 2021), greater prefrontal CT (Kirschner et al., 2021), reduced sensorimotor CT (Dukart et al., 2017; Vargas & Mittal, 2022)), other common structural findings were absent, such as thinning of insular (Gisselgård et al., 2018; van Lutterveld et al., 2014) and inferior/medial temporal cortex (Gisselgård et al., 2018; Jung et al., 2011; Takayanagi et al., 2020; van Lutterveld et al., 2014), decreased SA in anterior frontal and cingulate regions (ENIGMA Clinical High Risk for Psychosis Working Group et al., 2021; Jalbrzikowski et al., 2019), and precuneus abnormalities (Meller et al., 2020; Satterthwaite et al., 2016). However, this discrepancy is consistent with previous findings mainly reflecting either case-control differences or, occasionally, correlates of coarse 'positive' and 'negative' symptom clusters, in contrast to the more complex PS dimensions considered here. Instead, our observed correlation of the unique morphometric pattern of LV2 with the disturbed self-experience factor, but not other PS factors, is suggestive of an effect tapping into a brain signature related to this specific dimension of positive symptoms. These results broadly indicate that different symptom dimensions of the PS may reflect dissociable, targeted abnormalities across multiple cortical morphometric features, complementing dimensional cortical deficits observed in clinical populations (Kirschner, Shafiei, Markello, Makowski, et al., 2020).

Corroborating this idea, the MCPs shaping the second brain-behaviour pattern converge markedly with neuroanatomical substrates thought to underlie symptoms loading highly onto the disturbed self-experience PS dimension, namely delusional thoughts (e.g., 'paranoia', 'thought control') and depersonalization (e.g., 'loss of sense of self', 'detachment'). In psychosis patients, delusions have been associated with macrostructural abnormalities in the prefrontal cortex, insula, temporal pole and medial temporal cortex, as well as left parietal areas (Cascella et al., 2011; Prasad et al., 2004; J. Song et al., 2015; Whitford et al., 2009; Wolf et al., 2020; Zhu et al., 2016).

Depersonalization symptoms, which are also observed in both prodromal and disorder stages of psychosis (Büetiger et al., 2020; Madeira et al., 2016; Raballo et al., 2011), have been linked to a network of regions thought to be important for somatosensory integration and the generation of subjective experiences, which includes orbitofrontal and medial prefrontal cortex, primary sensory cortices, insula, and medial temporal cortex (Bonoldi et al., 2019; Büetiger et al., 2020; Daniels et al., 2015; Medford et al., 2016; Sierra et al., 2014). Thus, cortical regions historically implicated in the symptoms represented here by the 'disturbed self-experience' PS dimension were also well represented in the brain pattern correlated with this dimension in our analysis. Importantly, since relevant past studies primarily focused on volumetric abnormalities, the metric-specific weights of LV2 also provide a finer-grained view into the possible cortical morphometric signature of these delusion and depersonalization-like symptoms in the PS. The demographic features of LV2, meanwhile, provided additional insights into this putative PS dimension-cortical morphometry relationship. While the association of male sex and African American race with LV2 echoes previously reported demographic correlates of PS status among youth (Calkins et al., 2014), higher levels of PS symptoms have typically been linked to younger age (Calkins et al., 2014; Kelleher, Connor, et al., 2012), contrary to the inverse age effect captured by LV2. This finding may be concordant with evidence that while PS symptoms are more common in early adolescence, they become increasingly indicative of pathology with age (Kelleher, Keeley, et al., 2012), suggesting that the cortical morphometric pattern of LV2 may represent the neuroanatomical imprint of more aberrant psychological phenotypes in older youth.

Surprisingly, despite representing core clinical features of psychosis, the hallucinations/abnormal perceptions PS dimension did not contribute to either of the significant detected brain-behaviour relationships. This is possibly attributable to earlier stages of pathophysiology being captured by the young, non-help-seeking PS sample in the current study, in which anatomical concomitants of threshold-level hallucinations, which may imply progressive neural alterations, are likely to be less well-established. Nonetheless, both the sub-delusional and depersonalization symptoms represented by the disturbed self-experience dimension have been found to predict later transition to psychosis in at-risk cohorts (Cannon et al., 2008; Zammit et al., 2013), emphasizing the clinical relevance of the identified PS dimension-morphometry pattern for understanding emerging psychosis risk.

Overall, our bPLS analysis builds on previous work relating case-control differences or aggregate symptom measures to single indices of cortical structure in help-seeking patients. Our approach takes a step towards a more nuanced understanding of multimodal phenotypic axes of the PS at a critical age window, using an integrative framework that considers concise representations of complementary cortical features and symptom relationships simultaneously. We show that in doing so, parsimonious brain-behaviour patterns can be derived which capture more refined, yet still interpretable, mappings between developmentally relevant individual clinical variation and morphometric abnormalities.

6.4. The contribution of age to maturational MCP-behavioural LVs

While age contributed strongly to both the first and second brain-behaviour relationships, this effect was expected given the relatively large maturational window under investigation, which covers a period of extensive cortical remodeling (Keshavan et al., 2014; Paus et al., 2008). We note the alternative strategy of regressing age out of brain variables prior to PLS analysis, which has been used in attempts to isolate effects related more "purely" to pathology (Kirschner, Shafiei, Markello, Makowski, et al., 2020; Shan et al., 2022). However, given the normative sample of youth analyzed here and the known relationship between PS vulnerability and neurodevelopment (Calkins et al., 2014; Mennigen & Bearden, 2020), in the current study we were interested in the interaction of maturational processes with PS-related phenotypic variation. Thus, age was not treated as a cofounding variable to prevent masking important maturational effects (Mihalik et al., 2020).

6.5. Convergence of PS-related MCPs with relevant cognitive functions

Previous studies have shown a correspondence between NMF-delineated neuroanatomical covariance components and brain areas that are activated in related psychological processes (Robert et al., 2021; Shan et al., 2022), suggesting that shared covariation in macrostructural features may index functional coherency (Seidlitz et al., 2018). In the present report, we extend these findings to maturational cortical MCPs that integrate four different T1w morphometric features. Specifically, meta-analytic decoding using Neurosynth revealed specialized functions associated with each MCP, with minimal overlap in the top psychological terms correlated with each cortical pattern. We note that the marked specificity of the functional associations per MCP

provides an informal proof of concept for the choice of NMF decomposition resolution, as it supports that the 8 derived components capture meaningful intra-component similarity while also being distinguishable along multiple dimensions of cortical organization.

Significantly, the meta-analytic functional profiles of the MCPs that define the identified symptom-morphometry LV (i.e., MCPs 1, 2, 3, 4, and 6 in LV2) match cognitive processes thought to be perturbed in symptoms driving the associated PS dimension of disturbed self-experience. MCP 1 (anterior frontal) was related to cognitive control processes including "reasoning" and "decision[s]", which are impaired in the formation and maintenance of tenacious irrational beliefs central to delusion-like symptoms (Dudley et al., 2016). MCP 4 (ventral prefrontal/insular) was associated with affect terms such as "fear", "pleasant", and "unpleasant", which provides a mapping to the sense of emotional disconnect with one's life reported in psychosis (Büetiger et al., 2020; Wylie & Tregellas, 2010) and captured here in PS youth by the disturbed self-experience dimension. Furthermore, the term associations of MCP 4 are in line with theories that aberrant fear and anxiety processing contribute to the development of paranoid ideation (Perez et al., 2015), which also loads onto disturbed self-experience. MCP 6 (anterior/ventral temporal), which encompasses anterolateral and parts of inferior medial temporal cortex, was unsurprisingly related to semantic memory. The contribution of this MCP to the cortical pattern linked to disturbed self-experience (i.e., LV2) thus may reflect proposed links between aberrant semantic processing and both altered autobiographical memory, which is crucial for an intact sense of self (Berna et al., 2016; Mediavilla et al., 2021; Prebble et al., 2013), and delusional ideation (Kiang et al., 2013; Rossell et al., 1999). Finally, MCPs 2 (left lateralized sensorimotor/language) and 3 (visual) were correlated with verbal/non-verbal communication and visuo-spatial process terms, respectively. While the relatively lower-order functional specializations of these MCPs have less clear-cut relationships to the psychological disturbances shaping LV2, we posit that the implicated aberrant morphometry in these regions point more broadly to deficits in multisensory integration or perceptual coherence, which have been shown to be crucial for normal self-experience and reality representation (Postmes et al., 2014). Overall, this analysis illustrates a clear connection between the psychological functions subserved by MCPs contributing to LV2 and disturbances of self-experience, supporting that the morphometric pattern of this LV captures a clinically relevant dimension of the PS.

6.6. Cortical PS vulnerability and MCP organization along maturational functional gradients

There is evidence that intrinsic networks of cortical areas are ordered in anatomical space along macroscale gradients of functional organization of the cortex (Margulies et al., 2016). Significantly, the relative positions of networks along these gradients show non-uniform developmental changes as the principal gradient transitions to a mature unimodal-to-transmodal processing hierarchy (H.-M. Dong et al., 2021), suggesting that anatomical vulnerability to atypical neurodevelopment may also be governed locally by this reorganizing large-scale functional architecture.

Here, we found that MCPs in PS youth, which represent shared cortical "networks" based on morphological properties (Sotiras et al., 2017), varied in the specificity of their local functional topography within an established principal gradient in adolescents (H.-M. Dong et al., 2021). While some MCPs comprised vertices that clustered at similar positions along this gradient, such as MCP 2 (visual) or MCP 7 (paracentral), several others captured extensive ranges of gradient values that overlapped, such as MCP 3 (left-lateralized sensorimotor/language) and MCP 4 (ventral prefrontal/insular). Notably, the five MCPs related to disturbed self-experience by bPLS analysis were not preferentially localized to a specific position within the adolescent principal gradient, instead occupying both unimodal and transmodal functional territories. The results of this single-gradient analysis thus may be in line with recent evidence for an overall compressed sensorimotor-to-transmodal hierarchical organization in schizophrenia, which leads to diminished functional separation between sensory and association regions in gradient space (D. Dong et al., 2021). Namely, we showed that cortical areas with dissociable gradient positions in a typically developing cohort (H.-M. Dong et al., 2021) cluster into the same MCPs in PS youth, which could indicate macrostructural evidence of reduced unimodal-transmodal functional differentiation even in subclinical phenotypes. Furthermore, there is direct qualitative overlap between the MCPs linked to disturbed self-experience and regions of schizophrenia case-control difference in principal gradient value (D. Dong et al., 2021). One speculative interpretation is that patterns of morphometric alterations linked to psychosis risk, particularly to sub-delusional symptoms or incoherent subjective experience, may be coupled to aberrant functional connectivity that underpins a pathological global processing hierarchy of cortex.

While the wide distribution of PS-related MCPs along the unimodal-transmodal gradient was present throughout the child, adolescent, and adult gradient maps, we observed non-uniform maturational shifts in positions of MCPs within this emerging hierarchy. Notably, MCPs linked to disturbed self-experience comprised both MCPs that showed age-dependent changes in rank within the gradient (MCPs 2-4), implying continued refinement of their embedding within macroscale processing streams, as well as MCPs that represented more stable anchors of the developing transmodal-dominant gradient profile (MCP 1, MCP 6). Regardless of their trajectory within the hierarchy, however, all MCPs associated with this symptom dimension captured clear qualitative and quantitative changes in the local distributions of gradient values with age. Overall, these findings may suggest that regions undergoing protracted refinement within the global connectivity structure, namely to support increasing separation between primary sensory/motor and association cortex (H.-M. Dong et al., 2021), are also more vulnerable to PS-related changes. These findings complement evidence that an imbalance of information integration and segregation across sensorimotor and association areas, which is linked to abnormal development of an overarching unimodal-transmodal hierarchy, contributes to susceptibility for psychotic symptoms (D. Dong et al., 2021; Duan et al., 2019). We emphasize, however, the exploratory nature of these interpretations, as the gradients compared here with PS MCPs are representative of typically developing youth and healthy adults. Future work aligning MCPs and functional gradients both derived from PS data will be important for clarifying the relationship between morphometric abnormalities and macroscale functional organization in this early stage of neural risk for psychosis.

6.7. Transcriptional profiling of PS MCPs and putative links to structural vulnerability

6.7.1. An anterior frontotemporal-visual axis of MCP expression pattern differences

In an effort to bridge macroscale cortical patterns with putative molecular mechanisms, we explored whether MCP vulnerability to PS-related abnormalities may be underpinned by regional variation in gene expression. Since our bPLS analysis (i.e., LV2) linked feature-specific morphometric variation to PS symptoms at the level of MCPs, to connect this symptom-morphometry relationship to the underlying neurobiology, we first used mcPLS to isolate sets of genes whose expression patterns differentiated the PS-derived MCPs themselves. A single

significant transcriptional latent variable was found which maximally differentiated the ventral prefrontal/insular and anterior/medial temporal MCPs (MCPs 4 and 6, respectively) from the visual MCP (MCP 2). Notably, this axis of MCP expression pattern differences largely recapitulates the first principal component of transcriptional variation in the AHBA (PC1 of gene expression), which separates primary visual, sensorimotor, and auditory cortical areas at one end from transmodal frontal and temporal areas at the other (Burt et al., 2018; Hawrylycz et al., 2012). Both our transcriptional LV and the previously established PC1 of gene expression demonstrate a rough rostral-caudal organization. These overarching similarities make sense given that no *a priori* contrasts between MCPs were enforced in our exploratory mcPLS, permitting dominant axes of transcriptional structure to be detected. However, the spatial pattern of our transcriptional LV also bore distinct features. Specifically, although the sensorimotor MCP (3) shared the same *sign* of contrast value as the visual MCP (2) in this LV, indicating shared directionality with regards to the underlying expression pattern, MCP 2 had a clearly dominant contribution (i.e., contrast value *magnitude*) to the overall axis of differentiation. By contrast, in PC1 of gene expression, one end is more or less equally anchored in both sensorimotor and visual areas (Burt et al., 2018; Hawrylycz et al., 2012). While subtle, this difference may suggest that inter-regional morphometric coordination in PS youth, as summarized by MCPs, captures meaningful clusters of local transcription patterns that highlight a more strongly visual cortex-anchored axis of variation as opposed to a general sensorimotor to association organization (Huntenburg et al., 2018). For simplicity, we consider all contributing MCPs when contextualizing each dimension of the transcriptional LV below.

Within the context of the previously described symptom-morphometry relationship (Section 5.3), the LV of MCP gene expression differences separated three of the five MCPs linked to disturbed self-experience (i.e., MCPs 1 [anterior frontal], 4 [ventral prefrontal/insular], and 6 [anterior/medial temporal]) from all other MCPs. In other words, while the dominant pattern of MCP transcriptional differences was not entirely driven by our identified PS-related MCPs, it did capture a set of genes (denoted PLS+) with exclusively higher expression in anterior MCPs contributing to the symptom-morphometry pattern in our PS sample. The gene sets characterizing the positive versus negative dimension of this LV thus represented a window into possibly divergent molecular contributions of anterior frontotemporal MCPs versus visual/posterior MCPs, respectively, to PS phenotypes.

Here, genes over-expressed in anterior frontotemporal MCPs were associated positively with astrocytes, microglia, oligodendrocyte precursors, and neurons. Meanwhile, genes over-expressed in visual/posterior MCPs were associated with oligodendrocytes and endothelial cells. Recalling that anterior frontotemporal MCPs independently showed macrostructural changes linked to PS symptoms (brain-behaviour LV2), these results indicate enrichment for genetic signal of both neuronal and glial cells in heteromodal regions vulnerable to PS-related structural changes. This is consistent with prior reports of cellular correlates of schizophrenia CT signatures (Di Biase et al., 2022; Writing Committee for the Attention-Deficit/Hyperactivity Disorder et al., 2021), despite corresponding cell type signatures for other T1w imaging metrics being under-investigated. Nonetheless, given that brain-behaviour LV2 highlighted contributions of several feature alterations in anterior frontotemporal MCPs to a clinical-behavioural PS phenotype (i.e., higher CT and lower GI in MCP 1, lower GI in MCP 4, and lower SA in MCP 6), our results suggest that pathogenic interactions among multiple neural cell types likely lead to macroscale abnormalities in multiple inter-related cortical properties simultaneously.

Interestingly, the expression signature of the PS-related anterior frontotemporal MCPs was uniquely enriched for synaptic signalling processes in addition to processes of differentiation of cell types over-represented in this gene set. Convergent evidence for the role of synaptic dysfunction and pathology in psychosis risk has been found in both post-mortem (Berdenis van Berlekom et al., 2020) and neuroimaging analyses. In a morphometric similarity mapping study of psychosis patients, abnormal morphometric similarity in frontal and temporal cortical areas was related to expression of genes enriched for synaptic signalling (S. E. Morgan et al., 2019), consistent with the spatial enrichment pattern observed here. Moreover, in a typically developing cohort, the patterning of effects of schizophrenia polygenic risk score on CT in frontotemporal areas was associated with expression of dendrites and synapses (Kirschner et al., 2022), suggesting that aberrant synapse development may contribute to macrostructural changes even in nonclinical expressions of psychosis vulnerability. Extending these findings, our multi-scale analyses allude to the possibility that a diverse pattern of associations between CT, GI, and SA changes in frontotemporal MCPs and subclinical positive PS symptoms in youth may be linked to molecular susceptibility of signalling processes. Critically, emerging evidence that microglia and astrocytes can mediate pathological synaptic pruning, synapse formation, or glutamatergic signalling in

schizophrenia (R. Kim et al., 2018; Sellgren et al., 2019) further bridges the cellular and biological process enrichment patterns of this anterior frontotemporal system.

By contrast, the expression signature of the four visual/posterior MCPs (i.e., negative dimension of the transcriptional LV) was more heavily enriched for processes related to early central nervous system development and the production of supporting cells. Combined with the enrichment of this gene set for oligodendrocyte and endothelial cell markers but not neuron markers, these results possibly suggest that the MCPs contributing to this dimension that also weight onto the symptom-morphometry LV (i.e., MCP 2 [visual] and MCP 3 [left-lateralized sensorimotor/language]) are part of a differing neurobiological vulnerability pathway potentially related more closely to early precursor or glial cell development than protracted refinement of neuronal functions. Interestingly, this interpretation may be aligned with the known earlier maturation of primary sensorimotor and visual cortical areas compared to frontal and temporal association areas (Sydnor et al., 2021).

6.7.2. Putative neurobiological interpretations of the symptom-morphometry LV

Each of the four cortical morphometric features considered in the present report are influenced by multiple neurobiological processes throughout maturation. While we cannot derive feature-specific mechanisms for the latent symptom-morphometry pattern observed in our PS sample, we hypothesize based on our transcriptomic analysis results (Section 5.7.1) that cortical metric abnormalities implicated in the anterior frontotemporal MCPs may be disproportionately driven by factors related to synaptic organization. Specifically, CT has been shown to be sensitive to dendritic arborization and synaptic pruning (Huttenlocher, 1990; T. Jeon et al., 2015), with evidence supporting both synaptic loss driving the CT reductions observed in adults with schizophrenia (Berdenis van Berlekom et al., 2020; Carlo & Stevens, 2013), and a potentially delayed or amplified (i.e., higher peak, steeper decline) trajectory of pruning contributing to thicker cortex in children or adolescents at genetic risk for psychosis (Kirschner et al., 2022). Molecular correlates of psychosis abnormalities in SA and GI remain under-investigated; nonetheless, typical patterns of SA maturation have been linked to synaptogenesis as well as myelination in the neuropil (Budday et al., 2015b; Cafiero et al., 2019), and follow an earlier time course compared with CT (Wierenga et al., 2014). Relatedly, neurogenesis and neuropil growth are thought to represent cellular-level determinants of cortical GI (Llinares-Benadero & Borrell, 2019).

In contrast with these processes of synaptic growth and remodelling, we posit that the visual and sensorimotor MCP-specific feature alterations also contributing to the symptom-morphometry LV may be linked to early development of neural or glial scaffolding of cortex more broadly. For example, the PS-related cortical thinning in MCP 3 may be related to atypical glial support in cortical columns or myelination, factors that can also affect this metric (Natu et al., 2019; Rakic, 1988). The reduction in visual cortical MC, while less well understood, could be influenced by changes in mechanical properties or the stress state of cortical layers, characteristics typically established by early childhood, due to disruptions in radial migration of neural cells, oligodendrocyte development, or myelin production (Annese et al., 2004; Budday et al., 2015b). Importantly, it is conceivable that these changes have downstream effects on synaptic organization (Takahashi et al., 2011), underscoring that dissociable cellular-level processes likely interact to give rise to the spatially varying morphometric signature associated here with the disturbed self-experience PS dimension.

Overall, we hypothesize that the identified symptom-morphometry pattern in PS youth reflects multiple abnormal neurobiological trajectories, which may include delayed or amplified synaptic pruning, neuronal death, and impaired myelination, as well as early developmental vulnerability related to the maturation or patterning of neural precursor and support cells in the cortical sheet.

6.7.3. A gene expression signature of anterior frontotemporal MCPs is enriched for psychiatric disorders

By comparing gene sets characterizing the anterior frontotemporal (PLS+) versus visual/posterior (PLS-) dimensions of the transcriptomic LV to a large database of gene-disease associations (Piñero et al., 2017), we found significant enrichment of unique disorder terms in each system of MCPs. Notably, only PLS+ genes, whose over-expression was limited to PS-related MCPs, were significantly enriched for psychiatric disorder terms, supporting the psychopathological relevance of the anterior frontotemporal abnormalities in the PS symptom-morphometry LV. By contrast, the PLS- genes associated with visual/posterior MCPs showed nearly exclusive significant enrichment for intellectual and developmental disabilities. In the context of the bPLS-derived behavioural pattern shaped by disturbed self-experience in the PS, these enrichment results lend credence to the idea that differing types of neurobiological events may underlie the significant morphometric correlates found in the anterior frontal, ventral

prefrontal/insular, and anterior/ventral temporal MCPs versus the left-lateralized sensorimotor/language and visual MCPs.

While the psychiatric disorder enrichment of the anterior frontotemporal MCP gene set was driven by genes associated with affective disorders (e.g., bipolar disorder, unipolar depression), schizophrenia was also among the top over-represented terms. These results are consistent with the overlap in cortical gene expression profiles between psychotic and affective disorders, suggesting shared molecular underpinnings of macroscale disorder phenotypes (Gandal et al., 2018; Kirschner et al., 2022; Writing Committee for the Attention-Deficit/Hyperactivity Disorder et al., 2021). Moreover, the convergence of this enrichment signature with MCPs linked here to a PS symptom dimension is in line with evidence for the transdiagnostic psychiatric risk imparted by PS symptoms, particularly for the later development of mood disorders (Calkins et al., 2017; Giocondo et al., 2021; van Os & Reininghaus, 2016). This interpretation is also supported by a recent neuroimaging study, which showed that the transcriptional pattern correlated with schizotypy-related magnetization was enriched by genes differentially expressed in disorders including both schizophrenia and bipolar disorder (Romero-Garcia et al., 2020). Broadly, our findings suggest that the structural vulnerability to PS-related changes captured by MCPs may be embedded within a broader axis of molecular cortical organization. Specifically, we find evidence that this axis differentiates areas more closely associated with synaptic remodelling and expression of psychiatric disorder-related genes, from areas enriched for substrates of early cortical growth and genes related to intellectual disabilities.

6.8. Summary of key methodological strengths

A key strength of the present study was the focus on a community-based, non-help-seeking sample of PS youth. This enabled the characterization of cortical morphology in the PS during a critical neurobiological vulnerability window (Paus et al., 2008), while also helping to circumvent typical confounders in clinical psychosis populations, such as medication use or illness chronicity. In addition, the acquisition of all brain structural scans on a single scanner safeguarded against morphometric heterogeneity owing to batch or site effects. Another major strength of this work was the integration of multiple MRI-derived indices to delineate cortical MCPs. By harnessing complementary information from four morphometric features (CT, SA, MC, GI), we obtained representations of cortical variability in PS youth that permitted insights into local relationships of

different morphological metrics, contrasting with the unidimensional neurobiological perspectives offered by past studies of individual features. Furthermore, by demonstrating overall replicability of the identified MCPs in two non-overlapping samples, we reveal how integrating multiple measures allows us to develop stable cortical covariance phenotypes that may be recognizable in other age groups and diseases. Significantly, we also mapped individual morphometric variation to clinical-behavioural features of the PS using a single multivariate framework. This data-driven approach allowed interdependencies among both brain and behavioural features to be considered simultaneously, thus overcoming conceptual and statistical drawbacks of univariate analyses, which treat different cortical locations and phenotypic predictors as independent from one another (Genon et al., 2022). Meanwhile, by specifically performing the multivariate mapping with MCP-specific loadings and major dimensions of PS symptoms, we not only established a subject-to-feature ratio that would be at low risk of yielding unstable effects (Helmer et al., 2020), but ensured that resulting associations would still be interpretable despite their pleiotropic-like nature (e.g., in comparison to a model comprising many individual symptom items). In doing so, we were able to reveal a parsimonious symptom-morphometry pattern that, in concert with the original MCPs, provided a PS-linked neuroimaging foothold from which to interrogate underlying functional and molecular correlates.

6.9. Limitations and Future Directions

The present findings should be interpreted in light of several limitations. While our sample is larger than or comparable to most previous MRI studies of PS youth (e.g., (Jalbrzikowski et al., 2019)), its size is still limited relative to PS datasets attainable from newer population-based developmental neuroimaging cohorts with many thousands of participants, such as the ABCD study (Karcher, Loewy, et al., 2022). We note, however, that the PNC currently covers a much larger age range than the ABCD, which enabled characterization of age-related brain-behaviour relationships in the current work. More broadly, the spectrum of maturational stages (i.e., late childhood, early adolescence, late adolescence/early adulthood) and unique non-help-seeking symptom phenotypes captured by our PS sample make it difficult to find a comparable out-of-sample validation dataset. Nonetheless, future replication of the identified MCPs and symptom dimensions in an independent, conceptually related PS sample or more widely available clinical

high-risk cohorts could shed crucial insights into the generalizability of the brain-behaviour associations observed here.

Another limitation of the present work relates to the variation in smoothing level of each analyzed surface-based MRI metric, due to our choice to use the metric-specific recommended defaults for smoothing kernel size in either CIVET v2.1.1 (for CT, SA, and MC) (http://www.bic.mni.mcgill.ca/ServicesSoftware/CIVET) or surfaceratio v5 (for GI) (Toro et al., 2008). This choice was in line with previous applications of OPNMF on multi-metric imaging data (Ochi et al., 2022; R. Patel et al., 2022), as well as with kernel sizes employed in past vertex-wise analyses of the individual metrics investigated here (Lerch et al., 2006; Lyttelton et al., 2009; Toro et al., 2008). Nonetheless, it is possible that the differentially smoothed input data compromised the ability of the OPNMF-derived cortical MCPs to capture individual variability in each metric equally. Based on findings that smaller smoothing kernels may preserve more of the variability within CT data (Zeighami & Evans, 2021), follow-up work reproducing the MCPs using metrics smoothed with a smaller or consistent kernel size may be important for demonstrating the robustness of the identified cortical patterns.

As is often the case with unsupervised methods like NMF, the appropriate choice of number of components, or MCPs in this case, also represents a key methodological consideration. Here, we followed previous NMF studies in selecting an MCP resolution that achieved a suitable balance between pattern stability across subjects and capturing major changes in reconstruction accuracy (R. Patel et al., 2020; Sotiras et al., 2017). Importantly, while our choice of 8 MCPs satisfies an algorithmic concept of optimal dimensionality, it likely does not represent the "true" or definitive number of morphological patterns in the cortex. NMF decompositions demonstrate a hierarchical structure, in which higher resolutions of components subdivide the components at lower resolutions while largely respecting the boundaries of the coarser partitions (Ball et al., 2019; Sotiras et al., 2015, 2017). Thus, rather than being necessarily nearer to or farther from a ground truth of biological granularity, different component resolutions may localize cortical variability on a different scale, such that the "correct" resolution for a study could depend on the study aims and level of detail desired (Groves et al., 2012). In the context of our multi-metric implementation of NMF, 8 MCPs ensured a manageable number of subject-specific metric loadings (n = 32) for the downstream behavioural PLS analysis results to be easily interpretable at the level of each contributing morphometric feature. Similarly, whereas a very fine-grained decomposition

increases the complexity of contextualizing individual MCPs in terms of other modes of cortical organization, our chosen resolution could be easily imposed on external datasets such as Neurosynth, yielding coherent and dissociable functional specializations of MCPs. We note that alternative approaches may exist to analyzing a single resolution of MCPs. A recent application of NMF suggests that evaluating structural covariance components across a range of scales simultaneously can reveal more nuanced relationships with genetic architecture, and possibly provides more discriminative imaging signatures of illness (Wen et al., 2022). Future investigation of so-called "multi-scale" MCPs in the PS may thus enable the refinement of the observed clinical-anatomical associations within a multi-scale topology, and in turn, amplify their potential as a marker of individualized vulnerability to psychosis.

Another caveat of this study is that we did not consider cognitive measures in our PS sample aside from WRAT-4 Reading standard scores (as an IQ estimate), which notably did not attain significance in either of the identified brain-behaviour latent variables. Importantly, PS youth show deficits in multiple neurocognitive domains (Calkins et al., 2014; Gur et al., 2014), which have been found to be differentially associated with abnormalities in cortical morphology (Jalbrzikowski et al., 2019; Satterthwaite et al., 2016). Thus, additional research will be necessary to evaluate whether the observed relationship between MCP-feature alterations and the disturbed self-experience PS dimension may be modulated by neurocognitive functioning. In line with a multidimensional view of psychopathology, PS symptoms also often co-occur with symptoms of other psychopathology domains, including symptoms of depression, mania, and anxiety (Calkins et al., 2014; J. H. Taylor et al., 2020). Future examination of the impact of comorbid symptoms will be critical for establishing the specificity of the present brain-behavioural findings, as well as for a more holistic understanding of the three PS symptom dimensions detected here.

The external datasets used here also have associated methodological considerations. For one, the text-based mapping of psychological terms to functional activation coordinates in Neurosynth cannot distinguish activations from deactivations (Yarkoni et al., 2011). Thus, we identified cognitive functions associated with the spatial patterning of morphometric covariance across cortical regions, but cannot isolate the direction of effect. Additionally, since the AHBA was constructed using tissue samples from a small number of adult post-mortem brains (Hawrylycz et al., 2012), it is not fully representative of transcriptomic variation related to early life or maturational processes, contrary to the epoch of interest in the current work. We note that the

AHBA currently provides the best available spatial resolution for transcriptomic analysis of cortex-wide macrostructural patterns, as existing developmental gene expression atlases have significantly sparser anatomical coverage (Keil et al., 2018).

Given the cross-sectional nature of the PNC data, our findings also preclude conclusions about how atypical morphometry patterns across MCPs may be related to eventual help-seeking behaviour or onset of a first episode of psychosis. Importantly, there is evidence that distressing PS symptoms which are also persistent over time are associated with the most severe functional and mental health impairments in youth (Karcher, Loewy, et al., 2022). The use of longitudinal datasets capturing an extended period of development, as they become available, holds potential to substantiate the presented brain-behavioural relationships and clarify the extent to which cortical MCPs in the PS capture neural risk of transition to more severe psychopathological states.

7. Contributions and Conclusion

The present work adds to a growing understanding that individual psychosis spectrum symptoms do not occur in isolation, and neurobiologically reflect distributed changes across networks of areas rather than mapping precisely to individual loci. Leveraging an informative timeframe for psychopathology development, we delineate a succinct, data-driven representation of cortical morphometric organization in PS youth that integrates complementary information from cortical thickness, surface area, mean curvature, and local gyrification index. The identified 8 morphometric covariance patterns provide an alternative to existing anatomical atlas definitions that can be easily applied to new datasets and is readily comparable to other maps of cortical organization. We also uncover a novel multivariate mapping between individual morphometric variation in MCPs and a latent PS dimension defined by disturbed self-experience, and benchmark the contributing "PS-related" MCPs against functional imaging and molecular targets for the first time. We observe that MCP vulnerability to PS-related alterations is embedded in large-scale cognitive and cortical functional architectures, facilitating insights into PS brain-behaviour relationships in the context of structure-function coupling. Further, by incorporating whole-brain gene expression data, we reveal an anterior frontotemporal–visual transcriptional axis which separates anterior PS-related MCPs from all other MCPs. The corresponding anterior frontotemporal gene signature is enriched for neurons and certain glia, synaptic signalling

processes, and psychiatric disorder-related genes, thus bridging macroscale PS-related cortical patterns with established molecular substrates of psychosis vulnerability.

In summary, this study sheds novel insights into functionally and biologically grounded neuroanatomical concomitants of the developing PS. Our findings show that by harnessing shared variation among multiple MRI-derived metrics along with a dimensional approach to symptoms, a more nuanced understanding of neural PS signatures is possible. Taking this a step further, we illustrate how vulnerability in morphologically coordinated cortical units may be guided by multiple modes of cortical organization. Our integrated characterization of PS symptom–morphometry mappings provide a rich benchmark against which high-risk or psychotic disorder patient phenotypes can be evaluated, and holds potential to inform refined biomarkers of the transition to clinical psychosis.

8. Appendix

Appendix Figure 1. Quality control (QC) counts by T1w MRI processing stage.

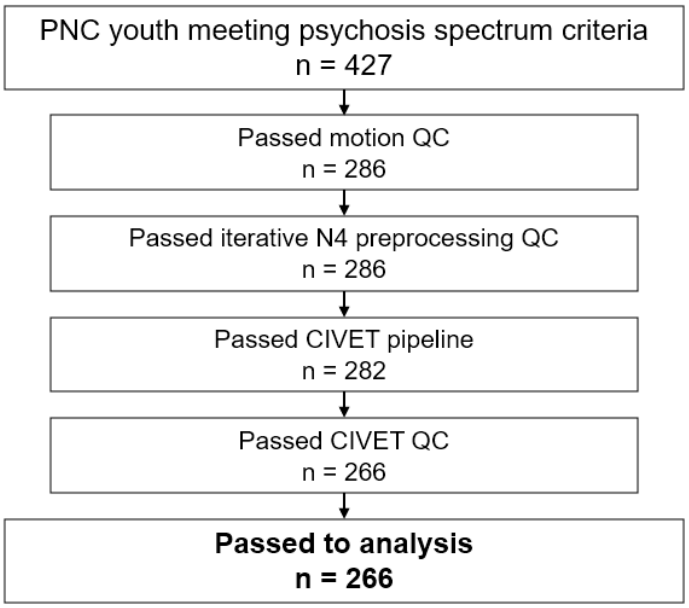

Appendix Figure 2. Generalizability of PS-derived MCPs. Comparison of the cortical maps of the 8 MCPs identified in the primary PS sample **(top)** with the 8-MCP solution for PNC youth who did not meet PS criteria **(middle)** and the 6-MCP solution Ziolkowski et al (2022, in prep) found to be stable in a sample of autism spectrum disorder (ASD) patients and matched neurotypical individuals **(bottom)**. Each set of MCPs is shown on the corresponding group-average brain.

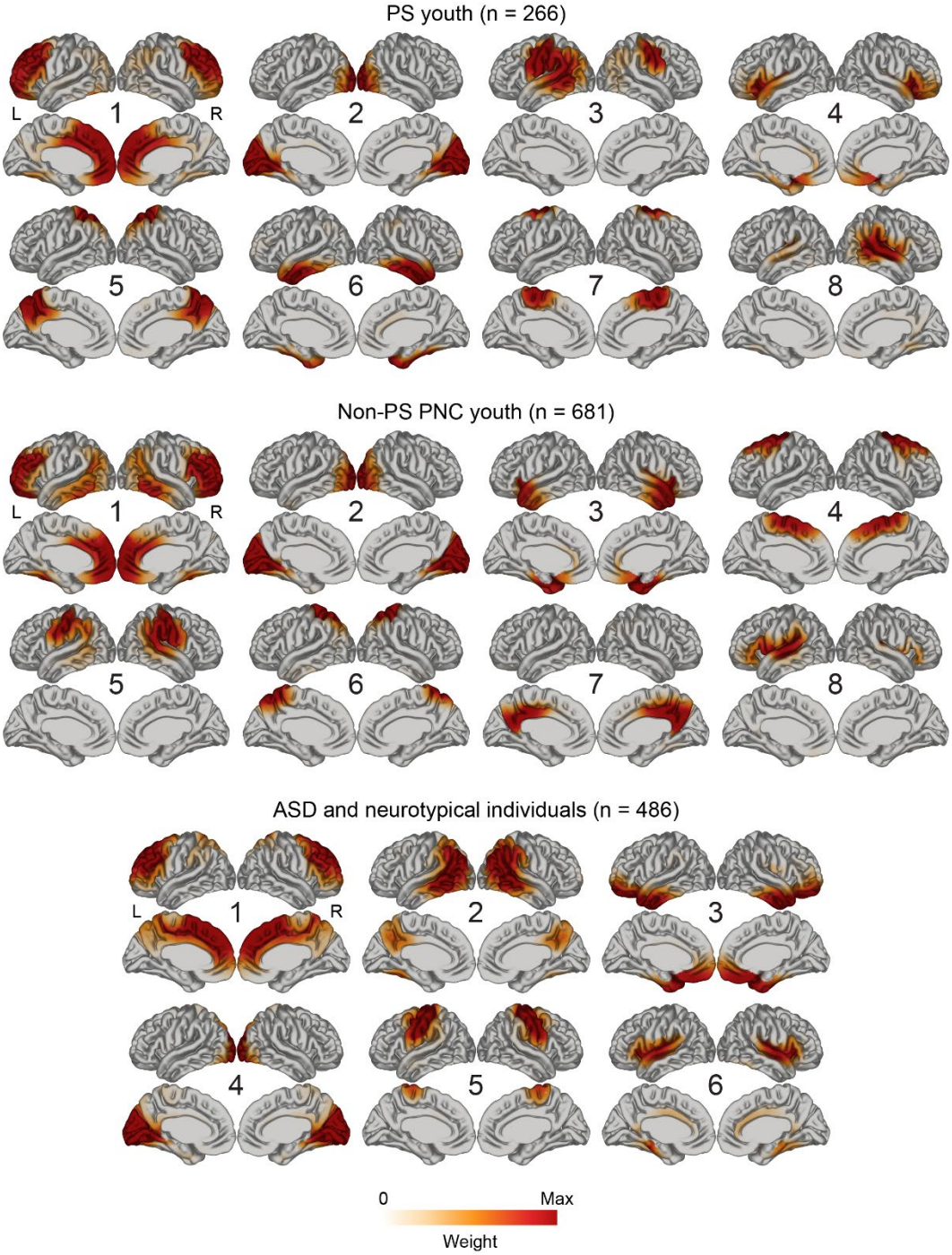

Appendix Figure 3. Split-half resampling results for behavioural PLS on subject-specific MCP loadings and clinical-behavioural features of PS youth. P-values of the split-half correlations (n = 200) of the left (Ucorr; red) and right (Vcorr; blue) singular vectors for all latent variables identified in the behavioural PLS analysis. The dashed line corresponds to p = 0.05. Only the first two latent variables attained p < 0.05 for both the left and right singular vector correlations (*) and were therefore considered reliable.

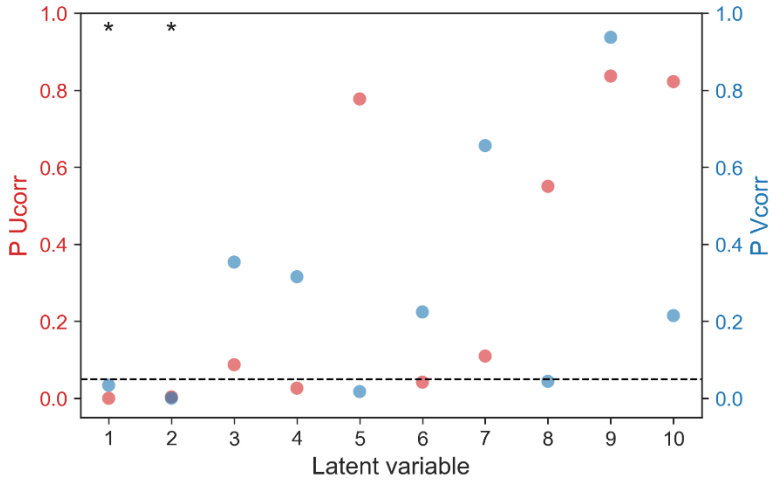

Appendix Table 1. Characteristics of the non-PS PNC and autism spectrum samples used to explore the generalizability of OPNMF-derived cortical MCPs in the primary PS dataset.

	Non-PS PNC (n = 681)			
Age, mean ± SD (range)	15.4 ± 3.6 (8.2–22.6)			
Sex, n (%)				
Female	384 (56.4)			
Male	297 (43.6)			
Race, n (%)				
African American or Black	232 (34.1)			
European American	371 (54.5)			
Mixed or other race	78 (11.5)			
Autism spectrum sample	**POND (n = 108)**	**SickKids (n = 196)**	**UK AIMS (n = 182)**	**Total (n = 486)**
Age range (median)	4.5–21.9	4–49	18–52	4–52 (18.4)
ASD:NT	64:44	79:117	100:82	243:243
Sex, ASD:NT				
Female	18:13	19:36	46:34	83:83
Male	46:31	60:81	54:48	160:160

POND = Province of Ontario Neurodevelopmental Disorders Network; SickKids = Margot Taylor Lab at the Hospital for Sick Children Toronto; UK AIMS = UK Medical Research Council Autism Imaging Multicentre Study Consortium

ASD = autism spectrum disorder; NT = neurotypical

Appendix Table 2. Biological process GO terms omitted from visualization. Terms and substrings used to systematically identify non-interesting biological process GO categories, which were categories that were enriched in the mPLS-derived gene sets but are non-specific or otherwise not directly related to neural function. Note that this list does not exhaustively capture all categories omitted from visualization, as others were manually excluded.

"actin"	"lipid"	"protein"
"cardiac"	"methyl"	"RNA"
"cell cycle"	"microtubule"	"transcription"
"complex assembly"	"phagy"	"translation"
"DNA"	"phospho"	

Appendix Table 3. PS symptom factor intercorrelations for the 2-factor, 3-factor, and 4-factor solutions. In the solution chosen for the main analyses (*), F1, F2, and F3 correspond to negative/disorganized symptoms, disturbed self-experience, and hallucinations/abnormal perceptions, respectively.

	2-Factor		**3-Factor***			**4-Factor**			
	F1	**F2**	**F1**	**F2**	**F3**	**F1**	**F2**	**F3**	**F4**
F1	1		1			1			
F2	0.08	1	0.23	1		0.32	1		
F3	-	-	-0.09	0.34	1	0.21	-0.11	1	
F4	-	-	-	-	-	0.19	0.04	0.32	1

Appendix Table 4. Details of PS symptom items from the GOASSESS interview that were included in the factor analysis, and their loadings in the final 3-factor solution. *(Continued on next page)* Loadings < 0.35 were removed. F1, F2, and F3 correspond to negative/disorganized symptoms, disturbed self-experience, and hallucinations/abnormal perceptions, respectively. *Two items derived from the PS-R screening tool ("Do people ever tell you that they can't understand you?", "Do people ever seem to have difficulty understanding you?") were very highly correlated across subjects, and thus were summed into a single "Communication difficulties" item for factor analysis. Kiddie Schedule for Affective Disorders and Schizophrenia; PS-R = PRIME Screen-Revised; SIPS = Structured Interview for Psychosis-risk Syndromes

Brief description	Tool	Item	F1	F2	F3
Verbal hallucination	K-SADS	Have you ever heard voices when no one was there?			.80
Auditory hallucination	K-SADS	Did you ever hear other sounds or noises that other people couldn't hear?			.51
Visual hallucination	K-SADS	Have you ever seen visions or seen things which other people could not see?			.64
Olfactory hallucination	K-SADS	Have you ever smelled strange odors other people could not smell?			.41
Tactile hallucination	K-SADS	Have you ever had strange feelings in your body like things were crawling on you or someone touching you and nothing or no one was there?			.74
Odd beliefs	K-SADS	Have you ever believed in things that most other people or your parents don't believe in?			.45
Persecutory	K-SADS	Have you ever believed in things and later found out they weren't true, like people being out to get you, or talking about you behind your back, or controlling what you do or think?			
Unusual thoughts	PS-R	I think that I have felt that there are odd or unusual things going on that I can't explain.		.39	
Predict future	PS-R	I think that I might be able to predict the future.			
Thought control	PS-R	I may have felt that there could possibly be something interrupting or controlling my thoughts, feelings, or actions.		.64	
Superstitions	PS-R	I have had the experience of doing something differently because of my superstitions.		.36	
Reality confusion	PS-R	I think I may get confused at times whether something I experience or perceive may be real or may be just part of my imagination or dreams.		.53	
Mind reading	PS-R	I have thought that it might be possible that other people can read my mind, or that I can read others' minds.		.58	
Paranoia	PS-R	I wonder if people may be planning to hurt me or even may be about to hurt me.		.53	
Grandiosity	PS-R	I believe that I have special natural or supernatural gifts beyond my talents and natural strengths.		.36	
Mind tricks	PS-R	I think I might feel like my mind is "playing tricks" on me.		.47	
Auditory perception	PS-R	I have had the experience of hearing faint or clear sounds of people or a person mumbling or talking when there is no one near me.			.77
Audible thoughts	PS-R	I think that I may hear my own thoughts being said out loud.		.49	
Sense of going crazy	PS-R	I have been concerned that I might be "going crazy."		.48	
Communication difficulties*	PS-R	Do people ever tell you that they can't understand you? Do people ever seem to have difficulty understanding you?			
Loss of sense of self	PS-R	Do you ever feel a loss of sense of self or feel disconnected from yourself or your life?		.59	
Detachment	PS-R	Has anyone pointed out to you that you are less emotional or connected to people than you used to be?		.51	
Loss of motivation	PS-R	Within the past 6 months, are you having a harder time getting your work or schoolwork done?	.68		
Loss of daily functioning	PS-R	Within the past 6 months, are you having a harder time getting normal activities done?	.80		
Attention	SIPS	Trouble With Focus and Attention: Severity Scale	.40		
Disorganized communication	SIPS	Changes in Speech, Disorganized communication, Tangential Speech: Severity Scale	.54		
Altered perception of self/world	SIPS	Changes in Perception of Self, Others, or the World in General: Severity Scale	.57		
Emotion expression	SIPS	Expression of Emotion: Severity Scale	.44		
Occupational functioning	SIPS	Occupational Functioning: Severity Scale	.91		
Avolition	SIPS	Avolition: Severity Scale	.78		

Appendix Table 5. Race differences in symptom factor scores. Using linear regression, subject scores for each factor were modelled as a function of race with age and sex as covariates. Results of pairwise comparisons using Tukey's test, averaged over sex, are shown. Note that no comparison attained statistical significance at the $p < 0.05$ level.

	African American - European American		**African American - Mixed/other race**		**European American - Mixed/other race**	
Factor	**t**	**p**	**t**	**p**	**t**	**p**
Negative/disorganized	-0.102	0.994	0.917	0.630	0.909	0.635
Disturbed self-experience	1.905	0.139	0.844	0.676	-0.515	0.864
Hallucinations/ abnormal perceptions	2.250	0.065	-0.230	0.971	-1.733	0.195

Appendix Table 6. Top 15 Disease Ontology terms and enrichment ratios for the PLS+ gene set from the mcPLS analysis. The preprocessed gene list from the Allen Human Brain Atlas (n = 15633) was served as the reference set.

Disease term*	Description	Enrichment ratio	p_{FDR}
C0024667	Animal Mammary Neoplasms	1.53	6.11×10^{-3}
C0041696	Unipolar Depression	1.40	6.11×10^{-3}
C0281966	reproductive system abnormality	2.39	6.11×10^{-3}
C0744356	genital abnormal	2.39	6.11×10^{-3}
C0023893	Liver Cirrhosis, Experimental	1.20	7.01×10^{-3}
C1269683	Major Depressive Disorder	1.36	1.62×10^{-2}
C0005586	Bipolar Disorder	1.23	1.90×10^{-2}
C0030567	Parkinson Disease	1.67	4.36×10^{-2}
C0019693	HIV Infections	1.50	6.13×10^{-2}
C1260899	Anemia, Diamond-Blackfan	2.21	6.76×10^{-2}
C0024668	Mammary Neoplasms, Experimental	1.37	1.11×10^{-1}
C0036341	Schizophrenia	1.13	1.78×10^{-1}
C0009241	Cognition Disorders	1.84	2.14×10^{-1}
C4021821	Abnormality of the urinary system	1.99	2.22×10^{-1}
C0026848	Myopathy	1.47	2.32×10^{-1}

* top 15 terms shown with DisGeNET identification codes

Appendix Table 7. Top 15 Disease Ontology terms and enrichment ratios of the PLS- gene set from the mcPLS analysis. The preprocessed gene list from the Allen Human Brain Atlas (n = 15633) served as the reference set.

Disease term*	Description	Enrichment ratio	p_{FDR}
C0014544	Epilepsy	1.37	1.56×10^{-2}
C3714756	Intellectual Disability	1.30	2.09×10^{-2}
C0557874	Global developmental delay	1.30	2.09×10^{-2}
C1864897	Cognitive delay	1.30	2.09×10^{-2}
C4020875	Mental and motor retardation	1.30	2.09×10^{-2}
C0025362	Mental Retardation	1.29	2.09×10^{-2}
C0423903	Low intelligence	1.29	2.09×10^{-2}
C0917816	Mental deficiency	1.29	2.09×10^{-2}
C1843367	Poor school performance	1.29	2.09×10^{-2}
C4020876	Dull intelligence	1.29	2.09×10^{-2}
C0678230	Congenital Epicanthus	1.55	5.40×10^{-2}
C0036572	Seizures	1.28	7.24×10^{-2}
C4024665	High-grade hypermetropia	2.53	1.50×10^{-1}
C0678222	Breast Carcinoma	2.40	1.65×10^{-1}
C0019572	Hirsutism	2.01	1.91×10^{-1}

* top 15 terms shown with DisGeNET identification codes

9. References

Ad-Dab'bagh, Y., Einarson, D., Lyttelton, O., J-S, M., Mok, K., Ivanov, O., Vincent, R. D., Lepage, C., Lerch, J., Fombonne, E., & Evans, A. C. (2006). The CIVET Image-Processing Environment: A Fully Automated Comprehensive Pipeline for Anatomical Neuroimaging Research. In M. Corbetta (Ed.), *Proceedings of the 12th Annual Meeting of the Organization for Human Brain Mapping*. http://www.bic.mni.mcgill.ca/users/yaddab/Yasser-HBM2006-Poster.pdf

Alexander-Bloch, A. F., Giedd, J. N., & Bullmore, E. (2013). Imaging structural co-variance between human brain regions. *Nature Reviews. Neuroscience*, *14*(5), 322–336.

Alexander-Bloch, A. F., Shou, H., Liu, S., Satterthwaite, T. D., Glahn, D. C., Shinohara, R. T., Vandekar, S. N., & Raznahan, A. (2018). On testing for spatial correspondence between maps of human brain structure and function. *NeuroImage*, *178*, 540–551.

Alonso, J., Saha, S., Lim, C. C. W., Aguilar-Gaxiola, S., Al-Hamzawi, A., Benjet, C., Bromet, E. J., Degenhardt, L., de Girolamo, G., Esan, O., Florescu, S., Gureje, O., Haro, J. M., Hu, C., Karam, E. G., Karam, G., Kovess-Masfety, V., Lepine, J.-P., Lee, S., … WHO World Mental Health Survey Collaborators. (2018). The association between psychotic experiences and health-related quality of life: a cross-national analysis based on World Mental Health Surveys. *Schizophrenia Research*, *201*, 46–53.

Amlien, I. K., Fjell, A. M., Tamnes, C. K., Grydeland, H., Krogsrud, S. K., Chaplin, T. A., Rosa, M. G. P., & Walhovd, K. B. (2016). Organizing Principles of Human Cortical Development--Thickness and Area from 4 to 30 Years: Insights from Comparative Primate Neuroanatomy. *Cerebral Cortex* , *26*(1), 257–267.

Andreou, C., & Borgwardt, S. (2020). Structural and functional imaging markers for susceptibility to psychosis. *Molecular Psychiatry*. https://doi.org/10.1038/s41380-020-0679-7

Annese, J., Pitiot, A., Dinov, I. D., & Toga, A. W. (2004). A myelo-architectonic method for the structural classification of cortical areas. *NeuroImage*, *21*(1), 15–26.

Armando, M., Nelson, B., Yung, A. R., Ross, M., Birchwood, M., Girardi, P., & Fiori Nastro, P. (2010). Psychotic-like experiences and correlation with distress and depressive symptoms in a community sample of adolescents and young adults. *Schizophrenia Research*, *119*(1–3), 258–265.

Arnatkeviciute, A., Fulcher, B. D., Bellgrove, M. A., & Fornito, A. (2021). Imaging Transcriptomics of Brain Disorders. *Biological Psychiatry Global Open Science*. https://doi.org/10.1016/j.bpsgos.2021.10.002

Arnatkeviciute, A., Fulcher, B. D., & Fornito, A. (2019). A practical guide to linking brain-wide gene expression and neuroimaging data. *NeuroImage*, *189*, 353–367.

Ashburner, M., Ball, C. A., Blake, J. A., Botstein, D., Butler, H., Cherry, J. M., Davis, A. P., Dolinski, K., Dwight, S. S., Eppig, J. T., Harris, M. A., Hill, D. P., Issel-Tarver, L., Kasarskis, A., Lewis, S., Matese, J. C., Richardson, J. E., Ringwald, M., Rubin, G. M., & Sherlock, G. (2000). Gene ontology: tool for the unification of biology. The Gene Ontology Consortium. *Nature Genetics*, *25*(1), 25–29.

Assari, S., & Mincy, R. (2021). Racism May Interrupt Age-related Brain Growth of African American Children in the United States. *Journal of Pediatrics & Child Health Care*, *6*(3). https://www.ncbi.nlm.nih.gov/pubmed/34966911

Ball, G., Beare, R., & Seal, M. L. (2019). Charting shared developmental trajectories of cortical thickness and structural connectivity in childhood and adolescence. *Human Brain Mapping*, *40*(16), 4630–4644.

Ball, G., Seidlitz, J., O'Muircheartaigh, J., Dimitrova, R., Fenchel, D., Makropoulos, A., Christiaens, D., Schuh, A., Passerat-Palmbach, J., Hutter, J., Cordero-Grande, L., Hughes, E., Price, A., Hajnal, J. V., Rueckert, D., Robinson, E. C., & Edwards, A. D. (2020). Cortical morphology at birth reflects spatiotemporal patterns of gene expression in the fetal human brain. *PLoS Biology*, *18*(11), e3000976.

Bedford, S. A., Park, M. T. M., Devenyi, G. A., Tullo, S., Germann, J., Patel, R., Anagnostou, E., Baron-Cohen, S., Bullmore, E. T., Chura, L. R., Craig, M. C., Ecker, C., Floris, D. L., Holt, R. J., Lenroot, R., Lerch, J. P., Lombardo, M. V., Murphy, D. G. M., Raznahan, A., … Chakravarty, M. M. (2020). Large-scale analyses of the relationship between sex, age and intelligence quotient heterogeneity and cortical morphometry in autism spectrum disorder. *Molecular Psychiatry*, *25*(3), 614–628.

Berdenis van Berlekom, A., Muflihah, C. H., Snijders, G. J. L. J., MacGillavry, H. D., Middeldorp, J., Hol, E. M., Kahn, R. S., & de Witte, L. D. (2020). Synapse Pathology in Schizophrenia: A Meta-analysis of Postsynaptic Elements in Postmortem Brain Studies. *Schizophrenia Bulletin*, *46*(2), 374–386.

Berna, F., Göritz, A. S., Schröder, J., Martin, B., Cermolacce, M., Allé, M. C., Danion, J.-M., Cuervo-Lombard, C. V., & Moritz, S. (2016). Self-disorders in individuals with attenuated psychotic symptoms: Contribution of a dysfunction of autobiographical memory. *Psychiatry Research*, *239*, 333–341.

Binder, J. R., Frost, J. A., Hammeke, T. A., Cox, R. W., Rao, S. M., & Prieto, T. (1997). Human brain language areas identified by functional magnetic resonance imaging. *The Journal of Neuroscience: The Official Journal of the Society for Neuroscience*, *17*(1), 353–362.

Bonoldi, I., Allen, P., Madeira, L., Tognin, S., Bossong, M. G., Azis, M., Samson, C., Quinn, B., Calem, M., Valmaggia, L., Modinos, G., Stone, J., Perez, J., Howes, O., Politi, P., Kempton, M. J., Fusar-Poli, P., & McGuire, P. (2019). Basic Self-Disturbances Related to Reduced Anterior Cingulate Volume in Subjects at Ultra-High Risk for Psychosis. *Frontiers in Psychiatry / Frontiers Research Foundation*, *10*, 254.

Bornovalova, M. A., Choate, A. M., Fatimah, H., Petersen, K. J., & Wiernik, B. M. (2020). Appropriate Use of Bifactor Analysis in Psychopathology Research: Appreciating Benefits and Limitations. *Biological Psychiatry*, *88*(1), 18–27.

Borrell, V. (2018). How Cells Fold the Cerebral Cortex. *The Journal of Neuroscience: The Official Journal of the Society for Neuroscience*, *38*(4), 776–783.

Boucher, M., Whitesides, S., & Evans, A. (2009). Depth potential function for folding pattern representation, registration and analysis. *Medical Image Analysis*, *13*(2), 203–214.

Boutsidis, C., & Gallopoulos, E. (2008). SVD based initialization: A head start for nonnegative matrix factorization. *Pattern Recognition*, *41*(4), 1350–1362.

Budday, S., Raybaud, C., & Kuhl, E. (2014). A mechanical model predicts morphological abnormalities in the developing human brain. *Scientific Reports*, *4*, 5644.

Budday, S., Steinmann, P., & Kuhl, E. (2015a). Secondary instabilities modulate cortical complexity in the mammalian brain. *Philosophical Magazine A*, *95*(28–30), 3244–3256.

Budday, S., Steinmann, P., & Kuhl, E. (2015b). Physical biology of human brain development. *Frontiers in Cellular Neuroscience*, *9*, 257.

Büetiger, J. R., Hubl, D., Kupferschmid, S., Schultze-Lutter, F., Schimmelmann, B. G., Federspiel, A., Hauf, M., Walther, S., Kaess, M., Michel, C., & Kindler, J. (2020). Trapped in a Glass Bell Jar: Neural Correlates of Depersonalization and Derealization in Subjects at Clinical High-Risk of Psychosis and Depersonalization-Derealization Disorder. *Frontiers in Psychiatry / Frontiers Research Foundation*, *11*, 535652.

Burkhard, C., Cicek, S., Barzilay, R., Radhakrishnan, R., & Guloksuz, S. (2021). Need for Ethnic and Population Diversity in Psychosis Research. *Schizophrenia Bulletin*, *47*(4), 889–895.

Burt, J. B., Demirtaş, M., Eckner, W. J., Navejar, N. M., Ji, J. L., Martin, W. J., Bernacchia, A., Anticevic, A., & Murray, J. D. (2018). Hierarchy of transcriptomic specialization across human cortex captured by structural neuroimaging topography. *Nature Neuroscience*, *21*(9), 1251–1259.

Buxton, R. B., & Frank, L. R. (1997). A model for the coupling between cerebral blood flow and oxygen metabolism during neural stimulation. *Journal of Cerebral Blood Flow and Metabolism: Official Journal of the International Society of Cerebral Blood Flow and Metabolism*, *17*(1), 64–72.

Buxton, R. B., Wong, E. C., & Frank, L. R. (1998). Dynamics of blood flow and oxygenation changes during brain activation: the balloon model. *Magnetic Resonance in Medicine: Official Journal of the Society of Magnetic Resonance in Medicine / Society of Magnetic Resonance in Medicine*, *39*(6), 855–864.

Cafiero, R., Brauer, J., Anwander, A., & Friederici, A. D. (2019). The Concurrence of Cortical Surface Area Expansion and White Matter Myelination in Human Brain Development. *Cerebral Cortex* , *29*(2), 827–837.

Calkins, M. E., Merikangas, K. R., Moore, T. M., Burstein, M., Behr, M. A., Satterthwaite, T. D., Ruparel, K., Wolf, D. H., Roalf, D. R., Mentch, F. D., Qiu, H., Chiavacci, R., Connolly, J. J., Sleiman, P. M. A., Gur, R. C., Hakonarson, H., & Gur, R. E. (2015). The Philadelphia Neurodevelopmental Cohort: constructing a deep phenotyping collaborative. *Journal of Child Psychology and Psychiatry, and Allied Disciplines*, *56*(12), 1356–1369.

Calkins, M. E., Moore, T. M., Merikangas, K. R., Burstein, M., Satterthwaite, T. D., Bilker, W. B., Ruparel, K., Chiavacci, R., Wolf, D. H., Mentch, F., Qiu, H., Connolly, J. J., Sleiman, P. A., Hakonarson, H., Gur, R. C., & Gur, R. E. (2014). The psychosis spectrum in a young U.S. community sample: findings from the Philadelphia Neurodevelopmental Cohort. *World Psychiatry: Official Journal of the World Psychiatric Association* , *13*(3), 296–305.

Calkins, M. E., Moore, T. M., Satterthwaite, T. D., Wolf, D. H., Turetsky, B. I., Roalf, D. R., Merikangas, K. R., Ruparel, K., Kohler, C. G., Gur, R. C., & Gur, R. E. (2017). Persistence of psychosis spectrum symptoms in the Philadelphia Neurodevelopmental Cohort: a

prospective two-year follow-up. *World Psychiatry: Official Journal of the World Psychiatric Association* , *16*(1), 62–76.

Cannon, T. D., Cadenhead, K., Cornblatt, B., Woods, S. W., Addington, J., Walker, E., Seidman, L. J., Perkins, D., Tsuang, M., McGlashan, T., & Heinssen, R. (2008). Prediction of psychosis in youth at high clinical risk: a multisite longitudinal study in North America. *Archives of General Psychiatry*, *65*(1), 28–37.

Cannon, T. D., Chung, Y., He, G., Sun, D., Jacobson, A., van Erp, T. G. M., McEwen, S., Addington, J., Bearden, C. E., Cadenhead, K., Cornblatt, B., Mathalon, D. H., McGlashan, T., Perkins, D., Jeffries, C., Seidman, L. J., Tsuang, M., Walker, E., Woods, S. W., … North American Prodrome Longitudinal Study Consortium. (2015). Progressive reduction in cortical thickness as psychosis develops: a multisite longitudinal neuroimaging study of youth at elevated clinical risk. *Biological Psychiatry*, *77*(2), 147–157.

Cardno, A. G., Jones, L. A., Murphy, K. C., Sanders, R. D., Asherson, P., Owen, M. J., & McGuffin, P. (1999). Dimensions of psychosis in affected sibling pairs. *Schizophrenia Bulletin*, *25*(4), 841–850.

Cardno, A. G., Sham, P. C., Murray, R. M., & McGuffin, P. (2001). Twin study of symptom dimensions in psychoses. *The British Journal of Psychiatry: The Journal of Mental Science*, *179*, 39–45.

Carlo, C. N., & Stevens, C. F. (2013). Structural uniformity of neocortex, revisited. *Proceedings of the National Academy of Sciences of the United States of America*, *110*(4), 1488–1493.

Cascella, N. G., Gerner, G. J., Fieldstone, S. C., Sawa, A., & Schretlen, D. J. (2011). The insula-claustrum region and delusions in schizophrenia. *Schizophrenia Research*, *133*(1–3), 77–81.

Cattell, R. B. (1966). The Scree Test For The Number Of Factors. *Multivariate Behavioral Research*, *1*(2), 245–276.

Cederlöf, M., Kuja-Halkola, R., Larsson, H., Sjölander, A., Östberg, P., Lundström, S., Kelleher, I., & Lichtenstein, P. (2017). A longitudinal study of adolescent psychotic experiences and later development of substance use disorder and suicidal behavior. *Schizophrenia Research*, *181*, 13–16.

Chang, L. J., Yarkoni, T., Khaw, M. W., & Sanfey, A. G. (2013). Decoding the role of the insula in human cognition: functional parcellation and large-scale reverse inference. *Cerebral Cortex* , *23*(3), 739–749.

Chang, W. C., Wong, C. S. M., Chen, E. Y. H., Lam, L. C. W., Chan, W. C., Ng, R. M. K., Hung, S. F., Cheung, E. F. C., Sham, P. C., Chiu, H. F. K., Lam, M., Lee, E. H. M., Chiang, T. P., Chan, L. K., Lau, G. K. W., Lee, A. T. C., Leung, G. T. Y., Leung, J. S. Y., Lau, J. T. F., … Bebbington, P. (2017). Lifetime Prevalence and Correlates of Schizophrenia-Spectrum, Affective, and Other Non-affective Psychotic Disorders in the Chinese Adult Population. *Schizophrenia Bulletin*, *43*(6), 1280–1290.

Chenn, A., & Walsh, C. A. (2002). Regulation of cerebral cortical size by control of cell cycle exit in neural precursors. *Science*, *297*(5580), 365–369.

Choi, Y. Y., Lee, J. J., Choi, K. Y., Seo, E. H., Choo, I. H., Kim, H., Song, M.-K., Choi, S.-M., Cho, S. H., Kim, B. C., & Lee, K. H. (2020). The Aging Slopes of Brain Structures Vary by Ethnicity and Sex: Evidence From a Large Magnetic Resonance Imaging Dataset From a Single Scanner of Cognitively Healthy Elderly People in Korea. *Frontiers in Aging Neuroscience*, *12*, 233.

Chung, Y. S., Hyatt, C. J., & Stevens, M. C. (2017). Adolescent maturation of the relationship between cortical gyrification and cognitive ability. *NeuroImage*, *158*, 319–331.

Clouchoux, C., Kudelski, D., Gholipour, A., Warfield, S. K., Viseur, S., Bouyssi-Kobar, M., Mari, J.-L., Evans, A. C., du Plessis, A. J., & Limperopoulos, C. (2012). Quantitative in vivo MRI measurement of cortical development in the fetus. *Brain Structure & Function*, *217*(1), 127–139.

Coifman, R. R., Lafon, S., Lee, A. B., Maggioni, M., Nadler, B., Warner, F., & Zucker, S. W. (2005). Geometric diffusions as a tool for harmonic analysis and structure definition of data: diffusion maps. *Proceedings of the National Academy of Sciences of the United States of America*, *102*(21), 7426–7431.

Collins, D. L., Neelin, P., Peters, T. M., & Evans, A. C. (1994). Automatic 3D intersubject registration of MR volumetric data in standardized Talairach space. *Journal of Computer Assisted Tomography*, *18*(2), 192–205.

Corlett, P. R., Taylor, J. R., Wang, X.-J., Fletcher, P. C., & Krystal, J. H. (2010). Toward a neurobiology of delusions. *Progress in Neurobiology*, *92*(3), 345–369.

Costello, A. B., & Osborne, J. (2005). Best practices in exploratory factor analysis: four recommendations for getting the most from your analysis. *Practical Assessment, Research, and Evaluation*, *10*(1), 7.

Cui, Y., & Wang, J. (2020). Impact of Dimension and Sample Size on the Performance of Imputation Methods. *Data Science*, 538–549.

Currie, S., Hoggard, N., Craven, I. J., Hadjivassiliou, M., & Wilkinson, I. D. (2013). Understanding MRI: basic MR physics for physicians. *Postgraduate Medical Journal*, *89*(1050), 209–223.

Cuthbert, B. N., & Insel, T. R. (2013). Toward the future of psychiatric diagnosis: the seven pillars of RDoC. *BMC Medicine*, *11*, 126.

Cuthbert, B. N., & Morris, S. E. (2021). Evolving Concepts of the Schizophrenia Spectrum: A Research Domain Criteria Perspective. *Frontiers in Psychiatry / Frontiers Research Foundation*, *12*, 641319.

Damme, K. S. F., Gupta, T., Nusslock, R., Bernard, J. A., Orr, J. M., & Mittal, V. A. (2019). Cortical Morphometry in the Psychosis Risk Period: A Comprehensive Perspective of Surface Features. *Biological Psychiatry. Cognitive Neuroscience and Neuroimaging*, *4*(5), 434–443.

Daniels, J. K., Gaebler, M., Lamke, J.-P., & Walter, H. (2015). Grey matter alterations in patients with depersonalization disorder: a voxel-based morphometry study. *Journal of Psychiatry & Neuroscience: JPN*, *40*(1), 19–27.

Darmanis, S., Sloan, S. A., Zhang, Y., Enge, M., Caneda, C., Shuer, L. M., Hayden Gephart, M. G., Barres, B. A., & Quake, S. R. (2015). A survey of human brain transcriptome diversity at the single cell level. *Proceedings of the National Academy of Sciences of the United States of America*, *112*(23), 7285–7290.

de Wit, S., Wierenga, L. M., Oranje, B., Ziermans, T. B., Schothorst, P. F., van Engeland, H., Kahn, R. S., & Durston, S. (2016). Brain development in adolescents at ultra-high risk for psychosis: Longitudinal changes related to resilience. *NeuroImage. Clinical*, *12*, 542–549.

Deppe, M., Marinell, J., Krämer, J., Duning, T., Ruck, T., Simon, O. J., Zipp, F., Wiendl, H., & Meuth, S. G. (2014). Increased cortical curvature reflects white matter atrophy in individual patients with early multiple sclerosis. *NeuroImage. Clinical*, *6*, 475–487.

Derome, M., Tonini, E., Zöller, D., Schaer, M., Eliez, S., & Debbané, M. (2020). Developmental Trajectories of Cortical Thickness in Relation to Schizotypy During Adolescence. *Schizophrenia Bulletin*. https://doi.org/10.1093/schbul/sbaa020

Di Biase, M. A., Geaghan, M. P., Reay, W. R., Seidlitz, J., Weickert, C. S., Pébay, A., Green, M. J., Quidé, Y., Atkins, J. R., Coleman, M. J., Bouix, S., Knyazhanskaya, E. E., Lyall, A. E., Pasternak, O., Kubicki, M., Rathi, Y., Visco, A., Gaunnac, M., Lv, J., … Zalesky, A. (2022). Cell type-specific manifestations of cortical thickness heterogeneity in schizophrenia. *Molecular Psychiatry*, 1–9.

DiStefano, C., Zhu, M., & Mîndrilã, D. (2009). Understanding and Using Factor Scores: Considerations for the Applied Researcher. *Practical Assessment, Research, and Evaluation*, *14*(1), 20.

Dolphin, L., Dooley, B., & Fitzgerald, A. (2015). Prevalence and correlates of psychotic like experiences in a nationally representative community sample of adolescents in Ireland. *Schizophrenia Research*, *169*(1–3), 241–247.

Dominguez, M.-G., Saka, M. C., Lieb, R., Wittchen, H.-U., & van Os, J. (2010). Early expression of negative/disorganized symptoms predicting psychotic experiences and subsequent clinical psychosis: a 10-year study. *The American Journal of Psychiatry*, *167*(9), 1075–1082.

Dominguez, M.-G., Wichers, M., Lieb, R., Wittchen, H.-U., & van Os, J. (2011). Evidence that onset of clinical psychosis is an outcome of progressively more persistent subclinical psychotic experiences: an 8-year cohort study. *Schizophrenia Bulletin*, *37*(1), 84–93.

Dong, D., Yao, D., Wang, Y., Hong, S.-J., Genon, S., Xin, F., Jung, K., He, H., Chang, X., Duan, M., Bernhardt, B. C., Margulies, D. S., Sepulcre, J., Eickhoff, S. B., & Luo, C. (2021). Compressed sensorimotor-to-transmodal hierarchical organization in schizophrenia. *Psychological Medicine*, 1–14.

Dong, H.-M., Margulies, D. S., Zuo, X.-N., & Holmes, A. J. (2021). Shifting gradients of macroscale cortical organization mark the transition from childhood to adolescence. *Proceedings of the National Academy of Sciences of the United States of America*, *118*(28). https://doi.org/10.1073/pnas.2024448118

Drakesmith, M., Dutt, A., Fonville, L., Zammit, S., Reichenberg, A., Evans, C. J., McGuire, P., Lewis, G., Jones, D. K., & David, A. S. (2016). Volumetric, relaxometric and diffusometric

correlates of psychotic experiences in a non-clinical sample of young adults. *NeuroImage. Clinical*, *12*, 550–558.

Drobinin, V., Van Gestel, H., Zwicker, A., MacKenzie, L., Cumby, J., Patterson, V. C., Vallis, E. H., Campbell, N., Hajek, T., Helmick, C. A., Schmidt, M. H., Alda, M., Bowen, C. V., & Uher, R. (2020). Psychotic symptoms are associated with lower cortical folding in youth at risk for mental illness. *Journal of Psychiatry & Neuroscience: JPN*, *45*(2), 125–133.

Duan, J., Xia, M., Womer, F. Y., Chang, M., Yin, Z., Zhou, Q., Zhu, Y., Liu, Z., Jiang, X., Wei, S., Anthony O'Neill, F., He, Y., Tang, Y., & Wang, F. (2019). Dynamic changes of functional segregation and integration in vulnerability and resilience to schizophrenia. *Human Brain Mapping*, *40*(7), 2200–2211.

Dudley, R., Taylor, P., Wickham, S., & Hutton, P. (2016). Psychosis, Delusions and the "Jumping to Conclusions" Reasoning Bias: A Systematic Review and Meta-analysis. *Schizophrenia Bulletin*, *42*(3), 652–665.

Dukart, J., Smieskova, R., Harrisberger, F., Lenz, C., Schmidt, A., Walter, A., Huber, C., Riecher-Rössler, A., Simon, A., Lang, U. E., Fusar-Poli, P., & Borgwardt, S. (2017). Age-related brain structural alterations as an intermediate phenotype of psychosis. *Journal of Psychiatry & Neuroscience: JPN*, *42*(5), 307–319.

Durran, D. R. (2013). *Numerical Methods for Wave Equations in Geophysical Fluid Dynamics*. Springer Science & Business Media.

Eckart, C., & Young, G. (1936). The approximation of one matrix by another of lower rank. *Psychometrika*, *1*(3), 211–218.

Elmaoğlu, M., & Çelik, A. (2011). *MRI Handbook: MR Physics, Patient Positioning, and Protocols*. Springer Science & Business Media.

ENIGMA Clinical High Risk for Psychosis Working Group, Jalbrzikowski, M., Hayes, R. A., Wood, S. J., Nordholm, D., Zhou, J. H., Fusar-Poli, P., Uhlhaas, P. J., Takahashi, T., Sugranyes, G., Kwak, Y. B., Mathalon, D. H., Katagiri, N., Hooker, C. I., Smigielski, L., Colibazzi, T., Via, E., Tang, J., Koike, S., … Hernaus, D. (2021). Association of Structural Magnetic Resonance Imaging Measures With Psychosis Onset in Individuals at Clinical High Risk for Developing Psychosis: An ENIGMA Working Group Mega-analysis. *JAMA Psychiatry* , *78*(7), 753–766.

Eskildsen, S. F., Coupé, P., Fonov, V., Manjón, J. V., Leung, K. K., Guizard, N., Wassef, S. N., Østergaard, L. R., Collins, D. L., & Alzheimer's Disease Neuroimaging Initiative. (2012). BEaST: brain extraction based on nonlocal segmentation technique. *NeuroImage*, *59*(3), 2362–2373.

Evermann, U., Gaser, C., Besteher, B., Langbein, K., & Nenadić, I. (2020). Cortical Gyrification, Psychotic-Like Experiences, and Cognitive Performance in Nonclinical Subjects. *Schizophrenia Bulletin*, *46*(6), 1524–1534.

Fava, G. A., & Kellner, R. (1991). Prodromal symptoms in affective disorders. *The American Journal of Psychiatry*, *148*(7), 823–830.

Fonov, V. S., Evans, A. C., McKinstry, R. C., Almli, C. R., & Collins, D. L. (2009). Unbiased nonlinear average age-appropriate brain templates from birth to adulthood. *NeuroImage*, *47*, S102.

Fonseca-Pedrero, E., Debbané, M., Ortuño-Sierra, J., Chan, R. C. K., Cicero, D. C., Zhang, L. C., Brenner, C., Barkus, E., Linscott, R. J., Kwapil, T., Barrantes-Vidal, N., Cohen, A., Raine, A., Compton, M. T., Tone, E. B., Suhr, J., Muñiz, J., Fumero, A., Giakoumaki, S., … Jablensky, A. (2018). The structure of schizotypal personality traits: a cross-national study. *Psychological Medicine*, *48*(3), 451–462.

Fonville, L., Drakesmith, M., Zammit, S., Lewis, G., Jones, D. K., & David, A. S. (2019). MRI Indices of Cortical Development in Young People With Psychotic Experiences: Influence of Genetic Risk and Persistence of Symptoms. *Schizophrenia Bulletin*, *45*(1), 169–179.

Fornberg, B. (1988). Generation of finite difference formulas on arbitrarily spaced grids. *Mathematics of Computation*, *51*(184), 699–706.

Fulcher, B. D., Arnatkeviciute, A., & Fornito, A. (2021). Overcoming false-positive gene-category enrichment in the analysis of spatially resolved transcriptomic brain atlas data. *Nature Communications*, *12*(1), 2669.

Fusar-Poli, P., Bonoldi, I., Yung, A. R., Borgwardt, S., Kempton, M. J., Valmaggia, L., Barale, F., Caverzasi, E., & McGuire, P. (2012). Predicting psychosis: meta-analysis of transition outcomes in individuals at high clinical risk. *Archives of General Psychiatry*, *69*(3), 220–229.

Fusar-Poli, P., Borgwardt, S., Bechdolf, A., Addington, J., Riecher-Rössler, A., Schultze-Lutter, F., Keshavan, M., Wood, S., Ruhrmann, S., Seidman, L. J., Valmaggia, L., Cannon, T., Velthorst, E., De Haan, L., Cornblatt, B., Bonoldi, I., Birchwood, M., McGlashan, T., Carpenter, W., … Yung, A. (2013). The psychosis high-risk state: a comprehensive state-of-the-art review. *JAMA Psychiatry* , *70*(1), 107–120.

Fusar-Poli, P., Borgwardt, S., Crescini, A., Deste, G., Kempton, M. J., Lawrie, S., Mc Guire, P., & Sacchetti, E. (2011). Neuroanatomy of vulnerability to psychosis: a voxel-based meta-analysis. *Neuroscience and Biobehavioral Reviews*, *35*(5), 1175–1185.

Fusar-Poli, P., Radua, J., McGuire, P., & Borgwardt, S. (2012). Neuroanatomical maps of psychosis onset: voxel-wise meta-analysis of antipsychotic-naive VBM studies. *Schizophrenia Bulletin*, *38*(6), 1297–1307.

Gandal, M. J., Haney, J. R., Parikshak, N. N., Leppa, V., Ramaswami, G., Hartl, C., Schork, A. J., Appadurai, V., Buil, A., Werge, T. M., Liu, C., White, K. P., CommonMind Consortium, PsychENCODE Consortium, iPSYCH-BROAD Working Group, Horvath, S., & Geschwind, D. H. (2018). Shared molecular neuropathology across major psychiatric disorders parallels polygenic overlap. *Science*, *359*(6376), 693–697.

Garavan, H., Bartsch, H., Conway, K., Decastro, A., Goldstein, R. Z., Heeringa, S., Jernigan, T., Potter, A., Thompson, W., & Zahs, D. (2018). Recruiting the ABCD sample: Design considerations and procedures. *Developmental Cognitive Neuroscience*, *32*, 16–22.

Garcia, K. E., Kroenke, C. D., & Bayly, P. V. (2018). Mechanics of cortical folding: stress, growth and stability. *Philosophical Transactions of the Royal Society of London. Series B, Biological Sciences*, *373*(1759). https://doi.org/10.1098/rstb.2017.0321

Gene Ontology Consortium. (2021). The Gene Ontology resource: enriching a GOld mine. *Nucleic Acids Research*, *49*(D1), D325–D334.

Genon, S., Eickhoff, S. B., & Kharabian, S. (2022). Linking interindividual variability in brain structure to behaviour. *Nature Reviews. Neuroscience*, *23*(5), 307–318.

Giocondo, J. G., Salum, G. A., Gadelha, A., Argolo, F. C., Simioni, A. R., Mari, J. J., Miguel, E. C., Bressan, R. A., Rohde, L. A., & Pan, P. M. (2021). Psychotic-like Experiences and Common Mental Disorders in Childhood and Adolescence: Bidirectional and Transdiagnostic Associations in a Longitudinal Community-based Study. *Schizophrenia Bulletin Open*, *2*(1). https://doi.org/10.1093/schizbullopen/sgab028

Gisselgård, J., Lebedev, A. V., Dæhli Kurz, K., Joa, I., Johannessen, J. O., & Brønnick, K. (2018). Structural and functional alterations in the brain during working memory in medication-naïve patients at clinical high-risk for psychosis. *PloS One*, *13*(5), e0196289.

Glasser, M. F., Coalson, T. S., Robinson, E. C., Hacker, C. D., Harwell, J., Yacoub, E., Ugurbil, K., Andersson, J., Beckmann, C. F., Jenkinson, M., Smith, S. M., & Van Essen, D. C. (2016). A multi-modal parcellation of human cerebral cortex. *Nature*, *536*(7615), 171–178.

Glover, G. H. (2011). Overview of functional magnetic resonance imaging. *Neurosurgery Clinics of North America*, *22*(2), 133–139, vii.

Groves, A. R., Smith, S. M., Fjell, A. M., Tamnes, C. K., Walhovd, K. B., Douaud, G., Woolrich, M. W., & Westlye, L. T. (2012). Benefits of multi-modal fusion analysis on a large-scale dataset: life-span patterns of inter-subject variability in cortical morphometry and white matter microstructure. *NeuroImage*, *63*(1), 365–380.

Gur, R. C., Calkins, M. E., Satterthwaite, T. D., Ruparel, K., Bilker, W. B., Moore, T. M., Savitt, A. P., Hakonarson, H., & Gur, R. E. (2014). Neurocognitive growth charting in psychosis spectrum youths. *JAMA Psychiatry* , *71*(4), 366–374.

Habib, N., Avraham-Davidi, I., Basu, A., Burks, T., Shekhar, K., Hofree, M., Choudhury, S. R., Aguet, F., Gelfand, E., Ardlie, K., Weitz, D. A., Rozenblatt-Rosen, O., Zhang, F., & Regev, A. (2017). Massively parallel single-nucleus RNA-seq with DroNc-seq. *Nature Methods*, *14*(10), 955–958.

Hansen, J. Y., Markello, R. D., Vogel, J. W., Seidlitz, J., Bzdok, D., & Misic, B. (2021). Mapping gene transcription and neurocognition across human neocortex. *Nature Human Behaviour*, 1–11.

Harman, H. H., & Jones, W. H. (1966). Factor analysis by minimizing residuals (minres). *Psychometrika*, *31*(3), 351–368.

Harnett, N. G. (2020). Neurobiological consequences of racial disparities and environmental risks: a critical gap in understanding psychiatric disorders. *Neuropsychopharmacology: Official Publication of the American College of Neuropsychopharmacology*, *45*(8), 1247–1250.

Hawrylycz, M. J., Lein, E. S., Guillozet-Bongaarts, A. L., Shen, E. H., Ng, L., Miller, J. A., van de Lagemaat, L. N., Smith, K. A., Ebbert, A., Riley, Z. L., Abajian, C., Beckmann, C. F., Bernard, A., Bertagnolli, D., Boe, A. F., Cartagena, P. M., Chakravarty, M. M., Chapin, M., Chong, J., … Jones, A. R. (2012). An anatomically comprehensive atlas of the adult human brain transcriptome. *Nature*, *489*(7416), 391–399.

Healy, C., Brannigan, R., Dooley, N., Coughlan, H., Clarke, M., Kelleher, I., & Cannon, M. (2019). Childhood and adolescent psychotic experiences and risk of mental disorder: a systematic review and meta-analysis. *Psychological Medicine*, *49*(10), 1589–1599.

Helmer, M., Warrington, S. D., Mohammadi-Nejad, A.-R., Ji, J. L., Howell, A., Rosand, B., Anticevic, A., Sotiropoulos, S. N., & Murray, J. D. (2020). *On stability of Canonical Correlation Analysis and Partial Least Squares with application to brain-behavior associations* (p. 2020.08.25.265546). https://doi.org/10.1101/2020.08.25.265546

Henson, R. K., & Roberts, J. K. (2006). Use of Exploratory Factor Analysis in Published Research: Common Errors and Some Comment on Improved Practice. *Educational and Psychological Measurement*, *66*(3), 393–416.

Hill, J., Dierker, D., Neil, J., Inder, T., Knutsen, A., Harwell, J., Coalson, T., & Van Essen, D. (2010). A surface-based analysis of hemispheric asymmetries and folding of cerebral cortex in term-born human infants. *The Journal of Neuroscience: The Official Journal of the Society for Neuroscience*, *30*(6), 2268–2276.

Hill, J., Inder, T., Neil, J., Dierker, D., Harwell, J., & Van Essen, D. (2010). Similar patterns of cortical expansion during human development and evolution. *Proceedings of the National Academy of Sciences of the United States of America*, *107*(29), 13135–13140.

Holgado–Tello, F. P., Chacón–Moscoso, S., Barbero–García, I., & Vila–Abad, E. (2008). Polychoric versus Pearson correlations in exploratory and confirmatory factor analysis of ordinal variables. *Quality & Quantity*, *44*(1), 153.

Hua, J. P. Y., Karcher, N. R., Straub, K. T., & Kerns, J. G. (2021). Associations between long-term psychosis risk, probabilistic category learning, and attenuated psychotic symptoms with cortical surface morphometry. *Brain Imaging and Behavior*. https://doi.org/10.1007/s11682-021-00479-8

Huntenburg, J. M., Bazin, P.-L., & Margulies, D. S. (2018). Large-Scale Gradients in Human Cortical Organization. *Trends in Cognitive Sciences*, *22*(1), 21–31.

Huttenlocher, P. R. (1990). Morphometric study of human cerebral cortex development. *Neuropsychologia*, *28*(6), 517–527.

Im, K., Lee, J.-M., Lyttelton, O., Kim, S. H., Evans, A. C., & Kim, S. I. (2008). Brain size and cortical structure in the adult human brain. *Cerebral Cortex* , *18*(9), 2181–2191.

Insel, T., Cuthbert, B., Garvey, M., Heinssen, R., Pine, D. S., Quinn, K., Sanislow, C., & Wang, P. (2010). Research domain criteria (RDoC): toward a new classification framework for research on mental disorders. *The American Journal of Psychiatry*, *167*(7), 748–751.

Isamah, N., Faison, W., Payne, M. E., MacFall, J., Steffens, D. C., Beyer, J. L., Krishnan, K. R., & Taylor, W. D. (2010). Variability in frontotemporal brain structure: the importance of recruitment of African Americans in neuroscience research. *PloS One*, *5*(10), e13642.

Jabbi, M., Swart, M., & Keysers, C. (2007). Empathy for positive and negative emotions in the gustatory cortex. *NeuroImage*, *34*(4), 1744–1753.

Jacobson, S., Kelleher, I., Harley, M., Murtagh, A., Clarke, M., Blanchard, M., Connolly, C., O'Hanlon, E., Garavan, H., & Cannon, M. (2010). Structural and functional brain

correlates of subclinical psychotic symptoms in 11-13 year old schoolchildren. *NeuroImage*, *49*(2), 1875–1885.

Jalbrzikowski, M., Freedman, D., Hegarty, C. E., Mennigen, E., Karlsgodt, K. H., Olde Loohuis, L. M., Ophoff, R. A., Gur, R. E., & Bearden, C. E. (2019). Structural Brain Alterations in Youth With Psychosis and Bipolar Spectrum Symptoms. *Journal of the American Academy of Child and Adolescent Psychiatry*, *58*(11), 1079–1091.

Jeon, S., Lepage, C., Lewis, L., Khalili-Mahani, N., Bermudez, P., Vincent, R. D., Zijdenbos, A., Omidyeganeh, M., Adalat, R., & Evans, A. C. (2017, June). Reproducibility of Cortical Thickness Measurement: CIVET (v2.1) vs. Freesurfer (v6.0-beta & v5.3). *23rd Annual Meeting of the Organization for Human Brain Mapping*. 23rd Annual Meeting of the Organization for Human Brain Mapping, Vancouver, BC, Canada. https://archive.aievolution.com/2017/hbm1701/index.cfm?do=abs.viewAbs&abs=3137

Jeon, T., Mishra, V., Ouyang, M., Chen, M., & Huang, H. (2015). Synchronous Changes of Cortical Thickness and Corresponding White Matter Microstructure During Brain Development Accessed by Diffusion MRI Tractography from Parcellated Cortex. *Frontiers in Neuroanatomy*, *9*, 158.

Jessen, K., Mandl, R. C. W., Fagerlund, B., Bojesen, K. B., Raghava, J. M., Obaid, H. G., Jensen, M. B., Johansen, L. B., Nielsen, M. Ø., Pantelis, C., Rostrup, E., Glenthøj, B. Y., & Ebdrup, B. H. (2019). Patterns of Cortical Structures and Cognition in Antipsychotic-Naïve Patients With First-Episode Schizophrenia: A Partial Least Squares Correlation Analysis. *Biological Psychiatry. Cognitive Neuroscience and Neuroimaging*, *4*(5), 444–453.

Johns, L. C., Cannon, M., Singleton, N., Murray, R. M., Farrell, M., Brugha, T., Bebbington, P., Jenkins, R., & Meltzer, H. (2004). Prevalence and correlates of self-reported psychotic symptoms in the British population. *The British Journal of Psychiatry: The Journal of Mental Science*, *185*, 298–305.

Jung, W. H., Kim, J. S., Jang, J. H., Choi, J.-S., Jung, M. H., Park, J.-Y., Han, J. Y., Choi, C.-H., Kang, D.-H., Chung, C. K., & Kwon, J. S. (2011). Cortical thickness reduction in individuals at ultra-high-risk for psychosis. *Schizophrenia Bulletin*, *37*(4), 839–849.

Kaczkurkin, A. N., Moore, T. M., Sotiras, A., Xia, C. H., Shinohara, R. T., & Satterthwaite, T. D. (2020). Approaches to Defining Common and Dissociable Neurobiological Deficits Associated With Psychopathology in Youth. *Biological Psychiatry*, *88*(1), 51–62.

Kaczkurkin, A. N., Park, S. S., Sotiras, A., Moore, T. M., Calkins, M. E., Cieslak, M., Rosen, A. F. G., Ciric, R., Xia, C. H., Cui, Z., Sharma, A., Wolf, D. H., Ruparel, K., Pine, D. S., Shinohara, R. T., Roalf, D. R., Gur, R. C., Davatzikos, C., Gur, R. E., & Satterthwaite, T. D. (2019). Evidence for Dissociable Linkage of Dimensions of Psychopathology to Brain Structure in Youths. *The American Journal of Psychiatry*, *176*(12), 1000–1009.

Kahl, M., Wagner, G., de la Cruz, F., Köhler, S., & Schultz, C. C. (2020). Resilience and cortical thickness: a MRI study. *European Archives of Psychiatry and Clinical Neuroscience*, *270*(5), 533–539.

Karcher, N. R., Klaunig, M. J., Elsayed, N. M., Taylor, R. L., Jay, S. Y., & Schiffman, J. (2022). Understanding Associations Between Race/Ethnicity, Experiences of Discrimination, and

Psychotic-like Experiences in Middle Childhood. *Journal of the American Academy of Child and Adolescent Psychiatry*. https://doi.org/10.1016/j.jaac.2022.03.025

Karcher, N. R., Loewy, R. L., Savill, M., Avenevoli, S., Huber, R. S., Makowski, C., Sher, K. J., & Barch, D. M. (2022). Persistent and distressing psychotic-like experiences using adolescent brain cognitive development[SM] study data. *Molecular Psychiatry*, *27*(3), 1490–1501.

Karcher, N. R., Paul, S. E., Johnson, E. C., Hatoum, A. S., Baranger, D. A. A., Agrawal, A., Thompson, W. K., Barch, D. M., & Bogdan, R. (2022). Psychotic-like Experiences and Polygenic Liability in the Adolescent Brain Cognitive Development Study. *Biological Psychiatry. Cognitive Neuroscience and Neuroimaging*, *7*(1), 45–55.

Kaufman, J., Birmaher, B., Brent, D., Rao, U., Flynn, C., Moreci, P., Williamson, D., & Ryan, N. (1997). Schedule for Affective Disorders and Schizophrenia for School-Age Children-Present and Lifetime Version (K-SADS-PL): initial reliability and validity data. *Journal of the American Academy of Child and Adolescent Psychiatry*, *36*(7), 980–988.

Kaymaz, N., Drukker, M., Lieb, R., Wittchen, H.-U., Werbeloff, N., Weiser, M., Lataster, T., & van Os, J. (2012). Do subthreshold psychotic experiences predict clinical outcomes in unselected non-help-seeking population-based samples? A systematic review and meta-analysis, enriched with new results. *Psychological Medicine*, *42*(11), 2239–2253.

Keil, J. M., Qalieh, A., & Kwan, K. Y. (2018). Brain Transcriptome Databases: A User's Guide. *The Journal of Neuroscience: The Official Journal of the Society for Neuroscience*, *38*(10), 2399–2412.

Kelleher, I., Clarke, M. C., Rawdon, C., Murphy, J., & Cannon, M. (2013). Neurocognition in the extended psychosis phenotype: performance of a community sample of adolescents with psychotic symptoms on the MATRICS neurocognitive battery. *Schizophrenia Bulletin*, *39*(5), 1018–1026.

Kelleher, I., Connor, D., Clarke, M. C., Devlin, N., Harley, M., & Cannon, M. (2012). Prevalence of psychotic symptoms in childhood and adolescence: a systematic review and meta-analysis of population-based studies. *Psychological Medicine*, *42*(9), 1857–1863.

Kelleher, I., Keeley, H., Corcoran, P., Lynch, F., Fitzpatrick, C., Devlin, N., Molloy, C., Roddy, S., Clarke, M. C., Harley, M., Arseneault, L., Wasserman, C., Carli, V., Sarchiapone, M., Hoven, C., Wasserman, D., & Cannon, M. (2012). Clinicopathological significance of psychotic experiences in non-psychotic young people: evidence from four population-based studies. *The British Journal of Psychiatry: The Journal of Mental Science*, *201*(1), 26–32.

Keshavan, M. S., Giedd, J., Lau, J. Y. F., Lewis, D. A., & Paus, T. (2014). Changes in the adolescent brain and the pathophysiology of psychotic disorders. *The Lancet. Psychiatry*, *1*(7), 549–558.

Kiang, M., Christensen, B. K., Streiner, D. L., Roy, C., Patriciu, I., & Zipursky, R. B. (2013). Association of abnormal semantic processing with delusion-like ideation in frequent cannabis users: an electrophysiological study. *Psychopharmacology*, *225*(1), 95–104.

Kim, J. S., Singh, V., Lee, J. K., Lerch, J., Ad-Dab'bagh, Y., MacDonald, D., Lee, J. M., Kim, S. I., & Evans, A. C. (2005). Automated 3-D extraction and evaluation of the inner and outer

cortical surfaces using a Laplacian map and partial volume effect classification. *NeuroImage*, *27*(1), 210–221.

Kim, R., Healey, K. L., Sepulveda-Orengo, M. T., & Reissner, K. J. (2018). Astroglial correlates of neuropsychiatric disease: From astrocytopathy to astrogliosis. *Progress in Neuro-Psychopharmacology & Biological Psychiatry*, *87*(Pt A), 126–146.

King, J. B., Lopez-Larson, M. P., & Yurgelun-Todd, D. A. (2016). Mean cortical curvature reflects cytoarchitecture restructuring in mild traumatic brain injury. *NeuroImage. Clinical*, *11*, 81–89.

Kirkbride, J. B., Barker, D., Cowden, F., Stamps, R., Yang, M., Jones, P. B., & Coid, J. W. (2008). Psychoses, ethnicity and socio-economic status. *The British Journal of Psychiatry: The Journal of Mental Science*, *193*(1), 18–24.

Kirschner, M., Hodzic-Santor, B., Antoniades, M., Nenadic, I., Kircher, T., Krug, A., Meller, T., Grotegerd, D., Fornito, A., Arnatkeviciute, A., Bellgrove, M. A., Tiego, J., Dannlowski, U., Koch, K., Hülsmann, C., Kugel, H., Enneking, V., Klug, M., Leehr, E. J., … Modinos, G. (2021). Cortical and subcortical neuroanatomical signatures of schizotypy in 3004 individuals assessed in a worldwide ENIGMA study. *Molecular Psychiatry*. https://doi.org/10.1038/s41380-021-01359-9

Kirschner, M., Paquola, C., Khundrakpam, B. S., Vainik, U., Bhutani, N., Hodzic-Santor, B., Georgiadis, F., Al-Sharif, N. B., Misic, B., Bernhardt, B., Evans, A. C., & Dagher, A. (2022). Schizophrenia polygenic risk during typical development reflects multiscale cortical organization. *Biological Psychiatry Global Open Science*. https://doi.org/10.1016/j.bpsgos.2022.08.003

Kirschner, M., Shafiei, G., Markello, R. D., Makowski, C., Talpalaru, A., Hodzic-Santor, B., Devenyi, G. A., Paquola, C., Bernhardt, B. C., Lepage, M., Chakravarty, M. M., Dagher, A., & Mišić, B. (2020). Latent Clinical-Anatomical Dimensions of Schizophrenia. *Schizophrenia Bulletin*. https://doi.org/10.1093/schbul/sbaa097

Kirschner, M., Shafiei, G., Markello, R. D., Markowski, C., Talpalaru, A., Hodzic-Santor, B., Devenyi, G. A., Lepage, M., Chakravarty, M. M., Dagher, A., & Misic, B. (2020). Clinical-Anatomical Phenotypes of Schizophrenia. *Biological Psychiatry*, *87*(9), S119–S120.

Kırlı, U., Binbay, T., Drukker, M., Elbi, H., Kayahan, B., Keskin Gökçelli, D., Özkınay, F., Onay, H., Alptekin, K., & van Os, J. (2019). DSM outcomes of psychotic experiences and associated risk factors: 6-year follow-up study in a community-based sample. *Psychological Medicine*, *49*(8), 1346–1356.

Klein, A., & Tourville, J. (2012). 101 labeled brain images and a consistent human cortical labeling protocol. *Frontiers in Neuroscience*, *6*, 171.

Klein, D., Rotarska-Jagiela, A., Genc, E., Sritharan, S., Mohr, H., Roux, F., Han, C. E., Kaiser, M., Singer, W., & Uhlhaas, P. J. (2014). Adolescent brain maturation and cortical folding: evidence for reductions in gyrification. *PloS One*, *9*(1), e84914.

Kobayashi, H., Nemoto, T., Koshikawa, H., Osono, Y., Yamazawa, R., Murakami, M., Kashima, H., & Mizuno, M. (2008). A self-reported instrument for prodromal symptoms of psychosis: testing the clinical validity of the PRIME Screen-Revised (PS-R) in a Japanese population. *Schizophrenia Research*, *106*(2–3), 356–362.

Kotov, R., Foti, D., Li, K., Bromet, E. J., Hajcak, G., & Ruggero, C. J. (2016). Validating dimensions of psychosis symptomatology: Neural correlates and 20-year outcomes. *Journal of Abnormal Psychology*, *125*(8), 1103–1119.

Kotov, R., Krueger, R. F., & Watson, D. (2018). A paradigm shift in psychiatric classification: the Hierarchical Taxonomy Of Psychopathology (HiTOP). *World Psychiatry: Official Journal of the World Psychiatric Association* , *17*(1), 24–25.

Kotov, R., Krueger, R. F., Watson, D., Achenbach, T. M., Althoff, R. R., Bagby, R. M., Brown, T. A., Carpenter, W. T., Caspi, A., Clark, L. A., Eaton, N. R., Forbes, M. K., Forbush, K. T., Goldberg, D., Hasin, D., Hyman, S. E., Ivanova, M. Y., Lynam, D. R., Markon, K., … Zimmerman, M. (2017). The Hierarchical Taxonomy of Psychopathology (HiTOP): A dimensional alternative to traditional nosologies. *Journal of Abnormal Psychology*, *126*(4), 454–477.

Kovacevic, N., Abdi, H., Beaton, D., & McIntosh, A. R. (2013). *Revisiting PLS Resampling: Comparing Significance Versus Reliability Across Range of Simulations*. *56*, 159–170.

Krishnan, A., Williams, L. J., McIntosh, A. R., & Abdi, H. (2011). Partial Least Squares (PLS) methods for neuroimaging: a tutorial and review. *NeuroImage*, *56*(2), 455–475.

Kroenke, C. D., & Bayly, P. V. (2018). How Forces Fold the Cerebral Cortex. *The Journal of Neuroscience: The Official Journal of the Society for Neuroscience*, *38*(4), 767–775.

Lake, B. B., Chen, S., Sos, B. C., Fan, J., Kaeser, G. E., Yung, Y. C., Duong, T. E., Gao, D., Chun, J., Kharchenko, P. V., & Zhang, K. (2018). Integrative single-cell analysis of transcriptional and epigenetic states in the human adult brain. *Nature Biotechnology*, *36*(1), 70–80.

Laurens, K. R., Hodgins, S., Maughan, B., Murray, R. M., Rutter, M. L., & Taylor, E. A. (2007). Community screening for psychotic-like experiences and other putative antecedents of schizophrenia in children aged 9-12 years. *Schizophrenia Research*, *90*(1–3), 130–146.

Laurens, K. R., West, S. A., Murray, R. M., & Hodgins, S. (2008). Psychotic-like experiences and other antecedents of schizophrenia in children aged 9-12 years: a comparison of ethnic and migrant groups in the United Kingdom. *Psychological Medicine*, *38*(8), 1103–1111.

Lee, J. S., Chun, J. W., Lee, S.-H., Kim, E., Lee, S.-K., & Kim, J.-J. (2015). Altered neural basis of the reality processing and its relation to cognitive insight in schizophrenia. *PloS One*, *10*(3), e0120478.

Lerch, J. P., & Evans, A. C. (2005). Cortical thickness analysis examined through power analysis and a population simulation. *NeuroImage*, *24*(1), 163–173.

Lerch, J. P., van der Kouwe, A. J. W., Raznahan, A., Paus, T., Johansen-Berg, H., Miller, K. L., Smith, S. M., Fischl, B., & Sotiropoulos, S. N. (2017). Studying neuroanatomy using MRI. *Nature Neuroscience*, *20*(3), 314–326.

Lerch, J. P., Worsley, K., Shaw, W. P., Greenstein, D. K., Lenroot, R. K., Giedd, J., & Evans, A. C. (2006). Mapping anatomical correlations across cerebral cortex (MACACC) using cortical thickness from MRI. *NeuroImage*, *31*(3), 993–1003.

Lewis, L., Lepage, C., Khalili-Mahani, N., Omidyeganeh, M., Jeon, S., Bermudez, P., Zijdenbos, A., Vincent, R. D., Adalat, R., & Evans, A. C. (2017, June). Robustness and reliability of

cortical surface reconstruction in CIVET and FreeSurfer. *23rd Annual Meeting of the Organization for Human Brain Mapping*. 23rd Annual Meeting of the Organization for Human Brain Mapping, Vancouver, BC, Canada. https://archive.aievolution.com/2017/hbm1701/index.cfm?do=abs.viewAbs&abs=1225

Li, G., Wang, L., Shi, F., Lyall, A. E., Lin, W., Gilmore, J. H., & Shen, D. (2014). Mapping longitudinal development of local cortical gyrification in infants from birth to 2 years of age. *The Journal of Neuroscience: The Official Journal of the Society for Neuroscience*, *34*(12), 4228–4238.

Li, M., Santpere, G., Kawasawa, Y. I., Evgrafov, O. V., Gulden, F. O., Pochareddy, S., Sunkin, S. M., Li, Z., Shin, Y., Zhu, Y., Sousa, A. M. M., Werling, D. M., Kitchen, R. R., Kang, H. J., Pletikos, M., Choi, J., Muchnik, S., Xu, X., Wang, D., … Li, Z. (2018). Integrative functional genomic analysis of human brain development and neuropsychiatric risks. *Science*, *362*(6420), eaat7615.

Liao, Y., Wang, J., Jaehnig, E. J., Shi, Z., & Zhang, B. (2019). WebGestalt 2019: gene set analysis toolkit with revamped UIs and APIs. *Nucleic Acids Research*, *47*(W1), W199–W205.

Liddle, P. F. (1987). The symptoms of chronic schizophrenia. A re-examination of the positive-negative dichotomy. *The British Journal of Psychiatry: The Journal of Mental Science*, *151*, 145–151.

Lin, Y., Li, M., Zhou, Y., Deng, W., Ma, X., Wang, Q., Guo, W., Li, Y., Jiang, L., Hu, X., Zhang, N., & Li, T. (2019). Age-Related Reduction in Cortical Thickness in First-Episode Treatment-Naïve Patients with Schizophrenia. *Neuroscience Bulletin*, *35*(4), 688–696.

Linscott, R. J., & van Os, J. (2013). An updated and conservative systematic review and meta-analysis of epidemiological evidence on psychotic experiences in children and adults: on the pathway from proneness to persistence to dimensional expression across mental disorders. *Psychological Medicine*, *43*(6), 1133–1149.

Liu, L., Cui, L.-B., Wu, X.-S., Fei, N.-B., Xu, Z.-L., Wu, D., Xi, Y.-B., Huang, P., von Deneen, K. M., Qi, S., Zhang, Y.-H., Wang, H.-N., Yin, H., & Qin, W. (2020). Cortical abnormalities and identification for first-episode schizophrenia via high-resolution magnetic resonance imaging. *Biomarkers in Neuropsychiatry*, *3*, 100022.

Llinares-Benadero, C., & Borrell, V. (2019). Deconstructing cortical folding: genetic, cellular and mechanical determinants. *Nature Reviews. Neuroscience*, *20*(3), 161–176.

Lyall, A. E., Shi, F., Geng, X., Woolson, S., Li, G., Wang, L., Hamer, R. M., Shen, D., & Gilmore, J. H. (2015). Dynamic Development of Regional Cortical Thickness and Surface Area in Early Childhood. *Cerebral Cortex* , *25*(8), 2204–2212.

Lyttelton, O. C., Karama, S., Ad-Dab'bagh, Y., Zatorre, R. J., Carbonell, F., Worsley, K., & Evans, A. C. (2009). Positional and surface area asymmetry of the human cerebral cortex. *NeuroImage*, *46*(4), 895–903.

Madeira, L., Bonoldi, I., Rocchetti, M., Brandizzi, M., Samson, C., Azis, M., Queen, B., Bossong, M., Allen, P., Perez, J., Howes, O. D., McGuire, P., & Fusar-Poli, P. (2016). Prevalence and implications of Truman symptoms in subjects at ultra high risk for psychosis. *Psychiatry Research*, *238*, 270–276.

Maj, M., van Os, J., De Hert, M., Gaebel, W., Galderisi, S., Green, M. F., Guloksuz, S., Harvey, P. D., Jones, P. B., Malaspina, D., McGorry, P., Miettunen, J., Murray, R. M., Nuechterlein, K. H., Peralta, V., Thornicroft, G., van Winkel, R., & Ventura, J. (2021). The clinical characterization of the patient with primary psychosis aimed at personalization of management. *World Psychiatry: Official Journal of the World Psychiatric Association* , *20*(1), 4–33.

Marek, S., Tervo-Clemmens, B., Calabro, F. J., Montez, D. F., Kay, B. P., Hatoum, A. S., Donohue, M. R., Foran, W., Miller, R. L., Hendrickson, T. J., Malone, S. M., Kandala, S., Feczko, E., Miranda-Dominguez, O., Graham, A. M., Earl, E. A., Perrone, A. J., Cordova, M., Doyle, O., … Dosenbach, N. U. F. (2022). Reproducible brain-wide association studies require thousands of individuals. *Nature*, 1–7.

Margulies, D. S., Ghosh, S. S., Goulas, A., Falkiewicz, M., Huntenburg, J. M., Langs, G., Bezgin, G., Eickhoff, S. B., Castellanos, F. X., Petrides, M., Jefferies, E., & Smallwood, J. (2016). Situating the default-mode network along a principal gradient of macroscale cortical organization. *Proceedings of the National Academy of Sciences of the United States of America*, *113*(44), 12574–12579.

Markello, R. D., Arnatkeviciute, A., Poline, J.-B., Fulcher, B. D., Fornito, A., & Misic, B. (2021). Standardizing workflows in imaging transcriptomics with the abagen toolbox. *ELife*, *10*. https://doi.org/10.7554/eLife.72129

Markello, R. D., Hansen, J. Y., Liu, Z.-Q., Bazinet, V., Shafiei, G., Suárez, L. E., Blostein, N., Seidlitz, J., Baillet, S., Satterthwaite, T. D., Chakravarty, M. M., Raznahan, A., & Misic, B. (2022). neuromaps: structural and functional interpretation of brain maps. *Nature Methods*, *19*(11), 1472–1479.

Martin, E. A., Jonas, K. G., Lian, W., Foti, D., Donaldson, K. R., Bromet, E. J., & Kotov, R. (2021). Predicting Long-Term Outcomes in First-Admission Psychosis: Does the Hierarchical Taxonomy of Psychopathology Aid DSM in Prognostication? *Schizophrenia Bulletin*, *47*(5), 1331–1341.

Martins, D., Giacomel, A., Williams, S. C. R., Turkheimer, F., Dipasquale, O., Veronese, M., & PET Templates Working Group. (2021). Imaging transcriptomics: Convergent cellular, transcriptomic, and molecular neuroimaging signatures in the healthy adult human brain. *Cell Reports*, *37*(13), 110173.

Matsuda, Y., & Ohi, K. (2018). Cortical gyrification in schizophrenia: current perspectives. *Neuropsychiatric Disease and Treatment*, *14*, 1861–1869.

McGlashan, T., Walsh, B., & Woods, S. (2010). *The Psychosis-Risk Syndrome: Handbook for Diagnosis and Follow-Up*. Oxford University Press, USA.

McGrath, J. J., Saha, S., Al-Hamzawi, A., Alonso, J., Bromet, E. J., Bruffaerts, R., Caldas-de-Almeida, J. M., Chiu, W. T., de Jonge, P., Fayyad, J., Florescu, S., Gureje, O., Haro, J. M., Hu, C., Kovess-Masfety, V., Lepine, J. P., Lim, C. C. W., Mora, M. E. M., Navarro-Mateu, F., … Kessler, R. C. (2015). Psychotic Experiences in the General Population: A Cross-National Analysis Based on 31,261 Respondents From 18 Countries. *JAMA Psychiatry* , *72*(7), 697–705.

McGrath, J. J., Saha, S., Al-Hamzawi, A., Andrade, L., Benjet, C., Bromet, E. J., Browne, M. O., Caldas de Almeida, J. M., Chiu, W. T., Demyttenaere, K., Fayyad, J., Florescu, S., de Girolamo, G., Gureje, O., Haro, J. M., Ten Have, M., Hu, C., Kovess-Masfety, V., Lim, C. C. W., … Kessler, R. C. (2016). The Bidirectional Associations Between Psychotic Experiences and DSM-IV Mental Disorders. *The American Journal of Psychiatry*, *173*(10), 997–1006.

McGrath, J. J., Saha, S., Al-Hamzawi, A. O., Alonso, J., Andrade, L., Borges, G., Bromet, E. J., Oakley Browne, M., Bruffaerts, R., Caldas de Almeida, J. M., Fayyad, J., Florescu, S., de Girolamo, G., Gureje, O., Hu, C., de Jonge, P., Kovess-Masfety, V., Lepine, J. P., Lim, C. C. W., … Kessler, R. C. (2016). Age of Onset and Lifetime Projected Risk of Psychotic Experiences: Cross-National Data From the World Mental Health Survey. *Schizophrenia Bulletin*, *42*(4), 933–941.

McIntosh, A. R., Chau, W. K., & Protzner, A. B. (2004). Spatiotemporal analysis of event-related fMRI data using partial least squares. *NeuroImage*, *23*(2), 764–775.

McIntosh, A. R., & Lobaugh, N. J. (2004). Partial least squares analysis of neuroimaging data: applications and advances. *NeuroImage*, *23 Suppl 1*, S250-63.

McIntosh, A. R., & Mišić, B. (2013). Multivariate statistical analyses for neuroimaging data. *Annual Review of Psychology*, *64*, 499–525.

Medford, N., Sierra, M., Stringaris, A., Giampietro, V., Brammer, M. J., & David, A. S. (2016). Emotional Experience and Awareness of Self: Functional MRI Studies of Depersonalization Disorder. *Frontiers in Psychology*, *7*, 432.

Mediavilla, R., López-Arroyo, M., Gómez-Arnau, J., Wiesepape, C., Lysaker, P. H., & Lahera, G. (2021). Autobiographical memory in schizophrenia: The role of metacognition. *Comprehensive Psychiatry*, *109*, 152254.

Meller, T., Schmitt, S., Ettinger, U., Grant, P., Stein, F., Brosch, K., Grotegerd, D., Dohm, K., Meinert, S., Förster, K., Hahn, T., Jansen, A., Dannlowski, U., Krug, A., Kircher, T., & Nenadić, I. (2020). Brain structural correlates of schizotypal signs and subclinical schizophrenia nuclear symptoms in healthy individuals. *Psychological Medicine*, 1–10.

Mennigen, E., & Bearden, C. E. (2020). Psychosis Risk and Development: What Do We Know From Population-Based Studies? *Biological Psychiatry*, *88*(4), 315–325.

Mihalik, A., Ferreira, F. S., Moutoussis, M., Ziegler, G., Adams, R. A., Rosa, M. J., Prabhu, G., de Oliveira, L., Pereira, M., Bullmore, E. T., Fonagy, P., Goodyer, I. M., Jones, P. B., NeuroScience in Psychiatry Network (NSPN) Consortium, Shawe-Taylor, J., Dolan, R., & Mourão-Miranda, J. (2020). Multiple Holdouts With Stability: Improving the Generalizability of Machine Learning Analyses of Brain-Behavior Relationships. *Biological Psychiatry*, *87*(4), 368–376.

Miller, T. J., McGlashan, T. H., Rosen, J. L., Cadenhead, K., Cannon, T., Ventura, J., McFarlane, W., Perkins, D. O., Pearlson, G. D., & Woods, S. W. (2003). Prodromal assessment with the structured interview for prodromal syndromes and the scale of prodromal symptoms: predictive validity, interrater reliability, and training to reliability. *Schizophrenia Bulletin*, *29*(4), 703–715.

Mollon, J., David, A. S., Morgan, C., Frissa, S., Glahn, D., Pilecka, I., Hatch, S. L., Hotopf, M., & Reichenberg, A. (2016). Psychotic Experiences and Neuropsychological Functioning in a Population-based Sample. *JAMA Psychiatry* , *73*(2), 129–138.

Moore, T. M., Martin, I. K., Gur, O. M., Jackson, C. T., Scott, J. C., Calkins, M. E., Ruparel, K., Port, A. M., Nivar, I., Krinsky, H. D., Gur, R. E., & Gur, R. C. (2016). Characterizing social environment's association with neurocognition using census and crime data linked to the Philadelphia Neurodevelopmental Cohort. *Psychological Medicine*, *46*(3), 599–610.

Morgan, C., Knowles, G., & Hutchinson, G. (2019). Migration, ethnicity and psychoses: evidence, models and future directions. *World Psychiatry: Official Journal of the World Psychiatric Association* , *18*(3), 247–258.

Morgan, S. E., Seidlitz, J., Whitaker, K. J., Romero-Garcia, R., Clifton, N. E., Scarpazza, C., van Amelsvoort, T., Marcelis, M., van Os, J., Donohoe, G., Mothersill, D., Corvin, A., Pocklington, A., Raznahan, A., McGuire, P., Vértes, P. E., & Bullmore, E. T. (2019). Cortical patterning of abnormal morphometric similarity in psychosis is associated with brain expression of schizophrenia-related genes. *Proceedings of the National Academy of Sciences of the United States of America*, *116*(19), 9604–9609.

Mueller, S., Wang, D., Fox, M. D., Yeo, B. T. T., Sepulcre, J., Sabuncu, M. R., Shafee, R., Lu, J., & Liu, H. (2013). Individual variability in functional connectivity architecture of the human brain. *Neuron*, *77*(3), 586–595.

Murray, R. M., Bhavsar, V., Tripoli, G., & Howes, O. (2017). 30 Years on: How the Neurodevelopmental Hypothesis of Schizophrenia Morphed Into the Developmental Risk Factor Model of Psychosis. *Schizophrenia Bulletin*, *43*(6), 1190–1196.

Mutlu, A. K., Schneider, M., Debbané, M., Badoud, D., Eliez, S., & Schaer, M. (2013). Sex differences in thickness, and folding developments throughout the cortex. *NeuroImage*, *82*, 200–207.

Natu, V. S., Gomez, J., Barnett, M., Jeska, B., Kirilina, E., Jaeger, C., Zhen, Z., Cox, S., Weiner, K. S., Weiskopf, N., & Grill-Spector, K. (2019). Apparent thinning of human visual cortex during childhood is associated with myelination. *Proceedings of the National Academy of Sciences of the United States of America*, *116*(41), 20750–20759.

Nelson, M. T., Seal, M. L., Pantelis, C., & Phillips, L. J. (2013). Evidence of a dimensional relationship between schizotypy and schizophrenia: a systematic review. *Neuroscience and Biobehavioral Reviews*, *37*(3), 317–327.

Nenadic, I., Dietzek, M., Schönfeld, N., Lorenz, C., Gussew, A., Reichenbach, J. R., Sauer, H., Gaser, C., & Smesny, S. (2015). Brain structure in people at ultra-high risk of psychosis, patients with first-episode schizophrenia, and healthy controls: a VBM study. *Schizophrenia Research*, *161*(2–3), 169–176.

Nenadic, I., Lorenz, C., Langbein, K., Dietzek, M., Smesny, S., Schönfeld, N., Fañanás, L., Sauer, H., & Gaser, C. (2015). Brain structural correlates of schizotypy and psychosis proneness in a non-clinical healthy volunteer sample. *Schizophrenia Research*, *168*(1–2), 37–43.

Neufeld, N. H., Kaczkurkin, A. N., Sotiras, A., Mulsant, B. H., Dickie, E. W., Flint, A. J., Meyers, B. S., Alexopoulos, G. S., Rothschild, A. J., Whyte, E. M., Mah, L., Nierenberg, J., Hoptman, M. J., Davatzikos, C., Satterthwaite, T. D., & Voineskos, A. N. (2020).

Structural brain networks in remitted psychotic depression. *Neuropsychopharmacology: Official Publication of the American College of Neuropsychopharmacology*, *45*(7), 1223–1231.

Nie, J., Guo, L., Li, K., Wang, Y., Chen, G., Li, L., Chen, H., Deng, F., Jiang, X., Zhang, T., Huang, L., Faraco, C., Zhang, D., Guo, C., Yap, P.-T., Hu, X., Li, G., Lv, J., Yuan, Y., … Liu, T. (2012). Axonal fiber terminations concentrate on gyri. *Cerebral Cortex* , *22*(12), 2831–2839.

Ochi, R., Plitman, E., Patel, R., Tarumi, R., Iwata, Y., Tsugawa, S., Kim, J., Honda, S., Noda, Y., Uchida, H., Devenyi, G. A., Mimura, M., Graff-Guerrero, A., Chakravarty, M. M., & Nakajima, S. (2022). Investigating structural subdivisions of the anterior cingulate cortex in schizophrenia, with implications for treatment resistance and glutamatergic levels. *Journal of Psychiatry & Neuroscience: JPN*, *47*(1), E1–E10.

Ochoa, S., Usall, J., Cobo, J., Labad, X., & Kulkarni, J. (2012). Gender differences in schizophrenia and first-episode psychosis: a comprehensive literature review. *Schizophrenia Research and Treatment*, *2012*, 916198.

Paksarian, D., Merikangas, K. R., Calkins, M. E., & Gur, R. E. (2016). Racial-ethnic disparities in empirically-derived subtypes of subclinical psychosis among a U.S. sample of youths. *Schizophrenia Research*, *170*(1), 205–210.

Palaniyappan, L., Mallikarjun, P., Joseph, V., White, T. P., & Liddle, P. F. (2011). Regional contraction of brain surface area involves three large-scale networks in schizophrenia. *Schizophrenia Research*, *129*(2–3), 163–168.

Panizzon, M. S., Fennema-Notestine, C., Eyler, L. T., Jernigan, T. L., Prom-Wormley, E., Neale, M., Jacobson, K., Lyons, M. J., Grant, M. D., Franz, C. E., Xian, H., Tsuang, M., Fischl, B., Seidman, L., Dale, A., & Kremen, W. S. (2009). Distinct genetic influences on cortical surface area and cortical thickness. *Cerebral Cortex* , *19*(11), 2728–2735.

Park, I., Kim, M., Lee, T. Y., Hwang, W. J., Bin Kwak, Y., Oh, S., Lho, S. K., Moon, S.-Y., & Kwon, J. S. (2021). Reduced cortical gyrification in the posteromedial cortex in unaffected relatives of schizophrenia patients with high genetic loading. *NPJ Schizophrenia*, *7*(1), 17.

Park, M. T. M., Raznahan, A., Shaw, P., Gogtay, N., Lerch, J. P., & Chakravarty, M. M. (2018). Neuroanatomical phenotypes in mental illness: identifying convergent and divergent cortical phenotypes across autism, ADHD and schizophrenia. *Journal of Psychiatry & Neuroscience: JPN*, *43*(3), 201–212.

Patel, R., Mackay, C. E., Jansen, M. G., Devenyi, G. A., O'Donoghue, M. C., Kivimäki, M., Singh-Manoux, A., Zsoldos, E., Ebmeier, K. P., Chakravarty, M. M., & Suri, S. (2022). Inter- and intra-individual variation in brain structural-cognition relationships in aging. *NeuroImage*, *257*, 119254.

Patel, R., Steele, C. J., Chen, A. G. X., Patel, S., Devenyi, G. A., Germann, J., Tardif, C. L., & Chakravarty, M. M. (2020). Investigating microstructural variation in the human hippocampus using non-negative matrix factorization. *NeuroImage*, *207*, 116348.

Patel, Y., Shin, J., Drakesmith, M., Evans, J., Pausova, Z., & Paus, T. (2020). Virtual histology of multi-modal magnetic resonance imaging of cerebral cortex in young men. *NeuroImage*, *218*, 116968.

Paus, T., Keshavan, M., & Giedd, J. N. (2008). Why do many psychiatric disorders emerge during adolescence? *Nature Reviews. Neuroscience*, *9*(12), 947–957.

Perälä, J., Suvisaari, J., Saarni, S. I., Kuoppasalmi, K., Isometsä, E., Pirkola, S., Partonen, T., Tuulio-Henriksson, A., Hintikka, J., Kieseppä, T., Härkänen, T., Koskinen, S., & Lönnqvist, J. (2007). Lifetime prevalence of psychotic and bipolar I disorders in a general population. *Archives of General Psychiatry*, *64*(1), 19–28.

Peralta, V., & Cuesta, M. J. (1999). Dimensional structure of psychotic symptoms: an item-level analysis of SAPS and SANS symptoms in psychotic disorders. *Schizophrenia Research*, *38*(1), 13–26.

Perez, D. L., Pan, H., Weisholtz, D. S., Root, J. C., Tuescher, O., Fischer, D. B., Butler, T., Vago, D. R., Isenberg, N., Epstein, J., Landa, Y., Smith, T. E., Savitz, A. J., Silbersweig, D. A., & Stern, E. (2015). Altered threat and safety neural processing linked to persecutory delusions in schizophrenia: a two-task fMRI study. *Psychiatry Research*, *233*(3), 352–366.

Pham, T. V., Sasabayashi, D., Takahashi, T., Takayanagi, Y., Kubota, M., Furuichi, A., Kido, M., Noguchi, K., & Suzuki, M. (2021). Longitudinal Changes in Brain Gyrification in Schizophrenia Spectrum Disorders. *Frontiers in Aging Neuroscience*, *13*, 752575.

Phan, K. L., Wager, T., Taylor, S. F., & Liberzon, I. (2002). Functional neuroanatomy of emotion: a meta-analysis of emotion activation studies in PET and fMRI. *NeuroImage*, *16*(2), 331–348.

Pienaar, R., Fischl, B., Caviness, V., Makris, N., & Grant, P. E. (2008). A METHODOLOGY FOR ANALYZING CURVATURE IN THE DEVELOPING BRAIN FROM PRETERM TO ADULT. *International Journal of Imaging Systems and Technology*, *18*(1), 42–68.

Pignon, B., Schürhoff, F., Szöke, A., Geoffroy, P. A., Jardri, R., Roelandt, J.-L., Rolland, B., Thomas, P., Vaiva, G., & Amad, A. (2018). Sociodemographic and clinical correlates of psychotic symptoms in the general population: Findings from the MHGP survey. *Schizophrenia Research*, *193*, 336–342.

Pina-Camacho, L., Martinez, K., Diaz-Caneja, C. M., Mezquida, G., Cuesta, M. J., Moreno, C., Amoretti, S., González-Pinto, A., Arango, C., Vieta, E., Castro-Fornieles, J., Lobo, A., Fraguas, D., Bernardo, M., Janssen, J., Parellada, M., & PEPs Group. (2022). Cortical thinning over two years after first-episode psychosis depends on age of onset. *Schizophrenia (Heidelberg, Germany)*, *8*(1), 20.

Piñero, J., Bravo, À., Queralt-Rosinach, N., Gutiérrez-Sacristán, A., Deu-Pons, J., Centeno, E., García-García, J., Sanz, F., & Furlong, L. I. (2017). DisGeNET: a comprehensive platform integrating information on human disease-associated genes and variants. *Nucleic Acids Research*, *45*(D1), D833–D839.

Postmes, L., Sno, H. N., Goedhart, S., van der Stel, J., Heering, H. D., & de Haan, L. (2014). Schizophrenia as a self-disorder due to perceptual incoherence. *Schizophrenia Research*, *152*(1), 41–50.

Potuzak, M., Ravichandran, C., Lewandowski, K. E., Ongür, D., & Cohen, B. M. (2012). Categorical vs dimensional classifications of psychotic disorders. *Comprehensive Psychiatry*, *53*(8), 1118–1129.

Prasad, K. M. R., Patel, A. R., Muddasani, S., Sweeney, J., & Keshavan, M. S. (2004). The entorhinal cortex in first-episode psychotic disorders: a structural magnetic resonance imaging study. *The American Journal of Psychiatry*, *161*(9), 1612–1619.

Prebble, S. C., Addis, D. R., & Tippett, L. J. (2013). Autobiographical memory and sense of self. *Psychological Bulletin*, *139*(4), 815–840.

Quarteroni, A., Sacco, R., & Saleri, F. (2007). Résolution des équations et des systèmes non linéaires. In Alfio Quarteroni, R. Sacco, & F. Saleri (Eds.), *Méthodes Numériques: Algorithmes, analyse et applications* (pp. 211–257). Springer Milan.

Raballo, A., Sæbye, D., & Parnas, J. (2011). Looking at the schizophrenia spectrum through the prism of self-disorders: an empirical study. *Schizophrenia Bulletin*, *37*(2), 344–351.

Rakic, P. (1988). Specification of cerebral cortical areas. *Science*, *241*(4862), 170–176.

Rakic, P. (1995). A small step for the cell, a giant leap for mankind: a hypothesis of neocortical expansion during evolution. *Trends in Neurosciences*, *18*(9), 383–388.

Rakic, P. (2009). Evolution of the neocortex: a perspective from developmental biology. *Nature Reviews. Neuroscience*, *10*(10), 724–735.

Rapoport, J. L., Giedd, J. N., & Gogtay, N. (2012). Neurodevelopmental model of schizophrenia: update 2012. *Molecular Psychiatry*, *17*(12), 1228–1238.

Ravichandran, C., Ongur, D., & Cohen, B. M. (2021). Clinical Features of Psychotic Disorders: Comparing Categorical and Dimensional Models. *Psychiatric Research and Clinical Practice*, *3*(1), 29–37.

Raznahan, A., Shaw, P., Lalonde, F., Stockman, M., Wallace, G. L., Greenstein, D., Clasen, L., Gogtay, N., & Giedd, J. N. (2011). How does your cortex grow? *The Journal of Neuroscience: The Official Journal of the Society for Neuroscience*, *31*(19), 7174–7177.

Reardon, P. K., Seidlitz, J., Vandekar, S., Liu, S., Patel, R., Park, M. T. M., Alexander-Bloch, A. F., Clasen, L. S., Blumenthal, J. D., Lalonde, F. M., Giedd, J. N., Gur, R. C., Gur, R. E., Lerch, J. P., Chakravarty, M. M., Satterthwaite, T. D., Shinohara, R. T., & Raznahan, A. (2018). Normative brain size variation and brain shape diversity in humans. *Science*, *360*(6394), 1222–1227.

Redolfi, A., Manset, D., Barkhof, F., Wahlund, L.-O., Glatard, T., Mangin, J.-F., Frisoni, G. B., & neuGRID Consortium, for the Alzheimer's Disease Neuroimaging Initiative. (2015). Head-to-head comparison of two popular cortical thickness extraction algorithms: a cross-sectional and longitudinal study. *PloS One*, *10*(3), e0117692.

Reininghaus, U., Priebe, S., & Bentall, R. P. (2013). Testing the psychopathology of psychosis: evidence for a general psychosis dimension. *Schizophrenia Bulletin*, *39*(4), 884–895.

Reise, S. P., Moore, T. M., & Haviland, M. G. (2010). Bifactor models and rotations: exploring the extent to which multidimensional data yield univocal scale scores. *Journal of Personality Assessment*, *92*(6), 544–559.

Remer, J., Croteau-Chonka, E., Dean, D. C., 3rd, D'Arpino, S., Dirks, H., Whiley, D., & Deoni, S. C. L. (2017). Quantifying cortical development in typically developing toddlers and young children, 1-6 years of age. *NeuroImage*, *153*, 246–261.

Rimol, L. M., Nesvåg, R., Hagler, D. J., Jr, Bergmann, O., Fennema-Notestine, C., Hartberg, C. B., Haukvik, U. K., Lange, E., Pung, C. J., Server, A., Melle, I., Andreassen, O. A., Agartz, I., & Dale, A. M. (2012). Cortical volume, surface area, and thickness in schizophrenia and bipolar disorder. *Biological Psychiatry*, *71*(6), 552–560.

Roalf, D. R., Quarmley, M., Calkins, M. E., Satterthwaite, T. D., Ruparel, K., Elliott, M. A., Moore, T. M., Gur, R. C., Gur, R. E., Moberg, P. J., & Turetsky, B. I. (2017). Temporal Lobe Volume Decrements in Psychosis Spectrum Youths. *Schizophrenia Bulletin*, *43*(3), 601–610.

Robert, C., Patel, R., Blostein, N., Steele, C. C., & Chakravarty, M. M. (2021). Analyses of microstructural variation in the human striatum using non-negative matrix factorization. *NeuroImage*, *246*, 118744.

Rodrigue, A. L., McDowell, J. E., Tandon, N., Keshavan, M. S., Tamminga, C. A., Pearlson, G. D., Sweeney, J. A., Gibbons, R. D., & Clementz, B. A. (2018). Multivariate Relationships Between Cognition and Brain Anatomy Across the Psychosis Spectrum. *Biological Psychiatry. Cognitive Neuroscience and Neuroimaging*, *3*(12), 992–1002.

Romero-Garcia, R., Seidlitz, J., Whitaker, K. J., Morgan, S. E., Fonagy, P., Dolan, R. J., Jones, P. B., Goodyer, I. M., Suckling, J., NSPN Consortium, Vértes, P. E., & Bullmore, E. T. (2020). Schizotypy-Related Magnetization of Cortex in Healthy Adolescence Is Colocated With Expression of Schizophrenia-Related Genes. *Biological Psychiatry*, *88*(3), 248–259.

Romero-Garcia, R., Warrier, V., Bullmore, E. T., Baron-Cohen, S., & Bethlehem, R. A. I. (2019). Synaptic and transcriptionally downregulated genes are associated with cortical thickness differences in autism. *Molecular Psychiatry*, *24*(7), 1053–1064.

Ronald, A., Sieradzka, D., Cardno, A. G., Haworth, C. M. A., McGuire, P., & Freeman, D. (2014). Characterization of psychotic experiences in adolescence using the specific psychotic experiences questionnaire: findings from a study of 5000 16-year-old twins. *Schizophrenia Bulletin*, *40*(4), 868–877.

Ronan, L., & Fletcher, P. C. (2015). From genes to folds: a review of cortical gyrification theory. *Brain Structure & Function*, *220*(5), 2475–2483.

Ronan, L., Pienaar, R., Williams, G., Bullmore, E., Crow, T. J., Roberts, N., Jones, P. B., Suckling, J., & Fletcher, P. C. (2011). Intrinsic curvature: a marker of millimeter-scale tangential cortico-cortical connectivity? *International Journal of Neural Systems*, *21*(5), 351–366.

Ronan, L., Voets, N., Rua, C., Alexander-Bloch, A. F., Hough, M., Mackay, C., Crow, T. J., James, A., Giedd, J. N., & Fletcher, P. C. (2013). Differential Tangential Expansion as a Mechanism for Cortical Gyrification. *Cerebral Cortex* , *24*(8), 2219–2228.

Rosenblad, A. (2009). Applied multivariate statistics for the social sciences, fifth edition by James P. stevens. *International Statistical Review = Revue Internationale de Statistique*, *77*(3), 476–476.

Rossell, S. L., Rabe-Hesketh, S., Shapleske, J., & David, A. S. (1999). Is Semantic Fluency Differentially Impaired in Schizophrenic Patients with Delusions? *Journal of Clinical and Experimental Neuropsychology*, *21*(5), 629–642.

Rousselet, G. A., Pernet, C. R., & Wilcox, R. R. (2017). Beyond differences in means: robust graphical methods to compare two groups in neuroscience. *The European Journal of Neuroscience*, *46*(2), 1738–1748.

Russell, D. W. (2002). In search of underlying dimensions: The use (and abuse) of factor analysis in Personality and Social Psychology Bulletin. *Personality & Social Psychology Bulletin*, *28*(12), 1629–1646.

Salo, T., Yarkoni, T., Nichols, T. E., Poline, J.-B., Kent, J. D., Gorgolewski, K. J., Glerean, E., Bottenhorn, K. L., Bilgel, M., Wright, J., Reeders, P., Kimbler, A., Nielson, D. N., Yanes, J. A., Pérez, A., Oudyk, K. M., Jarecka, D., Enge, A., Peraza, J. A., & Laird, A. R. (2022). *neurostuff/NiMARE: 0.0.12rc2*. https://doi.org/10.5281/zenodo.6329991

Sanfelici, R., Ruef, A., Antonucci, L. A., Penzel, N., Sotiras, A., Dong, M. S., Urquijo-Castro, M., Wenzel, J., Kambeitz-Ilankovic, L., Hettwer, M. D., Ruhrmann, S., Chisholm, K., Riecher-Rössler, A., Falkai, P., Pantelis, C., Salokangas, R. K. R., Lencer, R., Bertolino, A., Kambeitz, J., … PRONIA Consortium. (2021). Novel Gyrification Networks Reveal Links with Psychiatric Risk Factors in Early Illness. *Cerebral Cortex* . https://doi.org/10.1093/cercor/bhab288

Sasabayashi, D., Takayanagi, Y., Takahashi, T., Koike, S., Yamasue, H., Katagiri, N., Sakuma, A., Obara, C., Nakamura, M., Furuichi, A., Kido, M., Nishikawa, Y., Noguchi, K., Matsumoto, K., Mizuno, M., Kasai, K., & Suzuki, M. (2017). Increased Occipital Gyrification and Development of Psychotic Disorders in Individuals With an At-Risk Mental State: A Multicenter Study. *Biological Psychiatry*, *82*(10), 737–745.

Satterthwaite, T. D., Elliott, M. A., Ruparel, K., Loughead, J., Prabhakaran, K., Calkins, M. E., Hopson, R., Jackson, C., Keefe, J., Riley, M., Mentch, F. D., Sleiman, P., Verma, R., Davatzikos, C., Hakonarson, H., Gur, R. C., & Gur, R. E. (2014). Neuroimaging of the Philadelphia neurodevelopmental cohort. *NeuroImage*, *86*, 544–553.

Satterthwaite, T. D., Wolf, D. H., Calkins, M. E., Vandekar, S. N., Erus, G., Ruparel, K., Roalf, D. R., Linn, K. A., Elliott, M. A., Moore, T. M., Hakonarson, H., Shinohara, R. T., Davatzikos, C., Gur, R. C., & Gur, R. E. (2016). Structural Brain Abnormalities in Youth With Psychosis Spectrum Symptoms. *JAMA Psychiatry* , *73*(5), 515–524.

Schaer, M., Cuadra, M. B., Tamarit, L., Lazeyras, F., Eliez, S., & Thiran, J.-P. (2008). A surface-based approach to quantify local cortical gyrification. *IEEE Transactions on Medical Imaging*, *27*(2), 161–170.

Schimmelmann, B. G., Michel, C., Martz-Irngartinger, A., Linder, C., & Schultze-Lutter, F. (2015). Age matters in the prevalence and clinical significance of ultra-high-risk for psychosis symptoms and criteria in the general population: Findings from the BEAR and BEARS-kid studies. *World Psychiatry: Official Journal of the World Psychiatric Association* , *14*(2), 189–197.

Schoorl, J., Barbu, M. C., Shen, X., Harris, M. R., Adams, M. J., Whalley, H. C., & Lawrie, S. M. (2021). Grey and white matter associations of psychotic-like experiences in a general population sample (UK Biobank). *Translational Psychiatry*, *11*(1), 21.

Schultz, C. C., Koch, K., Wagner, G., Roebel, M., Nenadic, I., Gaser, C., Schachtzabel, C., Reichenbach, J. R., Sauer, H., & Schlösser, R. G. M. (2010). Increased parahippocampal

and lingual gyrification in first-episode schizophrenia. *Schizophrenia Research*, *123*(2–3), 137–144.

Schultze-Lutter, F., Michel, C., Schmidt, S. J., Schimmelmann, B. G., Maric, N. P., Salokangas, R. K. R., Riecher-Rössler, A., van der Gaag, M., Nordentoft, M., Raballo, A., Meneghelli, A., Marshall, M., Morrison, A., Ruhrmann, S., & Klosterkötter, J. (2015). EPA guidance on the early detection of clinical high risk states of psychoses. *European Psychiatry: The Journal of the Association of European Psychiatrists*, *30*(3), 405–416.

Schwartz, R. C., & Blankenship, D. M. (2014). Racial disparities in psychotic disorder diagnosis: A review of empirical literature. *World Journal of Psychiatry*, *4*(4), 133–140.

Seidlitz, J., Nadig, A., Liu, S., Bethlehem, R. A. I., Vértes, P. E., Morgan, S. E., Váša, F., Romero-Garcia, R., Lalonde, F. M., Clasen, L. S., Blumenthal, J. D., Paquola, C., Bernhardt, B., Wagstyl, K., Polioudakis, D., de la Torre-Ubieta, L., Geschwind, D. H., Han, J. C., Lee, N. R., … Raznahan, A. (2020). Transcriptomic and cellular decoding of regional brain vulnerability to neurogenetic disorders. *Nature Communications*, *11*(1), 3358.

Seidlitz, J., Váša, F., Shinn, M., Romero-Garcia, R., Whitaker, K. J., Vértes, P. E., Wagstyl, K., Kirkpatrick Reardon, P., Clasen, L., Liu, S., Messinger, A., Leopold, D. A., Fonagy, P., Dolan, R. J., Jones, P. B., Goodyer, I. M., NSPN Consortium, Raznahan, A., & Bullmore, E. T. (2018). Morphometric Similarity Networks Detect Microscale Cortical Organization and Predict Inter-Individual Cognitive Variation. *Neuron*, *97*(1), 231-247.e7.

Sellgren, C. M., Gracias, J., Watmuff, B., Biag, J. D., Thanos, J. M., Whittredge, P. B., Fu, T., Worringer, K., Brown, H. E., Wang, J., Kaykas, A., Karmacharya, R., Goold, C. P., Sheridan, S. D., & Perlis, R. H. (2019). Increased synapse elimination by microglia in schizophrenia patient-derived models of synaptic pruning. *Nature Neuroscience*, *22*(3), 374–385.

Shan, X., Uddin, L. Q., Xiao, J., He, C., Ling, Z., Li, L., Huang, X., Chen, H., & Duan, X. (2022). Mapping the Heterogeneous Brain Structural Phenotype of Autism Spectrum Disorder Using the Normative Model. *Biological Psychiatry*, *91*(11), 967–976.

Shevlin, M., McElroy, E., Bentall, R. P., Reininghaus, U., & Murphy, J. (2017). The Psychosis Continuum: Testing a Bifactor Model of Psychosis in a General Population Sample. *Schizophrenia Bulletin*, *43*(1), 133–141.

Shin, J., French, L., Xu, T., Leonard, G., Perron, M., Pike, G. B., Richer, L., Veillette, S., Pausova, Z., & Paus, T. (2018). Cell-Specific Gene-Expression Profiles and Cortical Thickness in the Human Brain. *Cerebral Cortex* , *28*(9), 3267–3277.

Sierra, M., Nestler, S., Jay, E.-L., Ecker, C., Feng, Y., & David, A. S. (2014). A structural MRI study of cortical thickness in depersonalisation disorder. *Psychiatry Research*, *224*(1), 1–7.

Siever, L. J., & Davis, K. L. (2004). The pathophysiology of schizophrenia disorders: perspectives from the spectrum. *The American Journal of Psychiatry*, *161*(3), 398–413.

Sled, J. G., Zijdenbos, A. P., & Evans, A. C. (1998). A nonparametric method for automatic correction of intensity nonuniformity in MRI data. *IEEE Transactions on Medical Imaging*, *17*(1), 87–97.

Smith, S. M., & Nichols, T. E. (2018). Statistical Challenges in “Big Data” Human Neuroimaging. *Neuron*, *97*(2), 263–268.

Song, C., Sandberg, K., Rutiku, R., & Kanai, R. (2022). Linking human behaviour to brain structure: further challenges and possible solutions [Review of *Linking human behaviour to brain structure: further challenges and possible solutions*]. *Nature Reviews. Neuroscience*, *23*(8), 517–518.

Song, J., Han, D. H., Kim, S. M., Hong, J. S., Min, K. J., Cheong, J. H., & Kim, B. N. (2015). Differences in gray matter volume corresponding to delusion and hallucination in patients with schizophrenia compared with patients who have bipolar disorder. *Neuropsychiatric Disease and Treatment*, *11*, 1211–1219.

Sotiras, A., Resnick, S. M., & Davatzikos, C. (2015). Finding imaging patterns of structural covariance via Non-Negative Matrix Factorization. *NeuroImage*, *108*, 1–16.

Sotiras, A., Toledo, J. B., Gur, R. E., Gur, R. C., Satterthwaite, T. D., & Davatzikos, C. (2017). Patterns of coordinated cortical remodeling during adolescence and their associations with functional specialization and evolutionary expansion. *Proceedings of the National Academy of Sciences of the United States of America*, *114*(13), 3527–3532.

Stainton, A., Chisholm, K., Woodall, T., Hallett, D., Reniers, R. L. E. P., Lin, A., & Wood, S. J. (2021). Gender differences in the experience of psychotic-like experiences and their associated factors: A study of adolescents from the general population. *Schizophrenia Research*, *228*, 410–416.

Stefanis, N. C., Hanssen, M., Smirnis, N. K., Avramopoulos, D. A., Evdokimidis, I. K., Stefanis, C. N., Verdoux, H., & van Os, J. (2002). Evidence that three dimensions of psychosis have a distribution in the general population. *Psychological Medicine*, *32*(2), 347–358.

Stekhoven, D. J., & Bühlmann, P. (2012). MissForest--non-parametric missing value imputation for mixed-type data. *Bioinformatics* , *28*(1), 112–118.

Sugranyes, G., de la Serna, E., Ilzarbe, D., Pariente, J. C., Borras, R., Romero, S., Rosa, M., Baeza, I., Moreno, M. D., Bernardo, M., Vieta, E., & Castro-Fornieles, J. (2021). Brain structural trajectories in youth at familial risk for schizophrenia or bipolar disorder according to development of psychosis spectrum symptoms. *Journal of Child Psychology and Psychiatry, and Allied Disciplines*, *62*(6), 780–789.

Sydnor, V. J., Larsen, B., Bassett, D. S., Alexander-Bloch, A. F., Fair, D. A., Liston, C., Mackey, A. P., Milham, M. P., Pines, A., Roalf, D. R., Seidlitz, J., Xu, T., Raznahan, A., & Satterthwaite, T. D. (2021). Neurodevelopment of the association cortices: Patterns, mechanisms, and implications for psychopathology. *Neuron*. https://doi.org/10.1016/j.neuron.2021.06.016

Takahashi, N., Sakurai, T., Davis, K. L., & Buxbaum, J. D. (2011). Linking oligodendrocyte and myelin dysfunction to neurocircuitry abnormalities in schizophrenia. *Progress in Neurobiology*, *93*(1), 13–24.

Takayanagi, Y., Sasabayashi, D., Takahashi, T., Furuichi, A., Kido, M., Nishikawa, Y., Nakamura, M., Noguchi, K., & Suzuki, M. (2020). Reduced Cortical Thickness in Schizophrenia and Schizotypal Disorder. *Schizophrenia Bulletin*, *46*(2), 387–394.

Taylor, J. H., Calkins, M. E., & Gur, R. E. (2020). Markers of Psychosis Risk in the General Population. *Biological Psychiatry*, *88*(4), 337–348.

Taylor, M. J., Freeman, D., & Ronald, A. (2016). Dimensional psychotic experiences in adolescence: Evidence from a taxometric study of a community-based sample. *Psychiatry Research*, *241*, 35–42.

Tohka, J., Zijdenbos, A., & Evans, A. (2004). Fast and robust parameter estimation for statistical partial volume models in brain MRI. *NeuroImage*, *23*(1), 84–97.

Toro, R., Perron, M., Pike, B., Richer, L., Veillette, S., Pausova, Z., & Paus, T. (2008). Brain size and folding of the human cerebral cortex. *Cerebral Cortex* , *18*(10), 2352–2357.

Tzourio-Mazoyer, N., Landeau, B., Papathanassiou, D., Crivello, F., Etard, O., Delcroix, N., Mazoyer, B., & Joliot, M. (2002). Automated anatomical labeling of activations in SPM using a macroscopic anatomical parcellation of the MNI MRI single-subject brain. *NeuroImage*, *15*(1), 273–289.

Unterrassner, L. (2018). Subtypes of Psychotic-Like Experiences and Their Significance for Mental Health. In *Psychosis - Biopsychosocial and Relational Perspectives*. unknown.

van der Werf, M., Hanssen, M., Köhler, S., Verkaaik, M., Verhey, F. R., RISE Investigators, van Winkel, R., van Os, J., & Allardyce, J. (2014). Systematic review and collaborative recalculation of 133,693 incident cases of schizophrenia. *Psychological Medicine*, *44*(1), 9–16.

van Erp, T. G. M., Walton, E., Hibar, D. P., Schmaal, L., Jiang, W., Glahn, D. C., Pearlson, G. D., Yao, N., Fukunaga, M., Hashimoto, R., Okada, N., Yamamori, H., Bustillo, J. R., Clark, V. P., Agartz, I., Mueller, B. A., Cahn, W., de Zwarte, S. M. C., Hulshoff Pol, H. E., … Turner, J. A. (2018). Cortical Brain Abnormalities in 4474 Individuals With Schizophrenia and 5098 Control Subjects via the Enhancing Neuro Imaging Genetics Through Meta Analysis (ENIGMA) Consortium. *Biological Psychiatry*, *84*(9), 644–654.

Van Essen, D. C., Drury, H. A., Joshi, S., & Miller, M. I. (1998). Functional and structural mapping of human cerebral cortex: Solutions are in the surfaces. *Proceedings of the National Academy of Sciences*, *95*(3), 788–795.

van Lutterveld, R., van den Heuvel, M. P., Diederen, K. M. J., de Weijer, A. D., Begemann, M. J. H., Brouwer, R. M., Daalman, K., Blom, J. D., Kahn, R. S., & Sommer, I. E. (2014). Cortical thickness in individuals with non-clinical and clinical psychotic symptoms. *Brain: A Journal of Neurology*, *137*(Pt 10), 2664–2669.

van Os, J., Hanssen, M., Bijl, R. V., & Ravelli, A. (2000). Strauss (1969) revisited: a psychosis continuum in the general population? *Schizophrenia Research*, *45*(1–2), 11–20.

van Os, J., & Kapur, S. (2009). Schizophrenia. *The Lancet*, *374*(9690), 635–645.

van Os, J., & Linscott, R. J. (2012). Introduction: The extended psychosis phenotype--relationship with schizophrenia and with ultrahigh risk status for psychosis. *Schizophrenia Bulletin*, *38*(2), 227–230.

van Os, J., Linscott, R. J., Myin-Germeys, I., Delespaul, P., & Krabbendam, L. (2009). A systematic review and meta-analysis of the psychosis continuum: evidence for a psychosis

proneness-persistence-impairment model of psychotic disorder. *Psychological Medicine*, *39*(2), 179–195.

van Os, J., & Reininghaus, U. (2016). Psychosis as a transdiagnostic and extended phenotype in the general population. *World Psychiatry: Official Journal of the World Psychiatric Association* , *15*(2), 118–124.

Vandekar, S. N., Shinohara, R. T., Raznahan, A., Hopson, R. D., Roalf, D. R., Ruparel, K., Gur, R. C., Gur, R. E., & Satterthwaite, T. D. (2016). Subject-level measurement of local cortical coupling. *NeuroImage*, *133*, 88–97.

Vandekar, S. N., Shinohara, R. T., Raznahan, A., Roalf, D. R., Ross, M., DeLeo, N., Ruparel, K., Verma, R., Wolf, D. H., Gur, R. C., Gur, R. E., & Satterthwaite, T. D. (2015). Topologically dissociable patterns of development of the human cerebral cortex. *The Journal of Neuroscience: The Official Journal of the Society for Neuroscience*, *35*(2), 599–609.

Vargas, T. G., & Mittal, V. A. (2022). Brain morphometry points to emerging patterns of psychosis, depression, and anxiety vulnerability over a 2-year period in childhood. *Psychological Medicine*, 1–13.

Varikuti, D. P., Genon, S., Sotiras, A., Schwender, H., Hoffstaedter, F., Patil, K. R., Jockwitz, C., Caspers, S., Moebus, S., Amunts, K., Davatzikos, C., & Eickhoff, S. B. (2018). Evaluation of non-negative matrix factorization of grey matter in age prediction. *NeuroImage*, *173*, 394–410.

Verdoux, H., & van Os, J. (2002). Psychotic symptoms in non-clinical populations and the continuum of psychosis. *Schizophrenia Research*, *54*(1–2), 59–65.

Vidal-Pineiro, D., Parker, N., Shin, J., French, L., Grydeland, H., Jackowski, A. P., Mowinckel, A. M., Patel, Y., Pausova, Z., Salum, G., Sørensen, Ø., Walhovd, K. B., Paus, T., Fjell, A. M., & Alzheimer's Disease Neuroimaging Initiative and the Australian Imaging Biomarkers and Lifestyle flagship study of ageing. (2020). Cellular correlates of cortical thinning throughout the lifespan. *Scientific Reports*, *10*(1), 21803.

Voineskos, A. N., Jacobs, G. R., & Ameis, S. H. (2020). Neuroimaging Heterogeneity in Psychosis: Neurobiological Underpinnings and Opportunities for Prognostic and Therapeutic Innovation. *Biological Psychiatry*, *88*(1), 95–102.

Wang, H.-T., Smallwood, J., Mourao-Miranda, J., Xia, C. H., Satterthwaite, T. D., Bassett, D. S., & Bzdok, D. (2020). Finding the needle in a high-dimensional haystack: Canonical correlation analysis for neuroscientists. *NeuroImage*, *216*, 116745.

Wen, J., Nasrallah, I. M., Abdulkadir, A., Satterthwaite, T. D., Yang, Z., Erus, G., Robert-Fitzgerald, T., Singh, A., Sotiras, A., Boquet-Pujadas, A., Mamourian, E., Doshi, J., Cui, Y., Srinivasan, D., Chen, J., Hwang, G., Bergman, M., Bao, J., Veturi, Y., … the AI4AD consortium. (2022). Novel genomic loci and pathways influence patterns of structural covariance in the human brain. In *bioRxiv*. https://doi.org/10.1101/2022.07.20.22277727

Werbeloff, N., Dohrenwend, B. P., Yoffe, R., van Os, J., Davidson, M., & Weiser, M. (2015). The association between negative symptoms, psychotic experiences and later schizophrenia: a population-based longitudinal study. *PloS One*, *10*(3), e0119852.

Werbeloff, N., Drukker, M., Dohrenwend, B. P., Levav, I., Yoffe, R., van Os, J., Davidson, M., & Weiser, M. (2012). Self-reported Attenuated Psychotic Symptoms as Forerunners of Severe Mental Disorders Later in Life. *Archives of General Psychiatry*, *69*(5), 467–475.

Whitaker, K. J., Vértes, P. E., Romero-Garcia, R., Váša, F., Moutoussis, M., Prabhu, G., Weiskopf, N., Callaghan, M. F., Wagstyl, K., Rittman, T., Tait, R., Ooi, C., Suckling, J., Inkster, B., Fonagy, P., Dolan, R. J., Jones, P. B., Goodyer, I. M., NSPN Consortium, & Bullmore, E. T. (2016). Adolescence is associated with genomically patterned consolidation of the hubs of the human brain connectome. *Proceedings of the National Academy of Sciences of the United States of America*, *113*(32), 9105–9110.

Whitford, T. J., Farrow, T. F. D., Williams, L. M., Gomes, L., Brennan, J., & Harris, A. W. F. (2009). Delusions and dorso-medial frontal cortex volume in first-episode schizophrenia: a voxel-based morphometry study. *Psychiatry Research*, *172*(3), 175–179.

Wierenga, L. M., Langen, M., Oranje, B., & Durston, S. (2014). Unique developmental trajectories of cortical thickness and surface area. *NeuroImage*, *87*, 120–126.

Wigman, J. T. W., Vollebergh, W. A. M., Raaijmakers, Q. A. W., Iedema, J., van Dorsselaer, S., Ormel, J., Verhulst, F. C., & van Os, J. (2011). The structure of the extended psychosis phenotype in early adolescence--a cross-sample replication. *Schizophrenia Bulletin*, *37*(4), 850–860.

Wilcox, R. R., Erceg-Hurn, D. M., Clark, F., & Carlson, M. (2014). Comparing two independent groups via the lower and upper quantiles. *Journal of Statistical Computation and Simulation*, *84*(7), 1543–1551.

Wilkinson, G. S., & Robertson, G. J. (2006). Wide Range Achievement Test: Fourth Edition. *Lutz, FL: Psychological Assessment Resources*. http://www.v-psyche.com/doc/MENTAL%20ABILITY/Wide%20Range%20Achievement%20Test%204%20(WRAT-4).doc

Winkler, A. M., Greve, D. N., Bjuland, K. J., Nichols, T. E., Sabuncu, M. R., Håberg, A. K., Skranes, J., & Rimol, L. M. (2018). Joint Analysis of Cortical Area and Thickness as a Replacement for the Analysis of the Volume of the Cerebral Cortex. *Cerebral Cortex* , *28*(2), 738–749.

Winkler, A. M., Kochunov, P., Blangero, J., Almasy, L., Zilles, K., Fox, P. T., Duggirala, R., & Glahn, D. C. (2010). Cortical thickness or grey matter volume? The importance of selecting the phenotype for imaging genetics studies. *NeuroImage*, *53*(3), 1135–1146.

Witthaus, H., Kaufmann, C., Bohner, G., Ozgürdal, S., Gudlowski, Y., Gallinat, J., Ruhrmann, S., Brüne, M., Heinz, A., Klingebiel, R., & Juckel, G. (2009). Gray matter abnormalities in subjects at ultra-high risk for schizophrenia and first-episode schizophrenic patients compared to healthy controls. *Psychiatry Research*, *173*(3), 163–169.

Wolf, R. C., Hildebrandt, V., Schmitgen, M. M., Pycha, R., Kirchler, E., Macina, C., Karner, M., Hirjak, D., Kubera, K. M., Romanov, D., Freudenmann, R. W., & Huber, M. (2020). Aberrant Gray Matter Volume and Cortical Surface in Paranoid-Type Delusional Disorder. *Neuropsychobiology*, *79*(4–5), 335–344.

Writing Committee for the Attention-Deficit/Hyperactivity Disorder, Autism Spectrum Disorder, Bipolar Disorder, Major Depressive Disorder, Obsessive-Compulsive Disorder, and

Schizophrenia ENIGMA Working Groups, Patel, Y., Parker, N., Shin, J., Howard, D., French, L., Thomopoulos, S. I., Pozzi, E., Abe, Y., Abé, C., Anticevic, A., Alda, M., Aleman, A., Alloza, C., … Paus, T. (2021). Virtual Histology of Cortical Thickness and Shared Neurobiology in 6 Psychiatric Disorders. *JAMA Psychiatry* , *78*(1), 47–63.

Wylie, K. P., & Tregellas, J. R. (2010). The role of the insula in schizophrenia. *Schizophrenia Research*, *123*(2–3), 93–104.

Xia, C. H., Ma, Z., Ciric, R., Gu, S., Betzel, R. F., Kaczkurkin, A. N., Calkins, M. E., Cook, P. A., García de la Garza, A., Vandekar, S. N., Cui, Z., Moore, T. M., Roalf, D. R., Ruparel, K., Wolf, D. H., Davatzikos, C., Gur, R. C., Gur, R. E., Shinohara, R. T., … Satterthwaite, T. D. (2018). Linked dimensions of psychopathology and connectivity in functional brain networks. *Nature Communications*, *9*(1), 3003.

Yang, Z., & Oja, E. (2010). Linear and nonlinear projective nonnegative matrix factorization. *IEEE Transactions on Neural Networks / a Publication of the IEEE Neural Networks Council*, *21*(5), 734–749.

Yarkoni, T., Poldrack, R. A., Nichols, T. E., Van Essen, D. C., & Wager, T. D. (2011). Large-scale automated synthesis of human functional neuroimaging data. *Nature Methods*, *8*(8), 665–670.

Yeo, B. T. T., Krienen, F. M., Sepulcre, J., Sabuncu, M. R., Lashkari, D., Hollinshead, M., Roffman, J. L., Smoller, J. W., Zöllei, L., Polimeni, J. R., Fischl, B., Liu, H., & Buckner, R. L. (2011). The organization of the human cerebral cortex estimated by intrinsic functional connectivity. *Journal of Neurophysiology*, *106*(3), 1125–1165.

Yung, A. R., Buckby, J. A., Cotton, S. M., Cosgrave, E. M., Killackey, E. J., Stanford, C., Godfrey, K., & McGorry, P. D. (2006). Psychotic-like experiences in nonpsychotic help-seekers: associations with distress, depression, and disability. *Schizophrenia Bulletin*, *32*(2), 352–359.

Yung, A. R., Nelson, B., Baker, K., Buckby, J. A., Baksheev, G., & Cosgrave, E. M. (2009). Psychotic-like experiences in a community sample of adolescents: implications for the continuum model of psychosis and prediction of schizophrenia. *The Australian and New Zealand Journal of Psychiatry*, *43*(2), 118–128.

Zammit, S., Kounali, D., Cannon, M., David, A. S., Gunnell, D., Heron, J., Jones, P. B., Lewis, S., Sullivan, S., Wolke, D., & Lewis, G. (2013). Psychotic experiences and psychotic disorders at age 18 in relation to psychotic experiences at age 12 in a longitudinal population-based cohort study. *The American Journal of Psychiatry*, *170*(7), 742–750.

Zeighami, Y., & Evans, A. C. (2021). Association vs. Prediction: The Impact of Cortical Surface Smoothing and Parcellation on Brain Age. *Frontiers in Big Data*, *4*, 637724.

Zeighami, Y., Fereshtehnejad, S.-M., Dadar, M., Collins, D. L., Postuma, R. B., Mišić, B., & Dagher, A. (2019). A clinical-anatomical signature of Parkinson's disease identified with partial least squares and magnetic resonance imaging. *NeuroImage*, *190*, 69–78.

Zhang, B., Kirov, S., & Snoddy, J. (2005). WebGestalt: an integrated system for exploring gene sets in various biological contexts. *Nucleic Acids Research*, *33*(Web Server issue), W741-8.

Zhang, Y., Sloan, S. A., Clarke, L. E., Caneda, C., Plaza, C. A., Blumenthal, P. D., Vogel, H., Steinberg, G. K., Edwards, M. S. B., Li, G., Duncan, J. A., 3rd, Cheshier, S. H., Shuer, L. M., Chang, E. F., Grant, G. A., Gephart, M. G. H., & Barres, B. A. (2016). Purification and Characterization of Progenitor and Mature Human Astrocytes Reveals Transcriptional and Functional Differences with Mouse. *Neuron*, *89*(1), 37–53.

Zhu, J., Zhuo, C., Liu, F., Xu, L., & Yu, C. (2016). Neural substrates underlying delusions in schizophrenia. *Scientific Reports*, *6*, 33857.

Ziermans, T. B., Schothorst, P. F., Schnack, H. G., Koolschijn, P. C. M. P., Kahn, R. S., van Engeland, H., & Durston, S. (2012). Progressive structural brain changes during development of psychosis. *Schizophrenia Bulletin*, *38*(3), 519–530.

Zijdenbos, A. P., Forghani, R., & Evans, A. C. (2002). Automatic "pipeline" analysis of 3-D MRI data for clinical trials: application to multiple sclerosis. *IEEE Transactions on Medical Imaging*, *21*(10), 1280–1291.

Ziolkowski, J. (2022). Investigating individual variability of morphometric covariance patterns in autism spectrum disorder [Manuscript in preparation]. Integrated Program in Neuroscience, McGill University.